University of Alberta

Flatness-Based Open and Closed-loop Control of a Flexible Beam System

by

Martin Barczyk

A thesis submitted to the Faculty of Graduate Studies and Research in partial fulfillment of the requirements for the degree of **Master of Science**.

Department of Electrical and Computer Engineering

Edmonton, Alberta
Fall 2005

0-494-09121-5

Library and Archives Canada

Published Heritage Branch

395 Wellington Street
Ottawa ON K1A 0N4
Canada

Bibliothèque et Archives Canada

Direction du Patrimoine de l'édition

395, rue Wellington
Ottawa ON K1A 0N4
Canada

Your file *Votre référence*
ISBN:
Our file *Notre référence*
ISBN:

NOTICE:
The author has granted a non-exclusive license allowing Library and Archives Canada to reproduce, publish, archive, preserve, conserve, communicate to the public by telecommunication or on the Internet, loan, distribute and sell theses worldwide, for commercial or non-commercial purposes, in microform, paper, electronic and/or any other formats.

The author retains copyright ownership and moral rights in this thesis. Neither the thesis nor substantial extracts from it may be printed or otherwise reproduced without the author's permission.

AVIS:
L'auteur a accordé une licence non exclusive permettant à la Bibliothèque et Archives Canada de reproduire, publier, archiver, sauvegarder, conserver, transmettre au public par télécommunication ou par l'Internet, prêter, distribuer et vendre des thèses partout dans le monde, à des fins commerciales ou autres, sur support microforme, papier, électronique et/ou autres formats.

L'auteur conserve la propriété du droit d'auteur et des droits moraux qui protège cette thèse. Ni la thèse ni des extraits substantiels de celle-ci ne doivent être imprimés ou autrement reproduits sans son autorisation.

In compliance with the Canadian Privacy Act some supporting forms may have been removed from this thesis.

While these forms may be included in the document page count, their removal does not represent any loss of content from the thesis.

Conformément à la loi canadienne sur la protection de la vie privée, quelques formulaires secondaires ont été enlevés de cette thèse.

Bien que ces formulaires aient inclus dans la pagination, il n'y aura aucun contenu manquant.

Canada

Abstract

Open and closed-loop flatness-based tracking control of flexible beams is considered. A rotating beam system is modeled using an Euler-Bernoulli partial differential equation. Flatness is used to derive an open-loop control by introducing a so-called flat output which parameterizes the system state and input in terms of an infinite series depending on the flat output and its time derivatives. The series are truncated to derive finite-dimensional state-space form system approximations for which linear estimated state feedback tracking laws are applied. A finite-element analysis model, required to simulate the performance of the proposed closed-loop design, is derived and implemented. Both open and closed-loop controls are successfully validated experimentally on a test stand. Generalization of the open-loop control for rotating beam systems with tip payload are presented, and a superposition-based open-loop control for a levitated beam is described.

Acknowledgements

I would like to thank my co-supervisors, Dr. Tongwen Chen, for believing in me and giving me a chance to study at the U of A, and Dr. Alan Lynch, for his continued help and endless patience throughout the work.

Regards to my colleagues in the research group. I am particularly grateful to Cesar Aguilar and Thomas Grochmal, for their encouragement, the many discussions, and for inspiring me to work hard and continue studying the field of control systems.

To my parents, Maria and Tomasz, for cheering me on and being there when I needed emotional support.

Finally, to all my fellow Faculté Saint-Jean residents, thanks for all the great times in res. I have grown as a person because of you.

Table of Contents

1 Introduction 1
- 1.1 Control of Flexible Structures . . . 1
- 1.2 Distributed Parameter Systems . . . 2
- 1.3 Flatness-based Control . . . 3
- 1.4 Flatness-based Control of Infinite-dimensional Systems . . . 4
- 1.5 Scope of the Research . . . 5
- 1.6 Overview of the Thesis . . . 5

2 System Description and Modeling 6
- 2.1 Description of the Plant . . . 6
- 2.2 Derivation of the Beam Model . . . 7
  - 2.2.1 Background . . . 7
  - 2.2.2 Euler-Bernoulli Beam PDE . . . 8
  - 2.2.3 Force and Moment Boundary Conditions . . . 10
- 2.3 Derivation of the Rotating Beam Model . . . 11
- 2.4 System Parameters . . . 14

3 Flatness-based Open-loop Control 16
- 3.1 Transformation of System Equations . . . 16
- 3.2 Transfer Function of the System . . . 17
- 3.3 Introducing the Flat Output . . . 18
- 3.4 Series Manipulations . . . 18
  - 3.4.1 Background . . . 19
  - 3.4.2 Series Representation of $P(x,s)$ . . . 20
  - 3.4.3 Series Representation of $Q(x,s)$ . . . 23
  - 3.4.4 Final Series Expressions . . . 25
- 3.5 Open-loop Control . . . 25
- 3.6 Calculation of Time Derivatives of $\eta_\gamma(t)$ . . . 28
- 3.7 Additional Series Expressions . . . 32
  - 3.7.1 Series Expression for $\theta(t)$ . . . 32
  - 3.7.2 Series Expression for $V(L,t)$ . . . 33

4 Flatness-based Closed-loop Tracking Control 34
- 4.1 Approximate State-space System Representation . . . 34
- 4.2 Observer Design . . . 38
- 4.3 State Feedback Tracking Controller Design . . . 39

5 Numerical Simulation 42
- 5.1 Series Computations . . . 42
- 5.2 Observer Testing . . . 44
- 5.3 FEA Model . . . 47
  - 5.3.1 FEA Formulation of a Single Beam Element . . . 47
  - 5.3.2 Superposition of Beam Elements . . . 49

5.3.3 Boundary Conditions in FEA . . . 50
5.3.4 State-space Representation of FEA model . . . 50
5.4 Validating the FEA Model . . . 51
5.5 Closed-loop Control Simulations . . . 51

6 Experimental Validation **56**
6.1 Overview of Experimental Setup . . . 56
6.2 Constant Gain Control . . . 56
6.3 Flatness-based Open-loop Control Experiment . . . 56
6.4 Flatness-Based Closed-loop Control Experiment . . . 59
6.4.1 Disturbance-Free Test, $N = 2$ Design . . . 59
6.4.2 External Disturbances Test, $N = 2$ Design . . . 59
6.4.3 Disturbance-Free Run, $N = 3$ Design . . . 61

7 Generalization of the Rotating Beam Model **62**
7.1 Derivation of the Rayleigh Beam Model . . . 62
7.1.1 Rayleigh Beam PDE . . . 62
7.1.2 Force and Moment Boundary Conditions . . . 63
7.2 Rotating Beam Model . . . 64
7.3 Alternative Series Solution . . . 67
7.4 Normalizing the Boundary-Value Problem . . . 68
7.5 Assumed Solution of Normalized BVP . . . 69
7.6 Series Manipulations . . . 72
7.6.1 Part I of $P(x, s)$ . . . 73
7.6.2 Part II of $P(x, s)$ . . . 74
7.6.3 Part III of $P(x, s)$ . . . 74
7.6.4 Part IV of $P(x, s)$ . . . 76
7.7 Conversion to Infinite Series . . . 77
7.8 Parameterizing the System Trajectories . . . 80
7.9 Undoing the Normalization . . . 80
7.10 Boundary Input Torque . . . 82

8 Levitating Flexible Beam and Superposition **86**
8.1 Introduction . . . 86
8.2 Input Superposition . . . 87
8.3 Boundary Conditions and Input Forces . . . 87
8.4 Problem Formulation for Single-input System . . . 88
8.5 Normalized Problem Formulation: Single-input . . . 91
8.6 Infinite Series Representation: Single-input . . . 93
8.6.1 Series Representation of $P(x, s)$ . . . 94
8.6.2 Series Representation of $Q(x, s)$ . . . 97
8.6.3 Series Representation of $R(x, s)$ . . . 98
8.7 Flat Output Parametrization: Single-input . . . 101
8.8 Simulation of Single-input System . . . 104
8.9 Two-input System . . . 104
8.10 Simulation of Two-input System . . . 105
8.11 Discussion and Future Work . . . 106

9 Conclusions and Future Work **107**

Bibliography **108**

A Electrical Drive Subsystem **113**

B Closed-loop Step Identification Test **115**

List of Tables

2.1 Physical parameters for the flexible beam plant 15

5.1 Calculation parameters for series simulation 42

8.1 Simulation parameters for a one-input beam 104
8.2 Simulation parameters for a two-input beam 106

List of Figures

1.1 Example of a flexible manipulator — the Canadarm 1
1.2 The kinematic car 4

2.1 Flexible beam system 6
2.2 Combined deformation and rigid-body translation of a flexible beam 7
2.3 Free-body diagram of infinitesimal beam segment 8
2.4 External force and moment acting on left beam edge 10
2.5 External force and moment acting on right beam edge 11
2.6 Rotating flexible beam model 12
2.7 Free-body diagram of hub 12
2.8 Free-body diagram of flexible beam 13
2.9 Beam cross-section diagram 14

3.1 Sample $\eta_\gamma(t)$ plots for $t_f = 1$ and $\gamma \in \{1.4, 10, 50\}$ 27

5.1 Results of series-based simulation 43
5.2 Observer testing Simulink diagram 44
5.3 Observer (—) versus actual (---) states, $N = 2$. 45
5.4 Observer (—) versus actual (---) states, $N = 3$. 45
5.5 Observer (—) versus actual (---) states, $N = 4$. 46
5.6 Single beam segment 47
5.7 Two-segment beam example for superposition 49
5.8 FEA model of rotating beam with N elements 50
5.9 FEA open-loop testing, Simulink implementation 51
5.10 Results of FEA simulation 52
5.11 Closed-loop system Simulink diagram 52
5.12 Controller subsystem Simulink implementation 53
5.13 Open-loop steering of beam with $\theta(0) = -10°$ 53
5.14 Closed-loop control of beam with $\theta(0) = -10°$, $N = 2$. 54
5.15 Closed-loop control of beam with $\theta(0) = -10°$, $N = 3$. 54
5.16 Closed-loop control of beam with $\theta(0) = -10°$, $N = 4$. Unstable operation. . 55

6.1 Proportional controller for rotating beam 56
6.2 90° transition using constant gain controller 57
6.3 Open-loop experimental testing setup 57
6.4 Experimental open-loop steering to 90° 58
6.5 Closed-loop experiment Simulink model 59
6.6 Closed-loop experiment, $\tau(t)$ to $u(t)$ conversion subsystem 59
6.7 Experimental 1 second 90° transition, $N = 2$ controller 60
6.8 Attempted 1 second 90° transition, subjected to manual interference. 60
6.9 Attempted 90° transition, $N = 3$ controller. Unstable operation. 61

7.1 Free-body diagram of infinitesimal Rayleigh beam segment 62
7.2 Rotating beam diagram 64

7.3 Free-body diagram of payload 65
7.4 Free-body diagram of hub 65
7.5 Forces and moments acting on Rayleigh beam 66

8.1 Active magnetic bearing 86
8.2 3-input system with 3 displacement fields 87
8.3 Graphical interpretation of superposition 87
8.4 Internal and external forces at inner beam boundary, $x = l$ 88
8.5 Two-segment beam with input at $x = l$ 88
8.6 Normalized 1-input 2-segment beam problem 91
8.7 Effect of input force location on final configuration 103
8.8 Simulation of 1-input beam 104
8.9 Simulation of 2-input beam 106

A.1 Electric drive system diagram 113

B.1 Closed-loop setup for parameter identification 116
B.2 Input/Output data for system step response 117

Chapter 1

Introduction

1.1 Control of Flexible Structures

The control of flexible structures is an established area of research with numerous important practical applications. An example of a controlled flexible structure is the Shuttle Remote Manipulator System, also known as the Canadarm [25] shown in Figure 1.1. Closer to home, applications include flexible robotic arms [1], construction cranes [54], heavy cables [56], piezoelectric microsystem positioning devices [22, 65], offshore oil and gas exploration equipment [12], and hard disk read/write head actuators [48].

Figure 1.1: Example of a flexible manipulator — the Canadarm

Flexible manipulators are intentionally slender to provide low mechanical inertia. This allows for fast motion control in weight critical applications. Such slender designs have low geometric stiffness and hence the control of lightly-damped oscillations becomes a key issue when trying to achieve motion planning objectives. As the speed of desired motion increases, especially in the presence of a tip payload mass, the system experiences larger inertial forces which can worsen vibrational problems. One way to reduce the level of oscillations is to control the manipulator in open-loop and move sufficiently slowly. This non-model-based simplistic approach to control is used to keep swaying at safe levels in the Canadarm, which translates at 6 cm/second fully loaded. However, this solution may not be acceptable in applications where accurate high-speed motions are critical. For example,

manufacturing robots must move fast to ensure the assembled product is profitable. Hence, it is natural to make use of a physical model of the system which accounts for flexibility in order to obtain better performance. For example, a closed-loop scheme might sense deformations of a manipulator and apply corrective actuator action using a model-based control strategy. Typical sensors include strain gages for measuring deflection, and encoders at the articulated joints to measure angular position and velocity. The actuator, typically a servo motor, applies torque to control the structure. The control of flexible manipulators has been studied extensively over the last two decades, especially in the context of robotics. A recent survey paper [5] classifies existing work in the area according to manipulator design (single versus multi-link), dynamic model (spring-mass discrete, continuous, Lagrangian formulation, finite-element decomposition, modal decomposition), control objective (end-effector position regulation, tracking of desired angular trajectory in rotating joints, tracking of end-effector trajectory) and control technique used (input-output linearization, PID, pole-placement, adaptive, neural network, sliding-mode, robust, optimal, and others). This thesis makes a contribution to the problem of controlling flexible structures by proposing flatness-based open and closed-loop control laws for flexible systems.

1.2 Distributed Parameter Systems

A distributed parameter system (DPS) is one whose behaviour can be naturally modeled by partial differential equations (PDEs). Such systems are a special case of infinite-dimensional systems whose state space has infinite dimension (e.g. a linear delay systems). In contrast to infinite-dimensional systems, lumped-parameter systems are described by ordinary differential equation (ODE) models. The behaviour of a DPS is described by dependent variables which are functions of at least two independent variables, usually time and space. On the other hand, lumped-parameter systems' variables depend on time alone. For example, the macroscopic description of the position and orientation of an airplane, or the voltage and current terminal characteristics of an analog circuit can be well-modeled using a lumped parameter ODE model. Distributed phenomena often results from a microscopic analysis and leads to a PDE model. For example, the vibration of an airplane wing or electric charge distribution inside a transistor are systems which have an infinite number of system variables or degrees of freedom and are best modeled using PDEs.

The study of controlled DPS is an interesting and challenging current area of research. Much of the challenge arises from the additional complexity of working with PDEs relative to ODEs. This increased complexity can be seen when investigating even fundamental issues indirectly related to control such as existence or uniqueness of solutions to PDEs. Existing control methods can be roughly divided into two categories.

1. *Indirect methods* which first spatially discretize the PDE model to obtain a system of ODEs. Spatial discretization can be performed in a number of ways including the use of modal decomposition and Finite-Element Analysis (FEA). Lumped parameter control design methods can then be readily applied to the resulting finite-dimensional model. Examples of this approach are in [28, 72, 10] which treat the motion control problem for rotating flexible beams. Robust H_∞-optimal control methods are applied to spatially discretized models [3, 69]. Such spatial discretization model-based methods are commonly used in practice but can lack theoretical justification for their underlying approximations.

2. *Direct methods* use the PDE model for design without explicitly performing a spatial discretization step and are a more modern approach [9, 2, 17, 75, 8]. Theoretical methods in [8] rely on a semigroup functional analysis framework in order to develop a theory for DPS similar to the established linear finite-dimensional state space system theory [6]. This thesis adopts a direct approach which generalizes the notion of differential flatness [13] to infinite-dimensional systems. Recent work in [45, 46] introduces practical methods for superimposing a closed-loop flatness-based control on top

of feedforward. Another body of work which adopts a direct approach to controlling DPS makes use of Lyapunov's method. Examples of such work include [50] and are typically focused on simple control structures which ensure closed-loop stability.

1.3 Flatness-based Control

Differential flatness-based control was originally developed for finite-dimensional nonlinear systems by Fliess et al. [13, 14]. An overview of recent results on flatness is in [43]. Although the concept of flatness originally arose in a differential algebraic framework, it is more easily explained as the ability to express system variables in terms of a so-called flat output function. The trajectories of a flat systems are completely parameterized differentially by the trajectories of a flat output which can be freely assigned (at least from a mathematical point of view). We consider a system in explicit state space form

$$\dot{x} = f(x, u) \tag{1.1}$$

where $x \in \mathbb{R}^n$ denotes the state and $u \in \mathbb{R}^m$ the input vector. If system (1.1) is flat, there exists a *flat output* vector $y \in \mathbb{R}^m$ with

$$y = h(x, u, \dot{u}, \ldots, u^{(r)})$$

for some smooth function h, and locally there exist smooth functions α, φ such that

$$\begin{aligned} x &= \varphi(y, \dot{y}, \ldots, y^{(q)}) \\ u &= \alpha(y, \dot{y}, \ldots, y^{(s)}) \end{aligned} \tag{1.2}$$

where r, q, s are finite integers. We remark the number of flat output components is equal to m, the number of system inputs. As well, the flat output y is *differentially independent*, which means there does not exist an ODE such that $\nu(y, \dot{y}, \ldots, y^{(p)}) = 0$.

A simple example of a flat system is the kinematic car [14] shown in Figure 1.2 and described by the ODE

$$\begin{aligned} \dot{x}_1 &= v\cos\theta \\ \dot{x}_2 &= v\sin\theta \\ \dot{x}_3 &= v\frac{\tan\phi}{l} \end{aligned} \tag{1.3}$$

where the linear velocity of the rear axle is denoted v, the position coordinate of the centre of the rear axle is (x_1, x_2), the angle the rear axle makes with the horizontal is θ, the angle the front axle makes with the frame of the car is ϕ, and the distance between the front and rear axle centers is denoted l. If we take the system input as $(v, \phi)^T$ and choose the flat output as position of the rear axle $y = (x_1, x_2)^T$, we have the following expressions for state ϕ and input $(v, \phi)^T$ in terms a finite number of time derivatives of y:

$$\begin{aligned} \theta &= \arctan\left(\frac{\dot{x}_2}{\dot{x}_1}\right) \\ v &= \pm\sqrt{\dot{x}_1^2 + \dot{x}_2^2} \\ \phi &= \arctan\left(\frac{l\dot{\theta}}{v}\right) = \pm\arctan\left(\frac{l(\ddot{x}_2\dot{x}_1 - \ddot{x}_1\dot{x}_2)}{(\dot{x}_1^2 + \dot{x}_2^2)^{3/2}}\right) \end{aligned}$$

Hence, the kinematic car is flat and we remark the local domain of definition of the functions α, φ introduced in (1.2).

The particular relationship between flat output and system variables (i.e., input and state), which involves only derivatives and no integration, allows us to readily incorporate

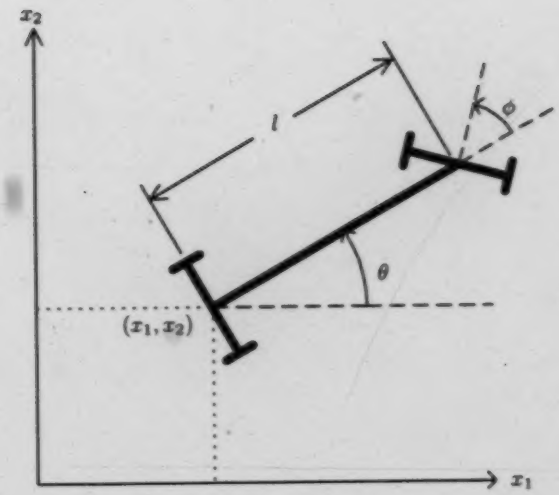

Figure 1.2: The kinematic car

motion planning objectives into the trajectory $t \mapsto y(t)$, and having fixed this trajectory an expression for the steering control follows by differentiation and algebraic computation. Flatness implies dynamic feedback linearizability and hence generalizes the important notion of static state feedback linearization [23, 27]. For example, the kinematic car (1.3) is flat but not static state feedback linearizable. A flatness-based control law also naturally leads to a closed-loop feedback with a linear tracking error dynamics system. Consequently, flatness-based feedback control provides robust tracking performance. A final important property of flatness is that, unlike feedback linearization, it can be generalized to the infinite-dimensional system case. In this thesis we will make extensive use of this fact which is discussed further in the following section.

1.4 Flatness-based Control of Infinite-dimensional Systems

An overview of flatness applied to infinite-dimensional systems is in [60, 63] with the presentation in [63] giving a particularly complete account. The original work in this area is [16] which considers a position tracking problem for a flexible rod with torsional flexibility. In this case a linear hyperbolic wave equation is reduced to a delay system and the open-loop input is parameterized by constant amplitude delays and predictions on the flat output trajectory and its time derivatives [49, 16]. Although a complete theoretical basis for flatness in the infinite-dimensional system case does not yet exist, the type of PDE (e.g. parabolic, hyperbolic, etc...) determines how the state and input is parameterized by the flat output. For example, for the hyperbolic undamped wave equation the parametrization is in terms of delays and advances of the flat output and its derivatives. Other hyperbolic equations modeling heat exchangers, telegraph lines, or heavy chains lead to finite distributed delay and prediction operators which require an integration of the flat output over a finite time interval [15, 62, 55, 56, 57]. Parabolic or biharmonic equations lead to infinite series parameterizations, e.g. [17]. Terms of these series depend on time derivatives of a flat output

chosen to be of Gevrey class at most 2 to ensure series convergence. Early work on the parabolic case considered a constant coefficient linear diffusion equation modeling a tubular reactor [18, 19] and linear heat equations [43]. Generalizations to the linear diffusion equation with spatially dependent coefficients is considered in [32, 33, 31, 30], and special cases of this work concern cylindrical coordinate models [59, 31]. Work on the biharmonic case includes the Euler-Bernoulli equation modeling a rotating flexible beam in a horizontal plane [17, 2], a vertical plane [35, 36], or a clamped-free piezoelectric positioning device [22, 65]. The case of a non-rotating Euler-Bernoulli beam with spatially varying beam parameters is in [66].

Most of the flatness-based work on infinite-dimensional systems to date and almost all work cited above has focused on the linear system case. Nonlinear extensions to the parabolic case are in [39, 38, 40, 41]. Other flatness-based work on the nonlinear infinite-dimensional case taking different approaches can be found in [11, 43, 61, 53, 57].

While flatness-based open-loop steering of infinite-dimensional systems has been extensively studied, closed-loop control has received much less attention. Of course in practice closed-loop control is required to reduce the effect of disturbances and model error. For experimental validation a common approach has been to augment the open-loop design with a simple PID control [2, 22]. In these last two references no rigorous way of determining suitable parameters of this PID controller were given. More recently published work [45, 46] gives a more systematic basis for designing the closed-loop component of the flatness-based control law. In this work the same series expressions used in open-loop motion planning are used to derive the closed-loop control. The technique has successfully been demonstrated in simulation for certain linear and nonlinear parabolic systems including a heat equation [46]. The work presented in this thesis makes use of the approach in [46] for a rotating flexible beam system.

1.5 Scope of the Research

The main objective of the research described in this thesis is to extend the closed-loop flatness-based tracking control design method [46] to a rotating flexible beam system. We derive the open-loop series expressions using hub torque as an input. We design a closed-loop estimated state feedback controller using series expressions derived for the open-loop control. To test the tracking feedback law, we derive a Finite-Element Analysis (FEA) model for the beam system. The controller is then implemented in simulation and experiment, demonstrating robust performance. Open-loop controls for a multi-input levitated flexible beam and rotating beam with payload are also considered as generalizations.

1.6 Overview of the Thesis

The thesis is organized as follows. Chapter 2 introduces the experimental flexible-beam plant and models the various subsystems from first principles. Chapter 3 derives the flatness-based open-loop design. Chapter 4 derives an estimated state feedback law based on the feedforward result in Chapter 3. Chapter 5 implements different techniques for simulating the beam system and tests the closed-loop design in simulation using the FEA model developed. Chapter 6 presents experimental validation results. Chapter 7 generalizes the rotating flexible beam model by including a payload and beam rotary inertia. Chapter 8 considers the open-loop control of a levitated flexible rotor, and makes use of a superposition technique which reduces the complexity of the multi-input system design.

Chapter 2

System Description and Modeling

In this chapter, we describe the model of the system to be controlled. This system is shown in Figure 2.1. Numerical values of the system's parameters are identified for the physical apparatus.

2.1 Description of the Plant

Figure 2.1: Flexible beam system

As shown in Figure 2.1, the system consists of a flexible steel ruler which is clamped to a hub. A DC motor drives the beam through a gear train. The motor is powered by a linear power amplifier, whose voltage is controlled from a computer via a Multi-I/O card. The hardware provides three output sensors. A strain gage is bonded to the base of the ruler, and is calibrated to measure the linear deflection of the tip during bending. An encoder attached to the rotating hub measures the angle $\theta(t)$. Finally, a tachometer measures the angular velocity of the hub, $\dot{\theta}(t)$. Further details on the experimental setup are contained in [58].

The control objective for this plant is rest-to-rest motion, i.e., rotating the flexible ruler between undeformed equilibrium configurations. The open-loop trajectory will be derived in Chapter 3 using flatness techniques applied to the infinite-dimensional model developed here.

2.2 Derivation of the Beam Model

We model the ruler as a flexible beam described by an *Euler-Bernoulli* PDE [26, Section 6.5]. In this section, we derive the beam equation, and work out the boundary conditions used to model the beam system.

2.2.1 Background

The following are some facts from mechanics which are relevant to the modeling [4, 44].

- The beam is *elastic* [7]. When it deforms, restoring internal loads appear which are proportional to the magnitude of the deflection. These restoring loads ensure the beam returns to its undeformed configuration if the deflecting input is removed.
- *Internal* loads (forces and moments) always appear in oppositely-directed pairs, creating a state of stress within the body, but not movement. By contrast, *external* loads, such as payload reaction forces and motor torque, appear alone and cause the body to accelerate, by Newton's second law.
- The displacement field $w(x,t)$ measures the transverse motion of the beam along its length at a given instant of time. It is measured from an inertial (non-accelerating) coordinate frame. This is schematically illustrated in Figure 2.2.
- The beam possesses two moments of inertia: I, the *area* moment of inertia, and J, the *mass* moment of inertia. Inertia I is a function of geometry only, and measures the bending stiffness of the body. J is a function of both mass and geometry, and is used in the moment balance [44].

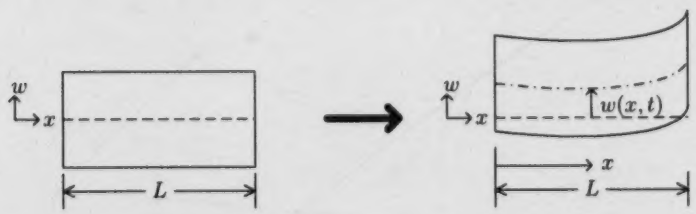

Figure 2.2: Combined deformation and rigid-body translation of a flexible beam

We also make the following simplifying assumptions about the beam being modeled.

- As the beam is deforming, its cross-sections remain plane to each other, i.e., do not rotate. This is also illustrated in Figure 2.2, where the beam's ends remain parallel, and the horizontal length L remains constant.
- The mass moment of inertia J about the beam's bending axis is negligibly small, and can be taken as zero. This assumption is used when performing a moment balance in Section 2.2.2.

- The beam is uniform along its length — the physical parameters (volumetric density ρ, Young's Modulus E) and geometric parameters (cross-sectional area A, area moment of inertia I) are taken as constants.

The first two points are necessary assumptions used to obtain the Euler-Bernoulli model. They are valid for long, slender beams with small deflections. As a general rule of thumb, a beam can be modeled using the Euler-Bernoulli PDE if its length is at least ten times greater than its width. Since this is the case for the plant's flexible ruler, we will use the Euler-Bernoulli equation as the beam model.

There exist more sophisticated PDE models of flexible beams, including the Rayleigh and Timoshenko models [73]. The Rayleigh model does not neglect rotational inertia, although it still assumes planar cross-sections. The Timoshenko model drops both assumptions by including a cross-section rotation field in addition to a displacement field, leading to a system of two coupled PDEs. Using either of these models increases the complexity of the control design [74, 63].

2.2.2 Euler-Bernoulli Beam PDE

Consider the free-body diagram of a deformed infinitesimal beam element, as shown in Figure 2.3. Note the end-sections remain plane, and restoring internal loads are present due to the beam deformation.

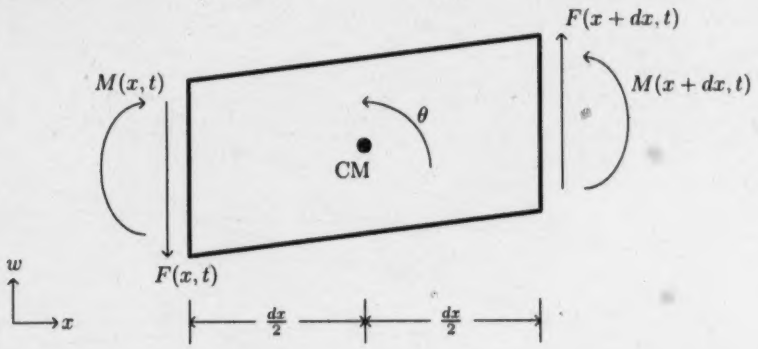

Figure 2.3: Free-body diagram of infinitesimal beam segment

Performing a force balance using Newton's second law we have

$$\sum F_w = m\frac{\partial^2 w(x,t)}{\partial t^2}$$
$$F(x+dx,t) - F(x,t) = \rho A dx \frac{\partial^2 w(x,t)}{\partial t^2} \tag{2.1}$$

Expanding $F(x+dx,t)$ about x using a first-order Taylor series expansion,

$$F(x+dx,t) = F(x,t) + \frac{\partial F(x,t)}{\partial x}(x+dx-x) + \underbrace{\text{HOT}}_{\approx 0} \tag{2.2}$$

Where the higher-order terms (HOT), containing the terms $(dx)^2, (dx)^3, \ldots$ are neglected

since the length of the segment dx is infinitesimally small. Substituting (2.2) into (2.1) gives

$$F(x,t) + \frac{\partial F(x,t)}{\partial x}dx - F(x,t) = \rho A dx \frac{\partial^2 w(x,t)}{\partial t^2}$$

$$\frac{\partial F(x,t)}{\partial x} = \rho A \frac{\partial^2 w(x,t)}{\partial t^2} \tag{2.3}$$

Next, performing a moment balance about the center of mass (CM) and using $J \approx 0$ according to the second Euler-Bernoulli assumption, we have

$$\sum M_{CM} = 0$$

$$M(x+dx,t) + \frac{dx}{2}F(x+dx,t) + \frac{dx}{2}F(x,t) - M(x,t) = 0 \tag{2.4}$$

Performing a Taylor series expansion of $M(x+dx,t)$ about x and neglecting the higher-order terms:

$$M(x+dx,t) = M(x,t) + \frac{\partial M(x,t)}{\partial x}dx + \underbrace{\text{HOT}}_{\approx 0} \tag{2.5}$$

Using (2.2) and (2.5) in (2.4) gives

$$M(x,t) + \frac{\partial M(x,t)}{\partial x}dx + \frac{dx}{2}\left(F(x,t) + \frac{\partial F(x,t)}{\partial x}dx\right) + \frac{dx}{2}F(x,t) - M(x,t) = 0$$

$$\frac{\partial M(x,t)}{\partial x}dx + F(x,t)dx + \frac{\partial F(x,t)}{\partial x}\underbrace{\frac{(dx)^2}{2}}_{\approx 0} = 0$$

$$\frac{\partial M(x,t)}{\partial x} + F(x,t) = 0 \tag{2.6}$$

where $(dx)^2$ is neglected as in the Taylor series expansion (2.2).

Next, we need to use a fundamental relationship from mechanics which relates internal restoring moment to beam curvature [4, pp. 187-192]:

$$M(x,t) = EI\frac{\partial^2 w(x,t)}{\partial x^2} \tag{2.7}$$

Employing (2.7) in (2.6) gives

$$EI\frac{\partial^3 w(x,t)}{\partial x^3}dx + F(x,t)dx = 0$$

$$F(x,t) = -EI\frac{\partial^3 w(x,t)}{\partial x^3} \tag{2.8}$$

Finally, substituting (2.8) into the force balance result (2.3) leads to the Euler-Bernoulli PDE

$$\frac{\partial}{\partial x}\left(-EI\frac{\partial^3 w(x,t)}{\partial x^3}\right) = \rho A\frac{\partial^2 w(x,t)}{\partial t^2}$$

$$EI\frac{\partial^4 w(x,t)}{\partial x^4} + \rho A\frac{\partial^2 w(x,t)}{\partial t^2} = 0 \tag{2.9}$$

Neglecting the higher-order terms $(dx)^2, (dx)^3, \ldots$ is standard practice in deriving the Euler-Bernoulli model, see for example [24, p. 157]. This approach is justified for a continuum which satisfies the infinitesimal deformation assumption of *linear elasticity* [7, pp. 34–37]. When higher order terms are not neglected, nonlinear *finite elasticity* PDE models result.

2.2.3 Force and Moment Boundary Conditions

In this section, we discuss how forces and moments acting on the beam edges can be expressed as boundary conditions for the Euler-Bernoulli PDE (2.9). This will be required in Section 2.3, and the equations are readily obtained from the previous discussion.

The left-hand side, with external force F_{ext} and external moment M_{ext} applied is shown in Figure 2.4.

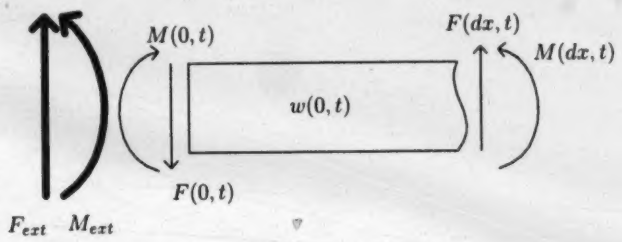

Figure 2.4: External force and moment acting on left beam edge

A force balance on the left-hand side of the beam, taking upwards as positive, gives

$$F_{ext} - F(0,t) = 0 \tag{2.10}$$

from (2.8), the internal force at $x = 0$ is

$$F(0,t) = -EI\frac{\partial^3 w(0,t)}{\partial x^3} \tag{2.11}$$

Using (2.10) in (2.11) gives

$$\begin{aligned} F_{ext} &= -EI\frac{\partial^3 w(0,t)}{\partial x^3} \\ \frac{\partial^3 w(0,t)}{\partial x^3} &= \frac{-F_{ext}}{EI} \end{aligned} \tag{2.12}$$

Now performing a moment balance on the left side, taking counter-clockwise as positive,

$$M_{ext} - M(0,t) = 0 \tag{2.13}$$

from (2.7), the internal moment at $x = 0$ is

$$M(0,t) = EI\frac{\partial^2 w(0,t)}{\partial x^2} \tag{2.14}$$

Using (2.13) in (2.14) gives

$$\begin{aligned} M_{ext} &= EI\frac{\partial^2 w(0,t)}{\partial x^2} \\ \frac{\partial^2 w(0,t)}{\partial x^2} &= \frac{M_{ext}}{EI} \end{aligned} \tag{2.15}$$

The beam's right-hand side is shown in Figure 2.5, again with an external force and moment applied.

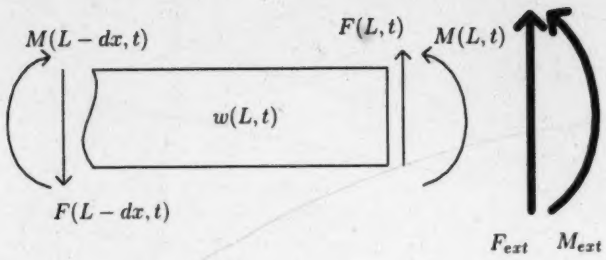

Figure 2.5: External force and moment acting on right beam edge

A force balance with upwards as positive, using (2.8) with $x = L$ leads to

$$\begin{aligned} F_{ext} + F(L,t) &= 0 \\ F_{ext} - EI\frac{\partial^3 w(L,t)}{\partial x^3} &= 0 \\ \frac{\partial^3 w(L,t)}{\partial x^3} &= \frac{F_{ext}}{EI} \end{aligned} \tag{2.16}$$

containing the opposite sign to (2.12). Next, we perform a moment balance at $x = L$ with counter-clockwise as positive and use (2.7):

$$\begin{aligned} M_{ext} + M(L,t) &= 0 \\ M_{ext} + EI\frac{\partial^2 w(L,t)}{\partial x^2} &= 0 \\ \frac{\partial^2 w(L,t)}{\partial x^2} &= \frac{-M_{ext}}{EI} \end{aligned} \tag{2.17}$$

Which, once again, has the opposite sign from (2.15).

When using the edge load to displacement conversions (2.12), (2.15), (2.16) and (2.17), the sign of F_{ext} is positive if facing upwards, while M_{ext} is positive if counter-clockwise.

2.3 Derivation of the Rotating Beam Model

We now derive the system equations for the ruler-hub assembly, modeled as an Euler-Bernoulli beam clamped to a rotating rigid body [2]. A schematic diagram of the system is shown in Figure 2.6

The governing Euler-Bernoulli PDE, which was derived by using a force and moment balance in a stationary frame, must be formulated using a displacement field measured in an inertial (non-accelerating) frame of reference. However, the $V(x,t)$ field in Figure 2.6 is measured in the frame of the beam, which is *non-inertial* due to rotation.

To deal with this, the governing PDE (2.9) will use $w(x,t) \equiv V(x,t) + x\,\theta(t)$ as the displacement field, made up of two components: $x\,\theta(t)$, which measures the curvilinear translation of a point on the beam due to rigid-body rotation; and $V(x,t)$, which measures the linear translation of the point due to elastic deformation.

The governing equation for the rotating beam in Figure 2.6 will be written in terms of the combined displacement field $w(x,t)$. Once an expression for the field is found, it is possible to separate $w(x,t)$ into its rigid and elastic components, by differentiating with

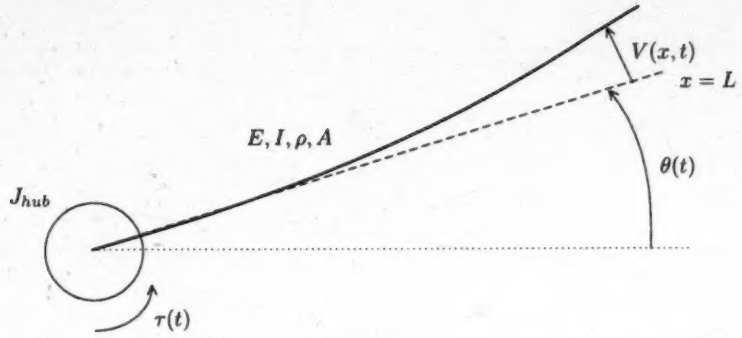

Figure 2.6: Rotating flexible beam model

respect to x and evaluating at $x = 0$, using the fact the beam is clamped to the hub:

$$\frac{\partial w(x,t)}{\partial x} = \frac{\partial V(x,t)}{\partial x} + \theta(t)$$

$$\frac{\partial w(0,t)}{\partial x} = \underbrace{\frac{\partial V(0,t)}{\partial x}}_{=0} + \theta(t)$$

$$\theta(t) = \frac{\partial w(0,t)}{\partial x} \tag{2.18}$$

Equation (2.18) gives the rigid-body component of the solution. The elastic component can be then obtained by

$$V(x,t) = w(x,t) - x\frac{\partial w(0,t)}{\partial x} \tag{2.19}$$

To model the rotating flexible beam from Figure 2.6, we start by looking at the rigid hub to which the input torque $\tau(t)$ is applied, and perform a moment balance. The free-body diagram is shown in Figure 2.7. The term M_{beam} represents the reaction moment *by* the beam *on* the hub.

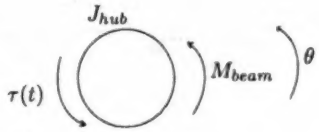

Figure 2.7: Free-body diagram of hub

$$\sum M = J_{hub}\frac{d^2\theta(t)}{dt^2}$$

$$M_{beam} + \tau(t) = J_{hub}\frac{d^2\theta(t)}{dt^2}$$

$$M_{beam} = J_{hub}\frac{d^2\theta(t)}{dt^2} - \tau(t) \tag{2.20}$$

The M_{beam} moment reaction (2.20) acts on the beam's left edge by Newton's third law, as shown in Figure 2.8. Note the direction of M_{beam} has changed direction from Figure 2.7, since it now represents the reaction *by* the hub *on* on the beam.

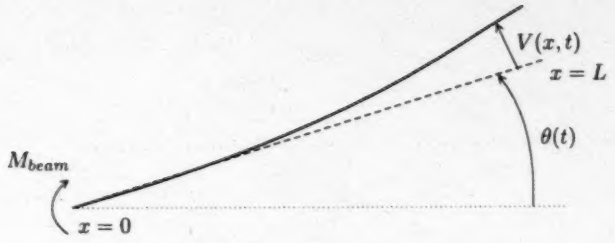

Figure 2.8: Free-body diagram of flexible beam

The reaction moment is used as a boundary condition for the beam PDE by converting $\theta(t)$ to $w(0,t)$ using (2.18), and making use of the boundary moment equivalence (2.15).

$$\frac{\partial^2 w(0,t)}{\partial x^2} = \frac{1}{EI}\left(J_{hub}\frac{\partial^3 w(0,t)}{\partial t^2 \partial x} - \tau(t)\right)$$

$$J_{hub}\frac{\partial^3 w(0,t)}{\partial t^2 \partial x} - EI\frac{\partial^2 w(0,t)}{\partial x^2} = \tau(t) \tag{2.21}$$

The three remaining BCs are deduced visually from Figures 2.6 and 2.8. The beam is pinned to the hub on the left edge, thus

$$w(0,t) = 0 \tag{2.22}$$

The beam is free from external moments on the right edge, so $M_{ext} = 0$ in (2.17)

$$\frac{\partial^2 w(L,t)}{\partial x^2} = 0 \tag{2.23}$$

The beam is also free from external forces on the right, so $F_{ext} = 0$ in (2.16)

$$\frac{\partial^3 w(L,t)}{\partial x^3} = 0 \tag{2.24}$$

Using the governing Euler-Bernoulli PDE (2.9) with boundary conditions (2.21), (2.22), (2.23) and (2.24) gives the BVP formulation of a rotating elastic beam with torque boundary input:

$$EI\frac{\partial^4 w(x,t)}{\partial x^4} + \rho A\frac{\partial^2 w(x,t)}{\partial t^2} = 0 \tag{2.25}$$

$$\begin{aligned} w(0,t) &= 0 \qquad \frac{\partial^2 w(L,t)}{\partial x^2} = 0 \\ J_{hub}\frac{\partial^3 w(0,t)}{\partial t^2 \partial x} - EI\frac{\partial^2 w(0,t)}{\partial x^2} &= \tau(t) \quad \frac{\partial^3 w(L,t)}{\partial x^3} = 0 \end{aligned} \tag{2.26}$$

The torque acting on the hub $\tau(t)$ is the input to the system model. In the experimental plant, a DC motor drives the hub through a gear train, with $u(t)$ as the controlled voltage input. To convert between voltage and torque, the following equation, derived in Appendix A, is used:

$$\tau(t) + \left(\frac{K_g^2 K_m K_b}{R_a} + b\right)\dot{\theta}(t) = \left(\frac{K_g K_m}{R_a}\right)u(t) \tag{2.27}$$

Where K_g is the gear ratio, K_m is motor torque constant, K_b is the back EMF constant, R_a is the armature resistance, and b is the viscous friction coefficient. The numerical values of these parameters are given in Section 2.4.

The hub angular velocity $\dot{\theta}(t)$ can be directly measured using a plant sensor, so (2.27) gives an algebraic relation between $\tau(t)$ and $u(t)$.

Using $\tau(t)$ instead of $u(t)$ for the PDE system input reduces expression complexity of the BVP boundary conditions (2.26). The importance of keeping the system equations as simple as possible will become apparent in Section 3.4.

2.4 System Parameters

The parameters used in the system model must be identified from the experimental hardware. The numerical values are required to produce numerical simulations in Chapter 5, and for experimental validation in Chapter 6.

The following parameters were straightforward to obtain, either from direct measurements or from reference tables. For easy reference, Table 2.1, provided at the end of this chapter, summaries the parameter values.

- Beam length $L = 0.440$ m. The distance from the ruler's rotation axis to the tip. Measured directly.
- Beam density $\rho = 780 \times 10^1$ kg/m^3. The volumetric mass density of the steel material. Obtained from reference tables.
- Beam cross-sectional area $A = 1.66 \times 10^{-5}$ m^2. The ruler's cross-section is shown in Figure 2.9. From direct measurements, $b = 20.7$mm, $h = 0.8$mm.
- Young's modulus of elasticity $E = 200 \times 10^9$ Pa. Measures the resistance of a material to deformation. Obtained from reference tables for steel.
- Area moment of inertia $I = 8.83 \times 10^{-13}$ m^4. The geometric stiffness of a solid to bending. For a rectangular cross-section bending about the axis shown in Figure 2.9, the calculation formula is $I = \frac{1}{12} b h^3$.
- Gear ratio $K_g = 70$. The multiplication factor of torque and reduction factor of speed, going from the DC motor to the hub.
- Motor torque constant $K_m = 0.00767$ N m/A. The relationship between armature current and torque produced by DC motor.
- Motor back EMF constant $K_b = 0.00767$ V s/rad. The relationship between motor speed and voltage loss across the terminals.
- Armature resistance $R_a = 2.60\,\Omega$. The total electrical resistance across the motor terminals.

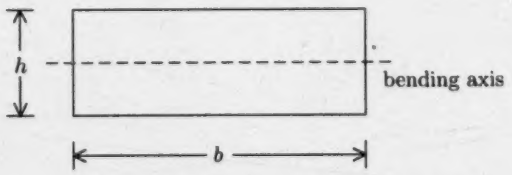

Figure 2.9: Beam cross-section diagram

The remaining two parameters are identified using a closed-loop step response test as described in Appendix B:

- Hub's mass moment of inertia $J_{\text{hub}} = 3.64 \times 10^{-3}$ kg m^2. The rotational inertia of the rigid hub, with the flexible ruler detached.
- Viscous friction coefficient $b = 2.09 \times 10^{-2}$ N m s. This parameter measures the friction in the gear train and motor.

Although more sophisticated methods for system identification could have used as described in [34], we observed little sensitivity of experimental controller performance to any error in the parameter values for J_{hub} and b. The complete list of system parameters, including their symbols and numerical values, is summarized in Table 2.1.

Parameter	Value
Modulus of elasticity – E	200×10^9 Pa
Area moment of inertia – I	8.83×10^{-13} m^4
Cross-sectional area – A	1.66×10^{-5} m^2
Density – ρ	780×10^1 kg/m^3
Length – L	0.440 m
Hub mass moment of inertia – J_{hub}	3.64×10^{-3} kg m^2
Gear ratio – K_g	70
Motor torque constant – K_m	0.00767 N m/A
Motor back-EMF constant – K_b	0.00767 V s/rad
Armature resistance – R_a	2.60 Ω
Viscous friction coefficient – b	2.09×10^{-2} N m s

Table 2.1: Physical parameters for the flexible beam plant

Chapter 3

Flatness-based Open-loop Control

In this chapter, we present the flatness-based open-loop control for the rotating beam system discussed in Chapter 2. The method used is based on work in [63, 17, 43].

3.1 Transformation of System Equations

The method used relies on applying a Laplace transform to a PDE in the dependent variable $w(x,t)$, treating x as constant. As a result, the PDE, containing derivatives with respect to x and t, gets transformed into an ODE containing derivatives with respect to x *only*. The system can then be put into transfer function form, the steering law is designed, and the inverse Laplace transform bring us back to the time domain.

We denote the Laplace transform of $w(x,t)$ as

$$W(x,s) = \mathcal{L}[w(x,t)]$$

We require the time-differentiation property of the Laplace transform:

$$\mathcal{L}\left[\frac{\partial w(x,t)}{\partial t}\right] = sW(x,s) - w(x,0)$$

$$\mathcal{L}\left[\frac{\partial^2 w(x,t)}{\partial t^2}\right] = s^2 W(x,s) - sw(x,0) - \frac{\partial w(x,0)}{\partial t}$$

Partial derivatives with respect to x remain unaffected by the transform:

$$\mathcal{L}\left[\frac{\partial w(x,t)}{\partial x}\right] = \frac{\partial W(x,s)}{\partial x}$$

$$\mathcal{L}\left[\frac{\partial^2 w(x,t)}{\partial x \partial t}\right] = s\frac{\partial W(x,s)}{\partial x} - \frac{\partial w(x,0)}{\partial x}$$

A BVP with zero initial conditions and one boundary input transforms into a transfer function form

$$W(x,s) = G(x,s)\,U(s)$$

where $U(s)$ denotes the Laplace transformed system input, and $G(x,s)$ the system's transfer function.

A more rigorous framework for the above process is Mikusiński operational calculus [47], where s is interpreted as an operator acting on the PDE. Transforming a PDE into the s domain is called taking the Mikusiński transform by some authors [63, 17, 30], and the Laplace transform by others [43, 46, 10]. From a practical point of view, there is little difference between the two in terms of the controls derived. Hence, to ease readability this thesis will use Laplace transform notation.

3.2 Transfer Function of the System

The BVP describing the system is given below. For compactness, we use J instead of J_{hub} to denote the mass moment of inertia of the hub.

$$EI\frac{\partial^4 w(x,t)}{\partial x^4} + \rho A\frac{\partial^2 w(x,t)}{\partial t^2} = 0 \tag{3.1}$$

$$\begin{aligned} w(0,t) &= 0 & \frac{\partial^2 w(L,t)}{\partial x^2} &= 0 \\ J\frac{\partial^3 w(0,t)}{\partial t^2 \partial x} - EI\frac{\partial^2 w(0,t)}{\partial x^2} &= \tau(t) & \frac{\partial^3 w(L,t)}{\partial x^3} &= 0 \end{aligned} \tag{3.2}$$

$$w(x,0) = 0 \qquad \frac{\partial w(x,0)}{\partial t} = 0 \tag{3.3}$$

Applying the Laplace transform to the PDE (3.1) and BCs (3.2) using zero ICs (3.3) yields

$$EI\frac{\partial^4 W(x,s)}{\partial x^4} + \rho A s^2 W(x,s) = 0 \tag{3.4}$$

$$\begin{aligned} W(0,s) &= 0 & \frac{\partial^2 W(L,s)}{\partial x^2} &= 0 \\ Js^2\frac{\partial W(0,s)}{\partial x} - EI\frac{\partial^2 W(0,s)}{\partial x^2} &= T(s) & \frac{\partial^3 W(L,s)}{\partial x^3} &= 0 \end{aligned} \tag{3.5}$$

where $T(s)$ denotes the transformation of the torque input $\tau(t)$. Equation (3.4) is an ODE for $W(x,s)$ with respect to independent variable x. The general solution for this ODE is

$$W(x,s) = C_1(s)e^{-\sqrt{is}x\left(\frac{\rho A}{EI}\right)^{1/4}} + C_2(s)e^{\sqrt{is}x\left(\frac{\rho A}{EI}\right)^{1/4}} + C_3(s)e^{-i\sqrt{is}x\left(\frac{\rho A}{EI}\right)^{1/4}} + C_4(s)e^{i\sqrt{is}x\left(\frac{\rho A}{EI}\right)^{1/4}}$$

Or using $\nu = \left(\frac{\rho A}{EI}\right)^{1/4}$ for compactness,

$$W(x,s) = C_1(s)e^{-\nu\sqrt{is}x} + C_2(s)e^{\nu\sqrt{is}x} + C_3(s)e^{-i\nu\sqrt{is}x} + C_4(s)e^{i\nu\sqrt{is}x} \tag{3.6}$$

We would like to change the basis functions of the solution (3.6) into a set of trigonometric functions. This is done by introducing the new terms

$$\begin{aligned} C_1(s) &= \frac{A(s)}{2} - \frac{B(s)}{2} & C_2(s) &= \frac{A(s)}{2} + \frac{B(s)}{2} \\ C_3(s) &= \frac{C(s)}{2} - \frac{D(s)}{2i} & C_4(s) &= \frac{C(s)}{2} + \frac{D(s)}{2i} \end{aligned}$$

which gives

$$\begin{aligned} W(x,s) &= \left(\frac{A(s)}{2} - \frac{B(s)}{2}\right)e^{-\nu\sqrt{is}x} + \left(\frac{A(s)}{2} + \frac{B(s)}{2}\right)e^{\nu\sqrt{is}x} \\ &\quad + \left(\frac{C(s)}{2} - \frac{D(s)}{2i}\right)e^{-i\nu\sqrt{is}x} + \left(\frac{C(s)}{2} + \frac{D(s)}{2i}\right)e^{i\nu\sqrt{is}x} \\ &= \frac{A(s)}{2}\left(e^{\nu\sqrt{is}x} + e^{-\nu\sqrt{is}x}\right) + \frac{B(s)}{2}\left(e^{\nu\sqrt{is}x} - e^{-\nu\sqrt{is}x}\right) \\ &\quad + \frac{C(s)}{2}\left(e^{i\nu\sqrt{is}x} + e^{-i\nu\sqrt{is}x}\right) + \frac{D(s)}{2i}\left(e^{i\nu\sqrt{is}x} - e^{-i\nu\sqrt{is}x}\right) \end{aligned}$$

Thus

$$W(x,s) = A(s)\cosh(\nu\sqrt{i\,s}\,x) + B(s)\sinh(\nu\sqrt{i\,s}\,x) + C(s)\cos(\nu\sqrt{i\,s}\,x) + D(s)\sin(\nu\sqrt{i\,s}\,x) \tag{3.7}$$

The transformed BCs in (3.5) lead to a linear system of four linear equations in four unknowns

$$\begin{aligned}
A(s) + C(s) &= 0 \\
-A(s)iEIs\nu^2 + B(s)J\sqrt{is}s^2\nu + C(s)iEIs\nu^2 + D(s)J\sqrt{is}s^2\nu &= T(s) \\
A(s)\cosh(L\sqrt{is}\nu) + B(s)\sinh(L\sqrt{is}\nu) - C(s)\cos(L\sqrt{is}\nu) - D(s)\sin(L\sqrt{is}\nu) &= 0 \\
A(s)\sinh(L\sqrt{is}\nu) + B(s)\cosh(L\sqrt{is}\nu) + C(s)\sin(L\sqrt{is}\nu) - D(s)\cos(L\sqrt{is}\nu) &= 0
\end{aligned} \tag{3.8}$$

We solve (3.8) for $A(s)$,$B(s)$,$C(s)$, $D(s)$ and substitute into (3.7). This results in the transfer function representation

$$W(x,s) = \frac{P(x,s)}{Q(x,s)}T(s) \tag{3.9}$$

where

$$\begin{aligned}
P(x,s) = \frac{1}{\sqrt{s}}\Big\{ &-\cos(\sqrt{is}x\nu)\sin[(1+i)L\sqrt{is}\nu] + \cosh(\sqrt{is}x\nu)\sin[(1+i)L\sqrt{is}\nu] \\
&- i\cos(L\sqrt{2s}\nu)\sin(\sqrt{is}x\nu) + \cosh(L\sqrt{2s}\nu)\sin(\sqrt{is}x\nu) \\
&+ (1-i)\sin(\sqrt{is}x\nu) + \cos(\sqrt{is}x\nu)\sinh[(1+i)L\sqrt{is}\nu] \\
&- \cosh(\sqrt{is}x\nu)\sinh[(1+i)L\sqrt{is}\nu] + \cos(L\sqrt{2s}\nu)\sinh(\sqrt{is}x\nu) \\
&- i\cosh(L\sqrt{2s}\nu)\sinh(\sqrt{is}x\nu) + (1-i)\sinh(\sqrt{is}x\nu)\Big\}
\end{aligned} \tag{3.10}$$

$$\begin{aligned}
Q(x,s) = 2\nu\sqrt{s}\Big\{ &(1-i)J\sqrt{is}s\cos(L\sqrt{is}\nu)\cosh(L\sqrt{is}\nu) + (1-i)J\sqrt{is}s \\
&- iEI\nu\sin[(1+i)L\sqrt{is}\nu] + iEI\nu\sinh[(1+i)L\sqrt{is}\nu]\Big\}
\end{aligned} \tag{3.11}$$

3.3 Introducing the Flat Output

The BVP in transfer function form is given in (3.9), where the input is the torque applied at the beam boundary, $T(s)$, and the output is the beam displacement field, $W(x,s)$. This form is Q-free controllable [63, p.96], leading to the parametrization of the system input as

$$T(s) = Q(x,s)Y(s) \tag{3.12}$$

where $Y(s)$ is the transformed system flat output $y(t)$. This choice immediately gives the system state parametrization

$$W(x,s) = \frac{P(x,s)}{Q(x,s)}\Big(Q(x,s)Y(s)\Big) = P(x,s)Y(s) \tag{3.13}$$

Note that this choice is not unique, since $P(x,s)$ and $Q(x,s)$ form a ratio in (3.9). It is therefore possible to multiply both terms by a common factor, giving a different system parametrization. For example, having $\frac{1}{2}$ instead of $\frac{1}{\sqrt{s}}$ multiplying $P(x,s)$ in (3.10), and νs in place of $2\nu\sqrt{s}$ in front of $Q(x,s)$ in (3.11) gives an alternate parametrization.

3.4 Series Manipulations

The parameterizations (3.12) and (3.13) are given in the s-domain. In order to obtain a time-domain expression for the control, we need to return to the time domain by performing an inverse Laplace transform.

The current expressions, $P(x,s)$ in (3.10) and $Q(x,s)$ in (3.11), have the s operator embedded in the arguments of trigonometric and hyperbolic functions, making a closed-form inversion impossible. To get around this, we will express both in terms of their infinite series expansions, which will make it possible to factor out the s operator and allow the inversion to be performed.

The series manipulation steps are conceptually straightforward:

1. Break up the s-domain expression into sums of individual functions, using trigonometric and hyperbolic identities
2. Convert each term into its infinite series representation
3. Combine all series into one
4. Factor out the s operator

Unfortunately, the process is tedious, due to the necessity of manipulating the series by hand. Computer algebra systems such as Mathematica cannot handle the complexity.

3.4.1 Background

The power series representations of trigonometric functions, expanded about $x = 0$, are given by

$$\cosh x = \sum_{k=0}^{\infty} \frac{x^{2k}}{(2k)!} \qquad \cos x = \sum_{k=0}^{\infty} \frac{(-1)^k x^{2k}}{(2k)!}$$

$$\sinh x = \sum_{k=0}^{\infty} \frac{x^{2k+1}}{(2k+1)!} \qquad \sin x = \sum_{k=0}^{\infty} \frac{(-1)^k x^{2k+1}}{(2k+1)!}$$

The hyperbolic addition theorems [67] use complex arguments:

$$\cosh(X \pm iY) = \cosh X \cos Y \pm i \sinh X \sin Y$$
$$\sinh(X \pm iY) = \sinh X \cos Y \pm i \cosh X \sin Y$$

Adding and subtracting the above leads to the identities

$$\cosh X \cos Y = \frac{\cosh(X+iY) + \cosh(X-iY)}{2}$$
$$\sinh X \cos Y = \frac{\sinh(X+iY) + \sinh(X-iY)}{2}$$
$$\sinh X \sin Y = \frac{\cosh(X+iY) - \cosh(X-iY)}{2i}$$
$$\cosh X \sin Y = \frac{\sinh(X+iY) - \sinh(X-iY)}{2i}$$

We need two more identities,

$$\sinh X \cosh Y = \frac{\sinh(X+Y) + \sinh(X-Y)}{2}$$
$$\sin X \cos Y = \frac{\sin(X+Y) + \sin(X-Y)}{2}$$

In order to simplify the use of the above identities, we will temporarily adopt the following conventions in the $P(x,s)$ and $Q(x,s)$ expressions (3.10) and (3.11):

$$A = \sqrt{s}$$
$$B = \sqrt{is}x\nu$$
$$C = (1+i)L\sqrt{is}\nu$$
$$D = L\sqrt{2s}\nu$$
$$V = s\sqrt{is}$$
$$W = L\sqrt{is}\nu$$

3.4.2 Series Representation of $P(x,s)$

Using the conventions from Section 3.4.1, expression (3.10) for $P(x,s)$ is rewritten as

$$P(x,s) = \frac{1}{A}\Big\{ -\cos B \sin C + \cosh B \sin C - i\cos D \sin B + \cosh D \sin B + (1-i)\sin B$$
$$+ \cos B \sinh C - \cosh B \sinh C + \cos D \sinh B - i\cosh D \sinh B + (1-i)\sinh B \Big\}$$

Using the trigonometric identities,

$$P(x,s) =$$
$$\frac{1}{A}\Big\{ -\left[\frac{\sin(C+B)+\sin(C-B)}{2}\right] + \left[\frac{\sinh(B+iC)-\sinh(B-iC)}{2i}\right]$$
$$- i\left[\frac{\sin(B+D)+\sin(B-D)}{2}\right] + \left[\frac{\sinh(D+iB)-\sinh(D-iB)}{2i}\right]$$
$$+ (1-i)\sin B + \left[\frac{\sinh(C+iB)+\sinh(C-iB)}{2}\right] - \left[\frac{\sinh(C+B)+\sinh(C-B)}{2}\right]$$
$$+ \left[\frac{\sinh(B+iD)+\sinh(B-iD)}{2}\right] - i\left[\frac{\sinh(B+D)+\sinh(B-D)}{2}\right]$$
$$+ (1-i)\sinh B \Big\}$$
$$= \frac{1}{A}\Big\{ -\frac{1}{2}\sin(C+B) - \frac{1}{2}\sin(C-B) - \frac{i}{2}\sin(B+D) - \frac{i}{2}\sin(B-D)$$
$$+ \frac{1}{2i}\sinh(B+iC) - \frac{1}{2i}\sinh(B-iC) + \frac{1}{2i}\sinh(D+iB) - \frac{1}{2i}\sinh(D-iB)$$
$$+ \frac{1}{2}\sinh(C+iB) + \frac{1}{2}\sinh(C-iB) - \frac{1}{2}\sinh(C+B) - \frac{1}{2}\sinh(C-B)$$
$$+ \frac{1}{2}\sinh(B+iD) + \frac{1}{2}\sinh(B-iD) - \frac{i}{2}\sinh(B+D) - \frac{i}{2}\sinh(B-D)$$
$$+ (1-i)\sin B + (1-i)\sinh B \Big\}$$
$$= \frac{1}{\sqrt{s}}\Big\{ -\frac{1}{2}\sin[\sqrt{is}\nu(L+iL+x)] - \frac{1}{2}\sin[\sqrt{is}\nu(L+iL-x)]$$
$$- \frac{i}{2}\sin[\sqrt{s}\nu(\sqrt{i}x+L\sqrt{2})] - \frac{i}{2}\sin[\sqrt{s}\nu(\sqrt{i}x-L\sqrt{2})]$$
$$+ \frac{1}{2i}\sinh[\sqrt{is}\nu(x+iL-L)] - \frac{1}{2i}\sinh[\sqrt{is}\nu(x-iL+L)]$$
$$+ \frac{1}{2i}\sinh[\sqrt{s}\nu(L\sqrt{2}+i\sqrt{i}x)] - \frac{1}{2i}\sinh[\sqrt{s}\nu(L\sqrt{2}-i\sqrt{i}x)]$$

$$
\begin{aligned}
&+\frac{1}{2}\sinh[\sqrt{is}\nu(L+iL+ix)]+\frac{1}{2}\sinh[\sqrt{is}\nu(L+iL-ix)]\\
&-\frac{1}{2}\sinh[\sqrt{is}\nu(L+iL+x)]-\frac{1}{2}\sinh[\sqrt{is}\nu(L+iL-x)]\\
&+\frac{1}{2}\sinh[\sqrt{s}\nu(\sqrt{i}x+iL\sqrt{2})]+\frac{1}{2}\sinh[\sqrt{s}\nu(\sqrt{i}x-iL\sqrt{2})]\\
&-\frac{i}{2}\sinh[\sqrt{s}\nu(\sqrt{i}x+L\sqrt{2})]-\frac{i}{2}\sinh[\sqrt{s}\nu(\sqrt{i}x-L\sqrt{2})]\\
&+(1-i)\sin[\sqrt{is}x\nu]+(1-i)\sinh[\sqrt{is}x\nu]\Big\}
\end{aligned}
$$

Converting to infinite series representation,

$$
\begin{aligned}
P(x,s)=\\
&\frac{1}{\sqrt{s}}\Big\{-\frac{1}{2}\sum_{k=0}^{\infty}\frac{(-1)^k(\sqrt{is}\nu)^{2k+1}(L+iL+x)^{2k+1}}{(2k+1)!}-\frac{1}{2}\sum_{k=0}^{\infty}\frac{(-1)^k(\sqrt{is}\nu)^{2k+1}(L+iL-x)^{2k+1}}{(2k+1)!}\\
&-\frac{i}{2}\sum_{k=0}^{\infty}\frac{(-1)^k(\sqrt{s}\nu)^{2k+1}(\sqrt{i}x+L\sqrt{2})^{2k+1}}{(2k+1)!}-\frac{i}{2}\sum_{k=0}^{\infty}\frac{(-1)^k(\sqrt{s}\nu)^{2k+1}(\sqrt{i}x-L\sqrt{2})^{2k+1}}{(2k+1)!}\\
&+\frac{1}{2i}\sum_{k=0}^{\infty}\frac{(\sqrt{is}\nu)^{2k+1}(x+iL-L)^{2k+1}}{(2k+1)!}-\frac{1}{2i}\sum_{k=0}^{\infty}\frac{(\sqrt{is}\nu)^{2k+1}(x-iL+L)^{2k+1}}{(2k+1)!}\\
&+\frac{1}{2i}\sum_{k=0}^{\infty}\frac{(\sqrt{s}\nu)^{2k+1}(L\sqrt{2}+i\sqrt{i}x)^{2k+1}}{(2k+1)!}-\frac{1}{2i}\sum_{k=0}^{\infty}\frac{(\sqrt{s}\nu)^{2k+1}(L\sqrt{2}-i\sqrt{i}x)^{2k+1}}{(2k+1)!}\\
&+\frac{1}{2}\sum_{k=0}^{\infty}\frac{(\sqrt{is}\nu)^{2k+1}(L+iL+ix)^{2k+1}}{(2k+1)!}+\frac{1}{2}\sum_{k=0}^{\infty}\frac{(\sqrt{is}\nu)^{2k+1}(L+iL-ix)^{2k+1}}{(2k+1)!}\\
&-\frac{1}{2}\sum_{k=0}^{\infty}\frac{(\sqrt{is}\nu)^{2k+1}(L+iL+x)^{2k+1}}{(2k+1)!}-\frac{1}{2}\sum_{k=0}^{\infty}\frac{(\sqrt{is}\nu)^{2k+1}(L+iL-x)^{2k+1}}{(2k+1)!}\\
&+\frac{1}{2}\sum_{k=0}^{\infty}\frac{(\sqrt{s}\nu)^{2k+1}(\sqrt{i}x+iL\sqrt{2})^{2k+1}}{(2k+1)!}+\frac{1}{2}\sum_{k=0}^{\infty}\frac{(\sqrt{s}\nu)^{2k+1}(\sqrt{i}x-iL\sqrt{2})^{2k+1}}{(2k+1)!}\\
&-\frac{i}{2}\sum_{k=0}^{\infty}\frac{(\sqrt{s}\nu)^{2k+1}(\sqrt{i}x+L\sqrt{2})^{2k+1}}{(2k+1)!}-\frac{i}{2}\sum_{k=0}^{\infty}\frac{(\sqrt{s}\nu)^{2k+1}(\sqrt{i}x-L\sqrt{2})^{2k+1}}{(2k+1)!}\\
&+(1-i)\sum_{k=0}^{\infty}\frac{(-1)^k(\sqrt{is}x\nu)^{2k+1}}{(2k+1)!}+(1-i)\sum_{k=0}^{\infty}\frac{(\sqrt{is}x\nu)^{2k+1}}{(2k+1)!}\Big\}
\end{aligned}
$$

Factoring into a single summation,

$$
\begin{aligned}
P(x,s)=\\
&\frac{1}{2\sqrt{s}}\sum_{k=0}^{\infty}\frac{(\sqrt{s}\nu)^{2k+1}}{(2k+1)!}\Big[-(-1)^k(\sqrt{i})^{2k+1}(L+iL+x)^{2k+1}-(-1)^k(\sqrt{i})^{2k+1}(L+iL-x)^{2k+1}\\
&\qquad-i(-1)^k(\sqrt{i}x+L\sqrt{2})^{2k+1}-i(-1)^k(\sqrt{i}x-L\sqrt{2})^{2k+1}\\
&\qquad-i(\sqrt{i})^{2k+1}(x+iL-L)^{2k+1}+i(\sqrt{i})^{2k+1}(x-iL+L)^{2k+1}\\
&\qquad-i(L\sqrt{2}+i\sqrt{i}x)^{2k+1}+i(L\sqrt{2}-i\sqrt{i}x)^{2k+1}\\
&\qquad+(\sqrt{i})^{2k+1}(L+iL+ix)^{2k+1}+(\sqrt{i})^{2k+1}(L+iL-ix)^{2k+1}\\
&\qquad-(\sqrt{i})^{2k+1}(L+iL+x)^{2k+1}-(\sqrt{i})^{2k+1}(L+iL-x)^{2k+1}\\
&\qquad+(\sqrt{i}x+iL\sqrt{2})^{2k+1}+(\sqrt{i}x-iL\sqrt{2})^{2k+1}
\end{aligned}
$$

$$- i(\sqrt{i}x + L\sqrt{2})^{2k+1} - i(\sqrt{i}x - L\sqrt{2})^{2k+1}$$
$$+ (2-2i)(-1)^k(\sqrt{i}x)^{2k+1} + (2-2i)(\sqrt{i}x)^{2k+1}\Big]$$

Note that the s operator has been factored out in the preceding step. This will enable the inverse transformation to be carried out.

$$P(x,s) =$$

$$\frac{\nu}{2}\sum_{k=0}^{\infty}\frac{s^k\nu^{2k}}{(2k+1)!}\Big[-(-1)^k(\sqrt{i})^{2k+1}(L+iL+x)^{2k+1} - (-1)^k(\sqrt{i})^{2k+1}(L+iL-x)^{2k+1}$$
$$- i(-1)^k(\sqrt{i}x + L\sqrt{2})^{2k+1} - i(-1)^k(\sqrt{i}x - L\sqrt{2})^{2k+1}$$
$$- i(\sqrt{i})^{2k+1}(x+iL-L)^{2k+1} + i(\sqrt{i})^{2k+1}(x-iL+L)^{2k+1}$$
$$- i(L\sqrt{2} + i\sqrt{i}x)^{2k+1} + i(L\sqrt{2} - i\sqrt{i}x)^{2k+1}$$
$$+ (\sqrt{i})^{2k+1}(L+iL+ix)^{2k+1} + (\sqrt{i})^{2k+1}(L+iL-ix)^{2k+1}$$
$$- (\sqrt{i})^{2k+1}(L+iL+x)^{2k+1} - (\sqrt{i})^{2k+1}(L+iL-x)^{2k+1}$$
$$+ (\sqrt{i}x + iL\sqrt{2})^{2k+1} + (\sqrt{i}x - iL\sqrt{2})^{2k+1}$$
$$- i(\sqrt{i}x + L\sqrt{2})^{2k+1} - i(\sqrt{i}x - L\sqrt{2})^{2k+1}$$
$$+ (2-2i)(-1)^k(\sqrt{i}x)^{2k+1} + (2-2i)(\sqrt{i}x)^{2k+1}\Big]$$

$$= \frac{\nu}{2}\sum_{k=0}^{\infty}\frac{s^k\nu^{2k}}{(2k+1)!}\Big[f(x,k)\Big]$$

The contents of the square bracket are a function of x and k only. It can be verified that

$$f(x,k) = 0 \qquad k = 1,3,5,\ldots$$
$$f(x,k) \neq 0 \in \mathbb{R} \qquad k = 0,2,4,\ldots$$

The fact that $f(x,k)$ is always real-valued is as expected, since this term remains unchanged during the inverse transformation of $W(x,s)$ into $w(x,t)$.

Returning to the series expression for $P(x,s)$, we let $k = 2m, m = 0,1,2,\ldots$ to guarantee that k is even:

$$P(x,s) =$$

$$\frac{\nu}{2}\sum_{m=0}^{\infty}\frac{s^{2m}\nu^{4m}}{(4m+1)!}\Big[-(-1)^{2m}(\sqrt{i})^{4m+1}(L+iL+x)^{4m+1}$$
$$- (-1)^{2m}(\sqrt{i})^{4m+1}(L+iL-x)^{4m+1}$$
$$- i(-1)^{2m}(\sqrt{i}x + L\sqrt{2})^{4m+1} - i(-1)^{2m}(\sqrt{i}x - L\sqrt{2})^{4m+1}$$
$$- i(\sqrt{i})^{4m+1}(x+iL-L)^{4m+1} + i(\sqrt{i})^{4m+1}(x-iL+L)^{4m+1}$$
$$- i(L\sqrt{2} + i\sqrt{i}x)^{4m+1} + i(L\sqrt{2} - i\sqrt{i}x)^{4m+1}$$
$$+ (\sqrt{i})^{4m+1}(L+iL+ix)^{4m+1} + (\sqrt{i})^{4m+1}(L+iL-ix)^{4m+1}$$
$$- (\sqrt{i})^{4m+1}(L+iL+x)^{4m+1} - (\sqrt{i})^{4m+1}(L+iL-x)^{4m+1}$$
$$+ (\sqrt{i}x + iL\sqrt{2})^{4m+1} + (\sqrt{i}x - iL\sqrt{2})^{4m+1}$$
$$- i(\sqrt{i}x + L\sqrt{2})^{4m+1} - i(\sqrt{i}x - L\sqrt{2})^{4m+1}$$

$$+ (2-2i)(-1)^{2m}(\sqrt{i}x)^{4m+1} + (2-2i)(\sqrt{i}x)^{4m+1}\Big]$$

$$= \frac{\nu}{2}\sum_{m=0}^{\infty}\frac{s^{2m}\nu^{4m}}{(4m+1)!}\Big[-2(\sqrt{i})^{4m+1}(L+iL+x)^{4m+1} - 2(\sqrt{i})^{4m+1}(L+iL-x)^{4m+1}$$
$$- 2i(\sqrt{i}x + L\sqrt{2})^{4m+1} - 2i(\sqrt{i}x - L\sqrt{2})^{4m+1}$$
$$+ 2(\sqrt{i})^{4m+1}(L+iL-ix)^{4m+1} + 2(\sqrt{i})^{4m+1}(L+iL+ix)^{4m+1}$$
$$+ 2(\sqrt{i}x - iL\sqrt{2})^{4m+1} + 2(\sqrt{i}x + iL\sqrt{2})^{4m+1}$$
$$+ 2(2-2i)(\sqrt{i}x)^{4m+1}\Big]$$

It can be verified that

$$-2(\sqrt{i})^{4m+1}(L+iL+x)^{4m+1} - 2(\sqrt{i})^{4m+1}(L+iL-x)^{4m+1}$$
$$- 2i(\sqrt{i}x + L\sqrt{2})^{4m+1} - 2i(\sqrt{i}x - L\sqrt{2})^{4m+1}$$
$$+ 2(\sqrt{i})^{4m+1}(L+iL-ix)^{4m+1} + 2(\sqrt{i})^{4m+1}(L+iL+ix)^{4m+1}$$
$$+ 2(\sqrt{i}x - iL\sqrt{2})^{4m+1} + 2(\sqrt{i}x + iL\sqrt{2})^{4m+1}$$
$$= (-1)^m\left[4\sqrt{2}\,\mathrm{Re}\left\{(x-L+iL)^{4m+1}\right\} - 4\sqrt{2}\,\mathrm{Im}\left\{(x-L-iL)^{4m+1}\right\}\right]$$

And

$$2(2-2i)(\sqrt{i}x)^{4m+1} = (-1)^m 4\sqrt{2}x^{4m+1}$$

Using these in the infinite series,

$$P(x,s) = \frac{\nu}{2}\sum_{m=0}^{\infty}\frac{s^{2m}\nu^{4m}}{(4m+1)!}\Big[(-1)^m\Big[4\sqrt{2}\,\mathrm{Re}\left\{(x-L+iL)^{4m+1}\right\}$$
$$- 4\sqrt{2}\,\mathrm{Im}\left\{(x-L-iL)^{4m+1}\right\}\Big] + (-1)^m 4\sqrt{2}x^{4m+1}\Big]$$

Cleaning up

$$P(x,s)$$
$$= 2\sqrt{2}\nu\sum_{m=0}^{\infty}\frac{(-1)^m s^{2m}\nu^{4m}}{(4m+1)!}\left[x^{4m+1} + \mathrm{Re}\left\{(x-L+iL)^{4m+1}\right\} - \mathrm{Im}\left\{(x-L-iL)^{4m+1}\right\}\right] \tag{3.14}$$

3.4.3 Series Representation of $Q(x,s)$

We start with the expression for $Q(x,s)$ from (3.11) and use the definitions for A, B, C, D, V, and W from Section 3.4.1:

$$Q(x,s) = 2\nu A\{(1-i)JV\cos W\cosh W + (1-i)JV - iEI\nu\sin C + iEI\nu\sinh C\}$$
$$= 2\nu A\left\{(1-i)JV\left[\frac{\cosh(W+iW)+\cosh(W-iW)}{2}\right] + (1-i)JV\right.$$
$$\left. - iEI\nu\sin C + iEI\nu\sinh C\right\}$$
$$= 2\nu A\left\{\left(\frac{1-i}{2}\right)JV\cosh(W+iW) + \left(\frac{1-i}{2}\right)JV\cosh(W-iW) + (1-i)JV\right.$$
$$\left. - iEI\nu\sin C + iEI\nu\sinh C\right\}$$

$$= 2\nu\sqrt{s}\Bigg\{\left(\frac{1-i}{2}\right)Js\sqrt{is}\cosh[L\sqrt{is}\nu(1+i)] + \left(\frac{1-i}{2}\right)Js\sqrt{is}\cosh[L\sqrt{is}\nu(1-i)]$$

$$+ (1-i)Js\sqrt{is} - iEI\nu\sin[(1+i)L\sqrt{is}\nu] + iEI\nu\sinh[(1+i)L\sqrt{is}\nu]\Bigg\}$$

$$= 2\nu\Bigg\{\left(\frac{1-i}{2}\right)Js^2\sqrt{i}\sum_{k=0}^{\infty}\frac{(L\sqrt{is}\nu)^{2k}(1+i)^{2k}}{(2k)!}$$

$$+ \left(\frac{1-i}{2}\right)Js^2\sqrt{i}\sum_{k=0}^{\infty}\frac{(L\sqrt{is}\nu)^{2k}(1-i)^{2k}}{(2k)!} + (1-i)Js^2\sqrt{i}$$

$$- i\sqrt{s}EI\nu\sum_{k=0}^{\infty}\frac{(-1)^k(L\sqrt{is}\nu)^{2k+1}(1+i)^{2k+1}}{(2k+1)!}$$

$$+ i\sqrt{s}EI\nu\sum_{k=0}^{\infty}\frac{(L\sqrt{is}\nu)^{2k+1}(1+i)^{2k+1}}{(2k+1)!}\Bigg\}$$

$$= 2\nu\Bigg\{(1-i)Js^2\sqrt{i} + \left(\frac{1-i}{2}\right)Js^2\sqrt{i}\sum_{k=0}^{\infty}\frac{(L\sqrt{is}\nu)^{2k}\left[(1+i)^{2k}+(1-i)^{2k}\right]}{(2k)!}$$

$$- i\sqrt{s}EI\nu\sum_{k=0}^{\infty}\frac{(L\sqrt{is}\nu)^{2k+1}(1+i)^{2k+1}\left[(-1)^k-1\right]}{(2k+1)!}\Bigg\}$$

$$= 2\nu\Bigg\{(1-i)Js^2\sqrt{i} + \left(\frac{1-i}{2}\right)Js^2\sqrt{i}\sum_{k=0}^{\infty}\frac{(L\nu)^{2k}(is)^k\left[(1+i)^{2k}+(1-i)^{2k}\right]}{(2k)!}$$

$$- i\sqrt{s}EI\nu(L\sqrt{is}\nu)(1+i)\sum_{k=0}^{\infty}\frac{(L\nu)^{2k}(is)^k(1+i)^{2k}\left[(-1)^k-1\right]}{(2k+1)!}\Bigg\}$$

It can be verified that:

$$(1-i)\sqrt{i} = \sqrt{2}$$
$$-i\sqrt{i}(1+i) = (1-i)\sqrt{i} = \sqrt{2}$$

So the expression becomes

$$Q(x,s) = 2\sqrt{2}\nu\Bigg\{Js^2 + \frac{1}{2}Js^2\sum_{k=0}^{\infty}\frac{(L\nu)^{2k}(is)^k\left[(1+i)^{2k}+(1-i)^{2k}\right]}{(2k)!}$$

$$+ sEI\nu^2L\sum_{k=0}^{\infty}\frac{(L\nu)^{2k}(is)^k(1+i)^{2k}\left[(-1)^k-1\right]}{(2k+1)!}\Bigg\}$$

It can be verified that:

$$(i)^k\left[(1+i)^{2k}+(1-i)^{2k}\right] = 0 \qquad k = 1,3,5,\ldots$$
$$= 2^{k+1} \qquad k = 0,2,4,\ldots$$

Thus, let $k = 2m, m = 0,1,2,\ldots$ in the first summation term of $Q(x,s)$. It can also be verified that:

$$(i)^k(1+i)^{2k}\left[(-1)^k-1\right] = 0 \qquad k = 0,2,4,\ldots$$
$$= 2^{k+1} \qquad k = 1,3,5,\ldots$$

Let $k = 2m+1, m = 0, 1, 2, \ldots$ in the second summation term. Returning to $Q(x,s)$:

$$\begin{aligned} Q(x,s) &= 2\sqrt{2}\nu\Bigg\{ Js^2 + \frac{1}{2}Js^2 \sum_{m=0}^{\infty} \frac{(L\nu)^{4m} s^{2m} 2^{2m+1}}{(4m)!} \\ &\qquad + sEI\nu^2 L \sum_{m=0}^{\infty} \frac{(L\nu)^{4m+2} s^{2m+1} 2^{2m+2}}{(4m+3)!} \Bigg\} \\ &= 2\sqrt{2}\nu\Bigg\{ Js^2 + J \sum_{m=0}^{\infty} \frac{(L\nu)^{4m} s^{2m+2} 4^m}{(4m)!} + 4EI\nu^4 L^3 \sum_{m=0}^{\infty} \frac{(L\nu)^{4m} s^{2m+2} 4^m}{(4m+3)!} \Bigg\} \end{aligned}$$

Combining into a single summation gives

$$Q(x,s) = 2\sqrt{2}\nu\Bigg\{ Js^2 + \sum_{m=0}^{\infty} \frac{(L\nu)^{4m} 4^m s^{2m+2}}{(4m+3)!} \Big[J(4m+3)(4m+2)(4m+1) + 4EI\nu^4 L^3 \Big] \Bigg\} \tag{3.15}$$

3.4.4 Final Series Expressions

A final set of adjustments is made to the infinite-series expressions for $P(x,s)$ (3.14) and $Q(x,s)$ (3.15):

- Both series have a $2\sqrt{2}\,\nu$ term in front. Since we are taking their ratio via (3.13), we can cancel this term out.
- The term ν^4 appears throughout the series. We define the new constant $\kappa = \nu^4 = \left(\frac{\rho A}{EI}\right)$.
- The summation index m is changed back to k.

With this, the final forms of the series expressions in the s-domain are

$$P(x,s) = \sum_{k=0}^{\infty} \frac{(-\kappa)^k}{(4k+1)!} \Big[x^{4k+1} + \mathrm{Re}\left\{ (x - L + iL)^{4k+1} \right\} - \mathrm{Im}\left\{ (x - L - iL)^{4k+1} \right\} \Big] s^{2k} \tag{3.16}$$

$$Q(x,s) = Js^2 + \sum_{k=0}^{\infty} \frac{L^{4k}(4\kappa)^k}{(4k+3)!} \Big[J(4k+3)(4k+2)(4k+1) + 4EI\kappa L^3 \Big] s^{2k+2} \tag{3.17}$$

3.5 Open-loop Control

Using the series expressions (3.16) and (3.17) in the system input and state parameterizations (3.12) and (3.13) gives

$$W(x,s) = \sum_{k=0}^{\infty} \frac{(-\kappa)^k}{(4k+1)!} \Big[x^{4k+1} + \mathrm{Re}\left\{ (x - L + iL)^{4k+1} \right\} - \mathrm{Im}\left\{ (x - L - iL)^{4k+1} \right\} \Big] s^{2k} Y(s) \tag{3.18}$$

$$T(s) = Js^2 Y(s) + \sum_{k=0}^{\infty} \frac{L^{4k}(4\kappa)^k}{(4k+3)!} \Big[J(4k+3)(4k+2)(4k+1) + 4EI\kappa L^3 \Big] s^{2k+2} Y(s) \tag{3.19}$$

For which the inverse Laplace transform is immediately available:

$$w(x,t) = \sum_{k=0}^{\infty} \frac{(-\kappa)^k}{(4k+1)!}\left[x^{4k+1} + \mathrm{Re}\left\{(x-L+iL)^{4k+1}\right\} - \mathrm{Im}\left\{(x-L-iL)^{4k+1}\right\}\right] y^{(2k)}(t) \tag{3.20}$$

$$\tau(t) = Jy^{(2)}(t) + \sum_{k=0}^{\infty} \frac{L^{4k}(4\kappa)^k}{(4k+3)!}\left[J(4k+3)(4k+2)(4k+1) + 4EI\kappa L^3\right] y^{(2k+2)}(t) \tag{3.21}$$

In other words, the flat output $y(t)$ and its (infinitely many) time derivatives parameterize both the system state and input.

In our control application, we wish to steer the flexible beam from rest to rest: $\theta(0) = 0, V(x,0) = 0, \forall x \in [0,L]$ and $\theta(t_f) = \Theta, V(x,t_f) = 0, \forall x \in [0,L]$, where $V(x,t)$ represents the beam's elastic deformation. In terms of $w(x,t)$, the desired system endpoints are written as

$$\begin{aligned} w(x,0) &= V(x,0) + x\,\theta(0) = 0 \\ w(x,t_f) &= V(x,t_f) + x\,\theta(t_f) = x\,\Theta \end{aligned} \tag{3.22}$$

We now develop some requirements for the steering function $y(t)$. The state expression (3.20) can be equivalently written as

$$w(x,t) = \sum_{k=0}^{\infty} g(x,k)\, y^{(2k)}(t) \tag{3.23}$$

Taking time derivatives of (3.23),

$$\begin{aligned} \frac{\partial w(x,t)}{\partial t} &= \sum_{k=0}^{\infty} g(x,k)\, y^{(2k+1)}(t) \\ \frac{\partial^2 w(x,t)}{\partial t^2} &= \sum_{k=0}^{\infty} g(x,k)\, y^{(2k+2)}(t) \end{aligned} \tag{3.24}$$

At the trajectory endpoints (3.22), $w(x,t_*), t_* \in \{0, t_f\}$ is a function of x *only*. From (3.24), this means

$$\begin{aligned} \frac{\partial w(x,t_*)}{\partial t} = 0 &= \sum_{k=0}^{\infty} g(x,k)\, y^{(2k+1)}(t_*) \\ \frac{\partial^2 w(x,t_*)}{\partial t^2} = 0 &= \sum_{k=0}^{\infty} g(x,k)\, y^{(2k+2)}(t_*) \end{aligned} \tag{3.25}$$

The $g(x,k)$ term in (3.25) cannot be 0, otherwise the $w(x,t)$ solution (3.23) is trivial. Thus,

$$y'(t_*) = y''(t_*) = \cdots = 0 \qquad t_* \in \{0, t_f\} \tag{3.26}$$

Expanding the $k = 0$ term from the series (3.23),

$$w(x,t) = g(x,0)\, y(t) + \sum_{k=1}^{\infty} g(x,k)\, y^{(2k)}(t) \tag{3.27}$$

The $g(x,0)$ term in (3.27) can be evaluated by returning to (3.20):

$$\begin{aligned} g(x,0) &= \frac{(-\kappa)^0}{(1)!}\left[x + \mathrm{Re}\left\{(x-L+iL)\right\} - \mathrm{Im}\left\{(x-L-iL)\right\}\right] \\ &= [x + x - L - (-L)] \\ &= 2x \end{aligned} \tag{3.28}$$

Evaluating (3.27) at the starting endpoint $t = 0$, making use of (3.22), (3.26) and (3.28), we obtain

$$\begin{aligned} \underbrace{w(x,0)}_{=0} &= \underbrace{g(x,0)}_{=2x} y(0) + \sum_{k=1}^{\infty} g(x,k) \underbrace{y^{(2k)}(0)}_{=0} \\ y(0) &= 0 \end{aligned} \tag{3.29}$$

The $t = t_f$ endpoint gives

$$\begin{aligned} \underbrace{w(x,t_f)}_{=x\,\Theta} &= \underbrace{g(x,0)}_{=2x} y(t_f) + \sum_{k=1}^{\infty} g(x,k) \underbrace{y^{(2k)}(t_f)}_{=0} \\ y(t_f) &= \frac{\Theta}{2} \end{aligned} \tag{3.30}$$

We need to find a steering function $y(t)$ which meets conditions (3.26), (3.29) and (3.30). Note this is not a trivial task, since the only analytical function which meets the requirement $y(0) = y'(0) = y''(0) = \cdots = 0$ is the trivial one $y(t) = 0$, which cannot reach $y(t_f) > 0$. For example, polynomial flat outputs, often used for finite dimensional system motion planning, cannot be used in this infinite-dimensional problem.

The steering function $y(t)$ must also meet the requirements of being:

- Smooth, of class C^{∞}
- Bounded for $t \geq 0$, for all derivative orders $y^{(k)}(t), k \geq 0$

A steering function which meets all the above requirements is given by [63, p.91]

$$\eta_\gamma(t) = \frac{1}{2} + \frac{1}{2} \tanh\left(\frac{2\left(2\frac{t}{t_f} - 1\right)}{\left(4\frac{t}{t_f}\left(1 - \frac{t}{t_f}\right)\right)^{\gamma}} \right) \qquad t \in [0, t_f] \tag{3.31}$$

belonging to the class of *Gevrey functions* [20]. Function (3.31) is plotted in Figure 3.1 for $t_f = 1$ and $\gamma \in \{1.4, 10, 50\}$. Note the amplitude of $\eta_\gamma(t)$ is always 1, and the γ parameter determines the "steepness" of the transition.

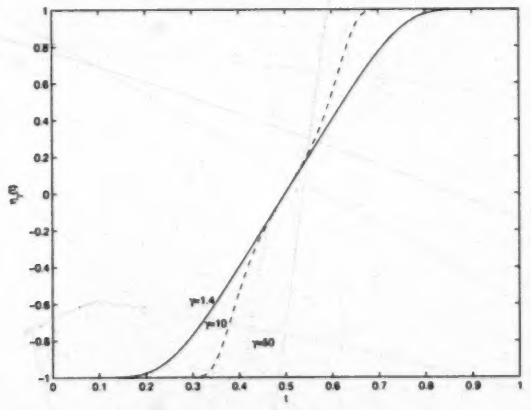

Figure 3.1: Sample $\eta_\gamma(t)$ plots for $t_f = 1$ and $\gamma \in \{1.4, 10, 50\}$

The Gevrey function (3.31) can be shown to have *Gevrey order* $\sigma = 1 + \frac{1}{\gamma}$. Gevrey functions are C^∞ on $[0, t_f]$ and satisfy

$$\sup_{t\in[0,t_f]} |\eta_\gamma^{(n)}(t)| \leq m\frac{(n!)^\sigma}{p^n} \qquad n \geq 0$$

where m,n and p are some real constants. Gevrey functions are non-analytic for $\sigma > 1$. It can be shown that the series (3.20), (3.21) have an infinite radius of convergence provided y is of Gevrey order $\sigma < 2$ [35, 63]. Hence, we require $1 < \sigma < 2$ or $1 < \gamma < \infty$.

Function (3.31) will be used to steer the flat output, using the endpoint relationship (3.30)

$$y(t) = \frac{\Theta}{2}\eta_\gamma(t) \tag{3.32}$$

The successive time derivatives of $y(t)$ in (3.32) can be calculated by recursion, as shown in the next section.

The open-loop design presented here provides rest-to-rest motion between specified beam angles. A generalization which allows for transitions between *non-stationary* configurations could be derived using the Fourier series-based results in [30]. In contrast to the finite-dimensional system case [29, 71, 42, 70], a flatness-based open-loop design for infinite-dimensional systems does seem to be readily extended to include a full range of motion planning constraints, e.g. bounds on the input or state amplitude during transition. A partial solution for infinite-dimensional systems is to split the desired motion into a number of smaller rest to rest motions, as in [2].

3.6 Calculation of Time Derivatives of $\eta_\gamma(t)$

We now derive a method for calculating the successive time derivatives of the steering function (3.31). Leaving out the constants, we work with the related function

$$y_c(t) = \tanh\left(\frac{2(2\frac{t}{t_f} - 1)}{(4\frac{t}{t_f}(1 - \frac{t}{t_f}))^\gamma}\right) \tag{3.33}$$

We need to calculate $y_c^{(n)}(t)$ derivatives of any order. The actual driving function will then be given by

$$y(t) = \frac{\Theta}{2}\left(\frac{1}{2} + \frac{1}{2}y_c(t)\right)$$
$$y^{(n)}(t) = \frac{\Theta}{2}\left(\frac{1}{2}y_c^{(n)}(t)\right) \qquad n \geq 1$$

The derivation presented is found in [64, Appendix A.2], although it has been generalized to allow the case of $t_f \neq 1$.

First, it can be verified that equation (3.33) is equivalent to

$$y_c = \tanh \dot{a} \tag{3.34}$$

where

$$a = \frac{t_f\left(4\frac{t}{t_f}\left(1 - \frac{t}{t_f}\right)\right)^{1-\gamma}}{2(\gamma - 1)} \tag{3.35}$$

Taking the time derivative of (3.34),

$$\begin{aligned} \dot{y}_c &= (\operatorname{sech}^2 \dot{a})\ddot{a} \\ &= (1 - \tanh^2 \dot{a})\ddot{a} \\ &= \ddot{a}(1 - y_c^2) \\ &= \ddot{a}z \end{aligned} \tag{3.36}$$

where we have introduced the new quantity

$$z = 1 - y_c^2 \tag{3.37}$$

Taking the time derivative of (3.36) a few more times, we recognize a binomial pattern in the coefficients:

$$\begin{aligned}
\ddot{y}_c &= \dot{z}\ddot{a} + za^{(3)} \\
y_c^{(3)} &= \ddot{z}\ddot{a} + 2\dot{z}a^{(3)} + za^{(4)} \\
y_c^{(4)} &= z^{(3)}\ddot{a} + 3\ddot{z}a^{(3)} + 3\dot{z}a^{(4)} + za^{(5)} \\
&\vdots \\
y_c^{(n)} &= \sum_{k=0}^{n-1} \binom{n-1}{k} a^{(k+2)} z^{(n-1-k)} \qquad n \geq 1
\end{aligned} \tag{3.38}$$

where

$$\binom{n}{k} = \frac{n!}{(n-k)!k!}$$

From (3.38), note $y_c^{(n)}$ requires knowing the values $z^{(n-1)}, \ldots, z$. We time differentiate equation (3.37) several times in order to find another pattern:

$$\begin{aligned}
z &= 1 - y_c^2 \\
\dot{z} &= -2y_c\dot{y}_c \\
&= -y_c\dot{y}_c - \dot{y}_c y_c \\
\ddot{z} &= -2\dot{y}_c\dot{y}_c - 2y_c\ddot{y}_c \\
&= -y_c\ddot{y}_c - 2\dot{y}_c\dot{y}_c - \ddot{y}_c y_c \\
z^{(3)} &= -6\dot{y}_c\ddot{y}_c - 2y_c y_c^{(3)} \\
&= -y_c y_c^{(3)} - 3\dot{y}_c\ddot{y}_c - 3\ddot{y}_c\dot{y}_c - y_c^{(3)} y_c \\
&\vdots \\
z^{(n)} &= -\sum_{k=0}^{n} \binom{n}{k} y_c^{(k)} y_c^{(n-k)} \qquad n \geq 2
\end{aligned} \tag{3.39}$$

Also from equation (3.38), $y_c^{(n)}$ requires $a^{(n+1)}, \ldots, a$, so we need a formula for $a^{(n)}$. Returning to equation (3.35), it can be verified that

$$\dot{a} = \frac{\left(2\frac{t}{t_f} - 1\right)(\gamma - 1)}{t\left(1 - \frac{t}{t_f}\right)} a \tag{3.40}$$

thus

$$\begin{aligned}
t\left(1 - \frac{t}{t_f}\right)\dot{a} &= \left(2\frac{t}{t_f} - 1\right)(\gamma - 1)a \\
F_1(t)\dot{a} &= F_2(t)(\gamma - 1)a
\end{aligned} \tag{3.41}$$

where we introduced the terms $F_1(t)$ and $F_2(t)$ for compactness. We again time differentiate

equation (3.41) a few times to find a pattern:

$$\frac{d}{dt}\Big(F_1(t)\dot{a} = F_2(t)(\gamma-1)a\Big)$$

$$\frac{d}{dt}\Big(F_1'(t)\dot{a} + F_1(t)\ddot{a} = (\gamma-1)\big\{F_2'(t)a + F_2(t)\dot{a}\big\}\Big)$$

$$\frac{d}{dt}\Big(F_1''(t)\dot{a} + 2F_1'(t)\ddot{a} + F_1(t)a^{(3)} = (\gamma-1)\big\{F_2''(t)a + 2F_2'(t)\dot{a} + F_2(t)\ddot{a}\big\}\Big)$$

$$F_1^{(3)}(t)\dot{a} + 3F_1''(t)\ddot{a} + 3F_1'(t)a^{(3)} + F_1(t)a^{(4)} = (\gamma-1)$$
$$\big\{F_2^{(3)}(t)a + 3F_2''(t)\dot{a} + 3F_2'(t)\ddot{a} + F_2(t)a^{(3)}\big\}$$

$$\vdots$$

$$\sum_{k=0}^{n-1}\binom{n-1}{k}a^{(n-k)}F_1^{(k)}(t) = (\gamma-1)\sum_{k=0}^{n-1}\binom{n-1}{k}a^{(n-k-1)}F_2^{(k)}(t) \tag{3.42}$$

We now isolate $a^{(n)}$ in (3.42):

$$\underbrace{\binom{n-1}{0}}_{=1}a^{(n)}F_1(t) + \sum_{k=1}^{n-1}\binom{n-1}{k}a^{(n-k)}F_1^{(k)}(t) = (\gamma-1)\sum_{k=0}^{n-1}\binom{n-1}{k}a^{(n-k-1)}F_2^{(k)}(t)$$

$$a^{(n)} = \frac{1}{F_1(t)}\left[(\gamma-1)\sum_{k=0}^{n-1}\binom{n-1}{k}a^{(n-k-1)}F_2^{(k)}(t)\right] - \frac{1}{F_1(t)}\left[\sum_{k=1}^{n-1}\binom{n-1}{k}a^{(n-k)}F_1^{(k)}(t)\right] \tag{3.43}$$

From the definitions of $F_1(t)$ and $F_2(t)$:

$$F_1(t) = t\left(1-\frac{t}{t_f}\right) \qquad F_2(t) = 2\frac{t}{t_f} - 1$$

$$F_1'(t) = 1 - 2\frac{t}{t_f} \qquad F_2'(t) = \frac{2}{t_f}$$

$$F_1''(t) = \frac{-2}{t_f} \qquad F_2''(t) = F_2^{(3)}(t) = \cdots = 0$$

$$F_1^{(3)}(t) = F_1^{(4)}(t) = \cdots = 0$$

Using the expressions for $F_1(t)$ and $F_2(t)$ in (3.43) we get

$$a^{(n)} = \frac{1}{t\left(1-\frac{t}{t_f}\right)}\left[(\gamma-1)\left\{\underbrace{\binom{n-1}{0}}_{=1}a^{(n-1)}\left(2\frac{t}{t_f}-1\right)+\underbrace{\binom{n-1}{1}}_{=n-1}a^{(n-2)}\left(\frac{2}{t_f}\right)\right\}\right.$$
$$\left.-\underbrace{\binom{n-1}{1}}_{=n-1}a^{(n-1)}\left(1-2\frac{t}{t_f}\right)-\underbrace{\binom{n-1}{2}}_{=\frac{(n-1)(n-2)}{2}}a^{(n-2)}\left(\frac{-2}{t_f}\right)\right] \qquad n\geq 2$$

$$= \frac{1}{t\left(1-\frac{t}{t_f}\right)}\left[(\gamma-1)a^{(n-1)}\left(2\frac{t}{t_f}-1\right)+(\gamma-1)(n-1)a^{(n-2)}\left(\frac{2}{t_f}\right)\right.$$
$$\left.-(n-1)a^{(n-1)}\left(1-2\frac{t}{t_f}\right)-\frac{(n-1)(n-2)}{2}a^{(n-2)}\left(\frac{-2}{t_f}\right)\right] \qquad n\geq 2$$

$$= \frac{1}{t\left(1-\frac{t}{t_f}\right)}\left[(\gamma-2+n)\left(2\frac{t}{t_f}-1\right)a^{(n-1)}+(n-1)a^{(n-2)}\left(\frac{2}{t_f}\right)\left[\gamma-1+\frac{(n-2)}{2}\right]\right]$$

$$a^{(n)} = \frac{1}{t\left(1-\frac{t}{t_f}\right)}\left[(\gamma-2+n)\left(2\frac{t}{t_f}-1\right)a^{(n-1)}+\frac{(n-1)}{t_f}(2\gamma-4+n)a^{(n-2)}\right] \qquad n\geq 2 \tag{3.44}$$

The recursion formulas from (3.44) and (3.39) can be used in (3.38) to find all orders of $y_c^{(n)}$ for $n \geq 1$.

Observe that because the recursion formulas cannot handle $n = 0$ (nor $n = 1$ for the $a^{(n)}$ expression), the values of y_c, z, a and $\dot{a}$ must be found using the original definitions in equations (3.33), (3.37), (3.35) and (3.34), respectively.

Finally, we summarize the recursion calculations. First we obtain the values

$$a = \frac{t_f\left(4\frac{t}{t_f}\left(1-\frac{t}{t_f}\right)\right)^{1-\gamma}}{2(\gamma-1)}$$
$$\dot{a} = \frac{2\left(2\frac{t}{t_f}-1\right)}{\left(4\frac{t}{t_f}\left(1-\frac{t}{t_f}\right)\right)^{\gamma}}$$
$$y_c = \tanh(\dot{a})$$
$$z = 1-y_c^2$$

And then loop through the following three equations for successive $n = 1, 2, \ldots, n_{max}$ to obtain $y_c', \ldots, y_c^{(n_{max})}$:

$$a^{(n+1)} = \frac{1}{t\left(1-\frac{t}{t_f}\right)}\left[(\gamma-1+n)\left(2\frac{t}{t_f}-1\right)a^{(n)}+\frac{n}{t_f}(2\gamma-3+n)a^{(n-1)}\right]$$
$$y_c^{(n)} = \sum_{k=0}^{n-1}\binom{n-1}{k}a^{(k+2)}z^{(n-1-k)}$$
$$z^{(n)} = -\sum_{k=0}^{n}\binom{n}{k}y_c^{(k)}y_c^{(n-k)}$$

The equations are recursive because

$$a^{(n+1)} = f\left(a^{(n)}, \ldots, a\right)$$
$$y_c^{(n)} = f\left(a^{(n)}, \ldots, a, z^{(n-1)}, \ldots, z\right)$$
$$z^{(n)} = f\left(y_c^{(n)}, \ldots, y_c\right)$$

3.7 Additional Series Expressions

Series (3.20) allows the calculation of the total displacement field $w(x,t)$ of the beam. It is possible to use expressions (2.18) and (2.19) to obtain series to calculate $\theta(t)$, the rigid-body angle, and $V(L,t)$, the elastic deflection of the tip. Plotting these alongside $w(x,t)$ will provide a clearer pictures of the beam's behaviour. The series will also be useful during the closed-loop design in Chapter 4 where they are the physically measured variables forcing the observer.

3.7.1 Series Expression for $\theta(t)$

Differentiating the $w(x,t)$ series (3.20) with respect to x gives

$$\frac{\partial w(x,t)}{\partial x} = \sum_{k=0}^{\infty} \frac{(-\kappa)^k}{(4k+1)!}\Big[(4k+1)x^{4k} + \mathrm{Re}\left\{(4k+1)(x-L+iL)^{4k}\right\} - \mathrm{Im}\left\{(4k+1)(x-L-iL)^{4k}\right\}\Big] y^{(2k)}(t)$$

$$\theta(t) = \frac{\partial w(0,t)}{\partial x} = \sum_{k=0}^{\infty} \frac{(-\kappa)^k}{(4k+1)!}(4k+1)(0)^{4k} y^{(2k)}(t) + \sum_{k=0}^{\infty} \frac{(-\kappa)^k}{(4k+1)!}\Big[\mathrm{Re}\left\{(4k+1)(-L+iL)^{4k}\right\} - \mathrm{Im}\left\{(4k+1)(-L-iL)^{4k}\right\}\Big] y^{(2k)}(t)$$

$$= \frac{(-\kappa)^0}{1!} y(t) + \sum_{k=0}^{\infty} \frac{(-\kappa)^k}{(4k+1)!}\Big[(4k+1)L^{4k}\mathrm{Re}\left\{(-1+i)^{4k}\right\} - (4k+1)(-L)^{4k}\mathrm{Im}\left\{(1+i)^{4k}\right\}\Big] y^{(2k)}(t)$$

$$= y(t) + \sum_{k=0}^{\infty} \frac{(-\kappa)^k}{(4k+1)!}\Big[(4k+1)L^{4k}\left(\mathrm{Re}\left\{(-1+i)^{4k}\right\} - \mathrm{Im}\left\{(1+i)^{4k}\right\}\right)\Big] y^{(2k)}(t)$$

It can be verified that

$$\mathrm{Re}\left\{(-1+i)^{4k}\right\} - \mathrm{Im}\left\{(1+i)^{4k}\right\} = (-4)^k \qquad k = 0, 1, 2, \ldots$$

Giving

$$\theta(t) = y(t) + \sum_{k=0}^{\infty} \frac{(4\kappa)^k L^{4k}}{(4k)!} y^{(2k)}(t) \tag{3.45}$$

3.7.2 Series Expression for $V(L,t)$

The elastic deflection of the tip of the beam $V(L,t)$ is directly measurable from a strain gage sensor in the experimental plant. Evaluating the $w(x,t)$ series in (3.20) at $x = L$,

$$w(L,t) = \sum_{k=0}^{\infty} \frac{(-\kappa)^k}{(4k+1)!}\left[L^{4k+1} + \mathrm{Re}\left\{(iL)^{4k+1}\right\} - \mathrm{Im}\left\{(-iL)^{4k+1}\right\}\right] y^{(2k)}(t)$$

It can be verified that

$$\begin{aligned} (i)^{4k+1} &= i \\ (-i)^{4k+1} &= -i \end{aligned} \qquad k = 0, 1, 2, \ldots$$

We then have

$$\begin{aligned} w(L,t) &= \sum_{k=0}^{\infty} \frac{(-\kappa)^k}{(4k+1)!}\left[L^{4k+1} + \mathrm{Re}\left\{iL^{4k+1}\right\} - \mathrm{Im}\left\{-iL^{4k+1}\right\}\right] y^{(2k)}(t) \\ &= \sum_{k=0}^{\infty} \frac{(-\kappa)^k}{(4k+1)!}\left[L^{4k+1} - \left(-L^{4k+1}\right)\right] y^{(2k)}(t) \\ &= \sum_{k=0}^{\infty} \frac{(-\kappa)^k 2L^{4k+1}}{(4k+1)!} y^{(2k)}(t) \end{aligned} \tag{3.46}$$

Taking (2.19) at $x = L$, then substituting in (3.45) and (3.46),

$$\begin{aligned} V(L,t) &= w(L,t) - L\theta(t) \\ &= \sum_{k=0}^{\infty} \frac{(-\kappa)^k 2L^{4k+1}}{(4k+1)!} y^{(2k)}(t) - Ly(t) - \sum_{k=0}^{\infty} \frac{(4\kappa)^k L^{4k+1}}{(4k)!} y^{(2k)}(t) \end{aligned}$$

which leads to

$$V(L,t) = -Ly(t) + \sum_{k=0}^{\infty} \frac{\kappa^k L^{4k+1}}{(4k+1)!}\left[(-1)^k 2 - 4^k(4k+1)\right] y^{(2k)}(t) \tag{3.47}$$

Chapter 4

Flatness-based Closed-loop Tracking Control

In this chapter, we augment the open-loop trajectory planning with an estimated state feedback tracking controller. This control, which is based on the infinite series developed in Chapter 3, is intended to compensate for initial tracking error, model uncertainty, and system disturbances.

4.1 Approximate State-space System Representation

The key step in designing the closed-loop controller is to convert the system series expressions into an approximate LTI state-space representation. The method uses results in [46] which considers the control of a diffusion PDE.

In the Laplace domain, the system state and input expressions (3.18) and (3.19) were found to be

$$W(x,s) = \sum_{k=0}^{\infty} \frac{(-\kappa)^k}{(4k+1)!}\left[x^{4k+1} + \mathrm{Re}\left\{(x-L+iL)^{4k+1}\right\} - \mathrm{Im}\left\{(x-L-iL)^{4k+1}\right\}\right] s^{2k} Y(s) \tag{4.1}$$

$$T(s) = Js^2 Y(s) + \sum_{k=0}^{\infty} \frac{L^{4k}(4\kappa)^k}{(4k+3)!}\left[J(4k+3)(4k+2)(4k+1) + 4EI\kappa L^3\right] s^{2k+2} Y(s) \tag{4.2}$$

Based on (4.1), we define the coefficient

$$A_{4k+1}(s) = \frac{(-\kappa)^k s^{2k} Y(s)}{(4k+1)!} \qquad k \geq 0 \tag{4.3}$$

Using definition (4.3), (4.1) becomes

$$W(x,s) = \sum_{k=0}^{\infty} A_{4k+1}(s)\left[x^{4k+1} + \mathrm{Re}\left\{(x-L+iL)^{4k+1}\right\} - \mathrm{Im}\left\{(x-L-iL)^{4k+1}\right\}\right]$$

or in time domain:

$$w(x,t) = \sum_{k=0}^{\infty} a_{4k+1}(t)\left[x^{4k+1} + \mathrm{Re}\left\{(x-L+iL)^{4k+1}\right\} - \mathrm{Im}\left\{(x-L-iL)^{4k+1}\right\}\right] \tag{4.4}$$

with $a_{4k+1}(t)$ being the inverse Laplace transform of $A_{4k+1}(s)$,

$$a_{4k+1}(t) = \frac{(-\kappa)^k y^{(2k)}(t)}{(4k+1)!} \qquad k \geq 0 \tag{4.5}$$

Using (4.5), we can find a recursion formula between successive coefficients. Observe that for $k = 0$ in (4.5) we have $a_1(t) = y(t)$: the flat output.

$$
\begin{aligned}
k = 0 \quad & a_1(t) = y(t) \\
k = 1 \quad & a_5(t) = \frac{(-\kappa)y''(t)}{5!} = \frac{-\kappa}{5!}\ddot{a}_1(t) \\
k = 2 \quad & a_9(t) = \frac{(-\kappa)^2 y^{(4)}(t)}{9!} = \frac{\kappa^2}{9!}\frac{d^2}{dt^2}[y''(t)] = \frac{\kappa^2}{9!}\frac{d^2}{dt^2}\left[\frac{a_5(t)5!}{-\kappa}\right] = \frac{-\kappa}{9\cdot 8\cdot 7\cdot 6}\ddot{a}_5(t) \\
k = 3 \quad & a_{13}(t) = \frac{(-\kappa)^3 y^{(6)}(t)}{13!} = \frac{-\kappa^3}{13!}\frac{d^2}{dt^2}\left[\frac{a_9(t)9!}{(-\kappa)^2}\right] = \frac{-\kappa}{13\cdot 12\cdot 11\cdot 10}\ddot{a}_9(t) \\
k = 4 \quad & a_{17}(t) = \frac{(-\kappa)^4 y^{(8)}(t)}{17!} = \frac{\kappa^4}{17!}\frac{d^2}{dt^2}\left[\frac{a_{13}(t)13!}{(-\kappa)^3}\right] = \frac{-\kappa}{17\cdot 16\cdot 15\cdot 14}\ddot{a}_{13}(t) \\
& \vdots \\
k = n+1 \quad & a_{4n+5}(t) = \frac{(-\kappa)^{n+1} y^{(2n+2)}(t)}{(4n+5)!} = \frac{(-1)^{n+1}\kappa^{n+1}}{(4n+5)!}\frac{d^2}{dt^2}\left[\frac{a_{4n+1}(t)(4n+1)!}{(-1)^n\kappa^n}\right]
\end{aligned}
$$

Using definition (4.5) in the last line above gives

$$
a_{4n+5}(t) = \frac{-\kappa\ddot{a}_{4n+1}(t)}{(4n+5)(4n+4)(4n+3)(4n+2)} \qquad n \geq 0 \tag{4.6}
$$

The recursion formula (4.6) will be used shortly. First, we introduce $A_{4k+1}(s)$ into the series (4.2) for $T(s)$. Using the change of variables $k' = k+1$, expression (4.2) becomes

$$
\begin{aligned}
T(s) &= Js^2Y(s) + \sum_{k'=1}^{\infty} \frac{L^{4(k'-1)}(4\kappa)^{k'-1}s^{2k'}Y(s)}{(4(k'-1)+3)!} \\
&\qquad \left[J(4(k'-1)+3)(4(k'-1)+2)(4(k'-1)+1) + 4EI\kappa L^3\right] \\
&= Js^2Y(s) + \sum_{k'=1}^{\infty} \frac{L^{4k'-4}(4\kappa)^{k'-1}s^{2k'}Y(s)}{(4k'-1)!}\left[J(4k'-1)(4k'-2)(4k'-3) + 4EI\kappa L^3\right]
\end{aligned}
$$

Rearranging this last expression we can introduce $A_{4k+1}(s)$:

$$
\begin{aligned}
T(s) &= J\left(\frac{-\kappa(5!)}{-\kappa(5!)}\right)s^2Y(s) \\
&\quad + \sum_{k=1}^{\infty}\left(\frac{(-1)^k(4k+1)(4k)}{(-1)^k(4k+1)(4k)}\right)\frac{L^{4k-4}(4\kappa)^{-1}4^k\kappa^k s^{2k}Y(s)}{(4k-1)!} \\
&\quad \left[J(4k-1)(4k-2)(4k-3) + 4EI\kappa L^3\right] \\
&= A_5(s)\left(\frac{J(5!)}{-\kappa}\right) + \sum_{k=1}^{\infty} A_{4k+1}(s)\left(\frac{(4k+1)(4k)L^{4k-4}4^k}{(-1)^k(4\kappa)}\right) \\
&\quad \left[J(4k-1)(4k-2)(4k-3) + 4EI\kappa L^3\right] \\
&= \frac{-120J}{\kappa}A_5(s) + \sum_{k=1}^{\infty} A_{4k+1}(s)\left(\frac{(4k+1)kL^{4k-4}(-4)^k}{\kappa}\right) \\
&\quad \left[J(4k-1)(4k-2)(4k-3) + 4EI\kappa L^3\right]
\end{aligned}
$$

Inverse transformation of the last expression gives

$$\tau(t) = a_5(t)\frac{-120J}{\kappa} + \sum_{k=1}^{\infty} a_{4k+1}(t)\frac{k(4k+1)L^{4k-4}(-4)^k}{\kappa}\left[J(4k-1)(4k-2)(4k-3)+4EI\kappa L^3\right] \tag{4.7}$$

At this point, (4.4) and (4.7) give the state $w(x,t)$ and the input $\tau(t)$ as functions of the coefficient $a_{4k+1}(t)$ from (4.5), which in turn possesses a recursion formula (4.6).

We now perform the key step of *truncating* the series (4.4) and (4.7), using N terms for the input $\tau(t)$ but only $N-1$ terms for the state $w(x,t)$. This gives the approximate relations

$$w(x,t) \approx \sum_{k=0}^{N-1} a_{4k+1}(t)\left[x^{4k+1} + \mathrm{Re}\left\{(x-L+iL)^{4k+1}\right\} - \mathrm{Im}\left\{(x-L-iL)^{4k+1}\right\}\right] \tag{4.8}$$

$$\tau(t) \approx a_5(t)\frac{-120J}{\kappa} + \sum_{k=1}^{N} a_{4k+1}(t)\frac{k(4k+1)L^{4k-4}(-4)^k}{\kappa}\left[J(4k-1)(4k-2)(4k-3)+4EI\kappa L^3\right] \tag{4.9}$$

Observe that the coefficient with the largest index which appears in (4.8) and (4.9) is $a_{4N+1}(t)$, and this coefficient only appears in the expression for $\tau(t)$. We consider a finite number of relations from the recursion formula (4.6):

$$\ddot{a}_{4n+1}(t) = \frac{-(4n+5)(4n+4)(4n+3)(4n+2)}{\kappa}\, a_{4n+5}(t) \qquad 0 \le n \le N-1 \tag{4.10}$$

where $n = N-1$ is the highest index value due to $a_{4N+1}(t)$ being the coefficient with the largest index.

Equation (4.10) represents a system of N second order ODE's, with $\{\ddot{a}_1, \cdots, \ddot{a}_{4N-3}\}$ terms on the left-hand side. We would like $\{a_1, \cdots, a_{4N-3}\}$ to appear on the right-hand side, so that the coefficients can be redefined using a set of states, and (4.10) can be put into state-space form. Currently, the extra term a_{4N+1} is present on the right-hand side of (4.10). To remove it, we use the truncated $\tau(t)$ expression (4.9), and isolate a_{4N+1} as a function of $\{a_1, \cdots, a_{4N-3}\}$ and the input $\tau(t)$:

$$\begin{aligned}\tau(t) = {} & a_5(t)\left(\frac{-120J}{\kappa}\right) \\ & + \sum_{k=1}^{N-1} a_{4k+1}(t)\left(\frac{k(4k+1)L^{4k-4}(-4)^k}{\kappa}\right)\left[J(4k-1)(4k-2)(4k-3)+4EI\kappa L^3\right] \\ & + a_{4N+1}(t)\frac{N(4N+1)L^{4N-4}(-4)^N}{\kappa}\left[J(4N-1)(4N-2)(4N-3)+4EI\kappa L^3\right]\end{aligned}$$

$$\begin{aligned}a_{4N+1}(t) = {} & \frac{\kappa}{N(4N+1)L^{4N-4}(-4)^N\left[J(4N-1)(4N-2)(4N-3)+4EI\kappa L^3\right]} \\ & \left\{\frac{120J}{\kappa}a_5(t) - \sum_{k=1}^{N-1} a_{4k+1}(t)\left(\frac{k(4k+1)L^{4k-4}(-4)^k}{\kappa}\right)\right. \\ & \left.\left[J(4k-1)(4k-2)(4k-3)+4EI\kappa L^3\right] + \tau(t)\right\}\end{aligned} \tag{4.11}$$

By using (4.11), the system (4.10) takes the form

$$(\ddot{a}_1, \cdots, \ddot{a}_{4N-3}) = f(a_1, \cdots, a_{4N-3}) + g(a_1, \cdots, a_{4N-3})\,\tau(t) \tag{4.12}$$

a set of N second order linear ODE's. (4.12) is put into state-space form by introducing $2N$ states $\{\zeta_1, \cdots, \zeta_{2N}\}$ as

$$\begin{aligned} a_{4k+1}(t) &= \zeta_{2k+1} \qquad 0 \le k \le N-1 \\ \dot{a}_{4k+1}(t) &= \zeta_{2k+2} \qquad 0 \le k \le N-1 \end{aligned} \tag{4.13}$$

The state definitions (4.13) are used in conjunction with the recursion formula (4.10) to derive a state-space representation of (4.12):

$$\begin{aligned} \dot{\zeta}_{2k+1} &= \dot{a}_{4k+1} = \zeta_{2k+2} && 0 \le k \le N-1 \\ \dot{\zeta}_{2k+2} &= \ddot{a}_{4k+1} = \frac{-(4k+5)(4k+4)(4k+3)(4k+2)}{\kappa}\zeta_{2k+3} && 0 \le k \le N-2 \end{aligned} \tag{4.14}$$

Equations (4.14) give $\{\dot{\zeta}_1, \cdots, \dot{\zeta}_{2N-1}\}$. The last term, $\dot{\zeta}_{2N}$, requires a different approach. From (4.13) and (4.10) we have

$$\begin{aligned} \zeta_{2N} &= \dot{a}_{4N-3}(t) \\ \dot{\zeta}_{2N} = \ddot{a}_{4N-3}(t) &= \frac{-(4(N-1)+5)(4(N-1)+4)(4(N-1)+3)(4(N-1)+2)}{\kappa} a_{4(N-1)+5}(t) \\ &= \frac{-(4N+1)(4N)(4N-1)(4N-2)}{\kappa} a_{4N+1}(t) \end{aligned}$$

Using (4.11) gives

$$\begin{aligned} \dot{\zeta}_{2N} = & \frac{-(4N+1)(4N)(4N-1)(4N-2)}{\kappa} \\ & \left(\frac{\kappa}{N(4N+1)L^{4N-4}(-4)^N\left[J(4N-1)(4N-2)(4N-3)+4EI\kappa L^3\right]}\right) \\ & \left\{\frac{120J}{\kappa}\zeta_3 - \sum_{k=1}^{N-1}\zeta_{2k+1}\left(\frac{k(4k+1)L^{4k-4}(-4)^k}{\kappa}\right)\left[J(4k-1)(4k-2)(4k-3)+4EI\kappa L^3\right]\right. \\ & \left. + \tau(t)\right\} \end{aligned}$$

Leading to

$$\begin{aligned} \dot{\zeta}_{2N} = & \frac{-4(4N-1)(4N-2)}{L^{4N-4}(-4)^N\left[J(4N-1)(4N-2)(4N-3)+4EI\kappa L^3\right]} \\ & \left\{\frac{120J}{\kappa}\zeta_3 - \sum_{k=1}^{N-1}\zeta_{2k+1}\left(\frac{k(4k+1)L^{4k-4}(-4)^k}{\kappa}\right)\left[J(4k-1)(4k-2)(4k-3)+4EI\kappa L^3\right]\right. \\ & \left. + \tau(t)\right\} \end{aligned} \tag{4.15}$$

Equations (4.14) and (4.15) define a state-space system representation of the form

$$\dot{\zeta} = A\zeta + B\tau$$

where $\zeta = \begin{bmatrix}\zeta_1 & \zeta_2 & \cdots & \zeta_{2N}\end{bmatrix}^T \in \mathbb{R}^{2N}$, and $A \in \mathbb{R}^{2N\times 2N}$, $B \in \mathbb{R}^{2N\times 1}$ are defined as

$$\dot{\zeta} = \underbrace{\begin{bmatrix} 0 & 1 & 0 & 0 & 0 & \cdots & 0 \\ 0 & 0 & -\frac{120}{\kappa} & 0 & 0 & \cdots & 0 \\ 0 & 0 & 0 & 1 & 0 & \cdots & 0 \\ 0 & 0 & 0 & 0 & -\frac{3024}{\kappa} & \cdots & 0 \\ \vdots & & & & & \ddots & \\ 0 & 0 & 0 & 0 & 0 & \cdots & 1 \\ 0 & 0 & \alpha_N\left(\frac{240J}{\kappa}+80EIL^3\right) & 0 & \alpha_N\left(\frac{-60480JL^4}{\kappa}-1152EIL^7\right) & \cdots & 0 \end{bmatrix}}_{A} \zeta + \underbrace{\begin{bmatrix} 0 \\ 0 \\ 0 \\ 0 \\ \vdots \\ 0 \\ \alpha_N \end{bmatrix}}_{B} \tau \tag{4.16}$$

$$\alpha_N = \frac{-4(4N-1)(4N-2)}{L^{4N-4}(-4)^N[J(4N-1)(4N-2)(4N-3)+4EI\kappa L^3]}$$

The system (4.16) is an approximation of the infinite-dimensional system (3.9).

4.2 Observer Design

The state ζ is not a directly measurable quantity. Hence, an observer is required in order to implement a state feedback law. For our experimental test stand the two measured outputs are the hub angle $\theta(t)$, and the tip deflection $V(L,t)$. To obtain a C matrix of the output equation $\psi = C\zeta$, we use the previously worked-out series expressions (3.45) and (3.46) for $\theta(t)$ and $V(L,t)$, respectively[1]:

$$\begin{aligned} \theta(t) &= y(t) + \sum_{k=0}^{\infty} \frac{(4\kappa)^k L^{4k}}{(4k)!} y^{(2k)}(t) \\ V(L,t) &= -Ly(t) + \sum_{k=0}^{\infty} \frac{\kappa^k L^{4k+1}}{(4k+1)!}\left[(-1)^k 2 - 4^k(4k+1)\right] y^{(2k)}(t) \end{aligned} \tag{4.17}$$

We will need to express the $y^{(k)}(t)$ flat outputs in terms of ζ. Using (4.13) and (4.5),

$$\begin{aligned} \zeta_{2k+1} &= a_{4k+1}(t) = \frac{(-\kappa)^k y^{(2k)}(t)}{(4k+1)!} \\ \zeta_{2k+2} &= \dot{a}_{4k+1}(t) = \frac{(-\kappa)^k y^{(2k+1)}(t)}{(4k+1)!} \end{aligned} \qquad 0 \le k \le N-1 \tag{4.18}$$

The series expressions (4.17) are rearranged to introduce (4.18):

$$\begin{aligned} \theta(t) &= y(t) + \sum_{k=0}^{\infty} \frac{(-4)^k(4k+1)(-\kappa)^k L^{4k}}{(4k+1)!} y^{(2k)}(t) \\ V(L,t) &= -Ly(t) + \sum_{k=0}^{\infty} \frac{(-\kappa)^k L^{4k+1}}{(4k+1)!}\left[2 - (-4)^k(4k+1)\right] y^{(2k)}(t) \end{aligned}$$

Using $N-1$ as the highest summation index leads to the output in terms of state:

$$\theta(t) = \zeta_1 + \sum_{k=0}^{N-1} (-4)^k(4k+1)L^{4k}\zeta_{2k+1} \tag{4.19}$$

$$V(L,t) = -L\zeta_1 + \sum_{k=0}^{N-1} \left[2 - (-4)^k(4k+1)\right] L^{4k+1}\zeta_{2k+1} \tag{4.20}$$

[1]The non-conventional notation $\psi(t)$ is used for the measured output to avoid confusion with the flat output $y(t)$.

In matrix form we have

$$\psi(t) = \begin{bmatrix} \theta(t) \\ V(L,t) \end{bmatrix} = C\zeta \qquad C \in \mathbb{R}^{2\times 2N} \tag{4.21}$$

We can shows the system is observable for all N by directly computing the rank of the observability matrix

$$\begin{bmatrix} C \\ CA \\ CA^2 \\ \vdots \\ CA^{2N-1} \end{bmatrix} \in \mathbb{R}^{4N\times 2N}$$

Since the system is observable, we can use a Luenberger observer of the form

$$\dot{\hat{\zeta}} = A\hat{\zeta} + B\tau + L(\psi - C\hat{\zeta}) \qquad L \in \mathbb{R}^{2N\times 2} \tag{4.22}$$

where L is the observer gain matrix. The observer error $\epsilon = \zeta - \hat{\zeta}$ is governed by

$$\dot{\epsilon} = (A - LC)\epsilon \tag{4.23}$$

and the dynamics of this error system can be arbitrarily assigned by placing the eigenvalues of $A - LC$.

4.3 State Feedback Tracking Controller Design

The feedforward open-loop control law derived in Chapter 3 steers the system and the closed-loop derived in this section provides (hopefully small) corrective action to account for model error, initial tracking error, and disturbances.

The state-space system (4.16) is *controllable* for any N, which can be verified by checking the rank of the controllability matrix

$$\begin{bmatrix} B & AB & A^2B & \cdots & A^{2N-1}B \end{bmatrix} \in \mathbb{R}^{2N\times 2N}$$

We design a closed-loop state feedback control to *track* arbitrarily smooth reference flat outputs $y^*(t)$. In order to achieve rest to rest motion, the output to be tracked can be taken as the flat output $y(t) = \zeta_1$. We time differentiate this output until the input appears. By inspection of (4.16), the input does not appear at any derivative order below $2N$. Using (4.18) in the $(2N-1)^{\text{th}}$ time derivative of $y(t)$,

$$\begin{aligned} y^{(2N-1)}(t) &= \frac{\zeta_{2(N-1)+2}\,(4(N-1)+1)!}{(-\kappa)^{N-1}} \\ &= \frac{\zeta_{2N}(4N-3)!}{(-\kappa)^{N-1}} \end{aligned} \tag{4.24}$$

Time differentiating (4.24) and using (4.15),

$$\begin{aligned} y^{(2N)}(t) =& \frac{\dot{\zeta}_{2N}(4N-3)!}{(-\kappa)^{N-1}} \\ =& \frac{(4N-3)!}{(-\kappa)^{N-1}} \left[\frac{-4(4N-1)(4N-2)}{L^{4N-4}(-4)^N\,[J(4N-1)(4N-2)(4N-3) + 4EI\kappa L^3]} \right. \\ & \left\{ \frac{120J}{\kappa}\zeta_3 - \sum_{k=1}^{N-1} \zeta_{2k+1} \left(\frac{k(4k+1)L^{4k-4}(-4)^k}{\kappa} \right) \right. \end{aligned}$$

$$\left[J(4k-1)(4k-2)(4k-3)+4EI\kappa L^3\right]+\tau(t)\Big\}\Big]$$

$$=\frac{(4N-1)!}{L^{4N-4}(4\kappa)^{N-1}\left[J(4N-1)(4N-2)(4N-3)+4EI\kappa L^3\right]}$$

$$\left\{\frac{120J}{\kappa}\zeta_3-\sum_{k=1}^{N-1}\zeta_{2k+1}\left(\frac{k(4k+1)L^{4k-4}(-4)^k}{\kappa}\right)\right.$$

$$\left.\left[J(4k-1)(4k-2)(4k-3)+4EI\kappa L^3\right]+\tau(t)\right\} \tag{4.25}$$

Hence, we have shown the relative degree of the systems is $2N$ and the system has no internal dynamics. This implies we can achieve asymptotic tracking of any smooth reference $y^*(t)$ [68].

Defining

$$a_N(\zeta)=\frac{(4N-1)!}{L^{4N-4}(4\kappa)^{N-1}\left[J(4N-1)(4N-2)(4N-3)+4EI\kappa L^3\right]}$$

$$\left\{\frac{120J}{\kappa}\zeta_3-\sum_{k=1}^{N-1}\zeta_{2k+1}\left(\frac{k(4k+1)L^{4k-4}(-4)^k}{\kappa}\right)\right. \tag{4.26}$$

$$\left.\left[J(4k-1)(4k-2)(4k-3)+4EI\kappa L^3\right]\right\}$$

$$b_N=\frac{(4N-1)!}{L^{4N-4}(4\kappa)^{N-1}\left[J(4N-1)(4N-2)(4N-3)+4EI\kappa L^3\right]} \tag{4.27}$$

we rewrite (4.25) as

$$y^{(2N)}(t)=a_N(\zeta)+b_N\tau(t) \tag{4.28}$$

Based on (4.28), the state feedback

$$\tau(t)=\frac{-a_N(\zeta)+v(t)}{b_N} \tag{4.29}$$

puts the system into a chain of integrators form

$$y^{(2N)}(t)=v(t) \tag{4.30}$$

Defining the tracking error between the actual and desired flat output as

$$e(t)=y(t)-y^*(t) \tag{4.31}$$

we assign the auxiliary input $v(t)$ in (4.30) to be

$$v(t)=y^{*(2N)}(t)-p_0\int_0^t e(t)dt-p_1e(t)-p_2\dot{e}(t)-\cdots-p_{2N}e^{(2N-1)}(t) \tag{4.32}$$

giving the tracking error dynamics

$$e^{(2N)}(t)+p_{2N}e^{(2N-1)}(t)+\cdots+p_2\dot{e}(t)+p_1e(t)+p_0\int_0^t e(t)dt=0 \tag{4.33}$$

The tracking error system (4.33) is a linear integro-differential equation and the asymptotic error convergence is ensured by choosing the roots of

$$s^{2N+1}+p_{2N}s^{2N}+\cdots+p_1s+p_0$$

in the open left-half plane.

Once the p_k coefficients of the characteristic polynomial are determined, they are substituted into the auxiliary input $v(t)$ given in (4.32), which in turn depends on $e(t) = y(t) - y^*(t)$. The reference $y^*(t)$ is pre-computed using the Gevrey steering function (3.32), while the observed ζ states are transformed to $y(t)$ using (4.18). The actual control law $\tau(t)$ is then obtained from (4.29). The expression for the closed-loop torque is

$$\tau(t) = \frac{-120J}{\kappa}\zeta_3 + \sum_{k=1}^{N-1} \zeta_{2k+1} \frac{k(4k+1)L^{4k-4}(-4)^k}{\kappa}\left[J(4k-1)(4k-2)(4k-3) + 4EI\kappa L^3\right]$$
$$+ \frac{L^{4N-4}(4\kappa)^{N-1}\left[J(4N-1)(4N-2)(4N-3) + 4EI\kappa L^3\right]}{(4N-1)!}$$
$$\left(y^{*(2N)}(t) - p_0\int_0^t (\zeta_1 - y^*(t))\,dt - \sum_{k=0}^{N-1} p_{2k+1}\left[\frac{(4k+1)!\zeta_{2k+1}}{(-\kappa)^k} - y^{*(2k)}(t)\right]\right.$$
$$\left. - \sum_{k=0}^{N-1} p_{2k+2}\left[\frac{(4k+1)!\zeta_{2k+2}}{(-\kappa)^k} - y^{*(2k+1)}(t)\right]\right)$$

Chapter 5

Numerical Simulation

In this chapter we numerically simulate the rotating beam system in both open and closed-loop modes. An FEA model of the plant is developed in order to test the control described in Chapters 3 and 4.

5.1 Series Computations

The first approach of calculating the PDE system response is to use the infinite series expressions developed in Chapter 3. The series for state $w(x,t)$ (3.20), input torque $\tau(t)$ (3.21), rigid-body angle $\theta(t)$ (3.45) and elastic tip deflection $V(L,t)$ (3.47) will be evaluated.

The infinite series are parameterized by the flat output function (3.32):

$$y(t) = \frac{\Theta}{2}\eta_\gamma(t) \tag{5.1}$$

with t_f the transition time, Θ the beam's end equilibrium rotation angle, and $\eta_\gamma(t)$ the Gevrey function from (3.31):

$$\eta_\gamma(t) = \frac{1}{2} + \frac{1}{2}\tanh\left(\frac{2(2\frac{t}{t_f} - 1)}{(4\frac{t}{t_f}(1 - \frac{t}{t_f}))^\gamma}\right) \tag{5.2}$$

To obtain the system response, the infinite series are expanded to a finite number of terms. The truncated expressions are then evaluated at a set of discrete grid of time and space points. Evaluating the series requires the calculations of successive time derivatives of the flat output (5.1). This is done efficiently using the recursion formulas derived in Section 3.6.

Simulation is carried out using the parameters given in Table 5.1. The physical system parameters are taken from Table 2.1 on Page 15.

Calculation parameter	Value
Series truncation order	25
Gevrey function parameter	$\gamma = 1.4$
Transition time	$t_f = 1$s
End beam angle	$\Theta = 90°$
# of time points	1000
# of space points	1000

Table 5.1: Calculation parameters for series simulation

The results are plotted in Figure 5.1. The simulated beam behaviour is consistent with physical intuition. A positive torque accelerates the beam, then a negative torque decelerates

it to rest at $\theta(t_f) = 90°$. It first bends downwards due to the counter-clockwise positive moment, then upwards due to the clockwise negative one. The beam is undeformed at its equilibrium positions.

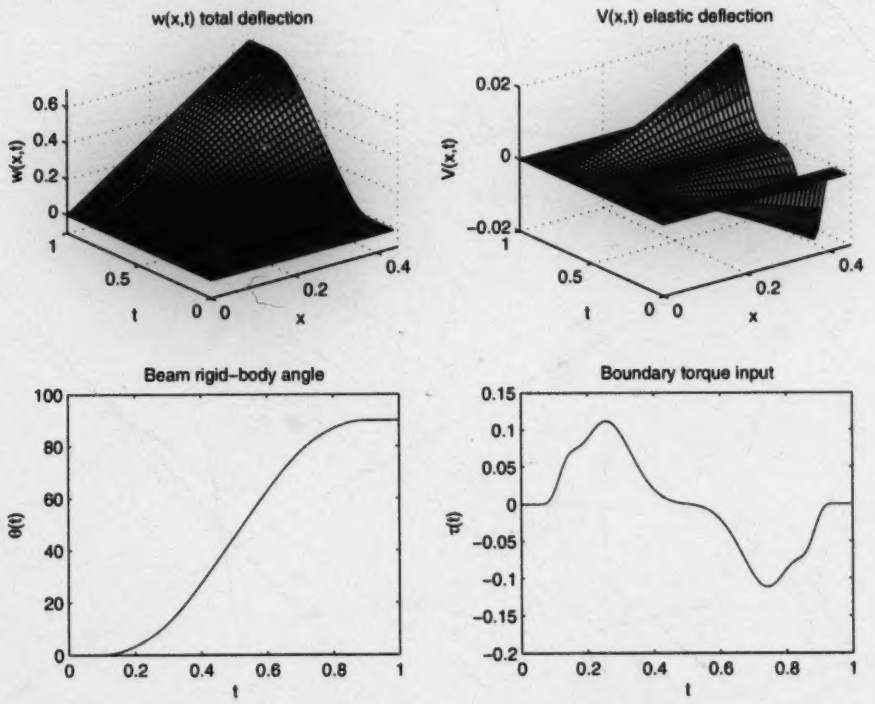

Figure 5.1: Results of series-based simulation

5.2 Observer Testing

The observer designed in Section 4.2 will be used to check the accuracy of the approximate system (4.16).

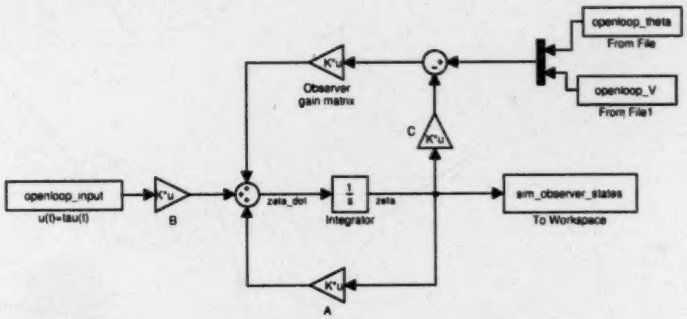

Figure 5.2: Observer testing Simulink diagram

The Simulink diagram used for testing the observer is shown in Figure 5.2. The three inputs are the boundary torque $\tau(t)$, the rigid-body angle $\theta(t)$ and the tip elastic deflection $V(L,t)$, which have been calculated for in open-loop using the series given in the previous section. The observer output is the estimated state vector $\hat{\zeta}$, which is compared to the actual state ζ obtained by using $y(t)$ defined in (5.1) in (4.18).

For the first test run, the value $N = 2$ is used, generating a fourth-order state-space system. The state estimate error system eigenvalues are chosen to be

$$\lambda_{obs} = \{-30, -35, -40, -45\}$$

. The actual and observed states are then plotted in Figure 5.3. The plots show good agreement between the estimated and actual ζ states, even at the low state-space order of $N = 2$. In a second run, we take $N = 3$ and

$$\lambda_{obs} = \{-70, -75, -80, -85, -90, -95\}$$

. The results are shown in Figure 5.4. Here again, we see good agreement between the series and observer states. For a final run, we have $N = 4$ and

$$\lambda_{obs} = \{-60, -65, -70, -75, -80, -85, -90, -95\}$$

, plotted in Figure 5.5. The lower states are well estimated, but the higher-order ones exhibit noise.

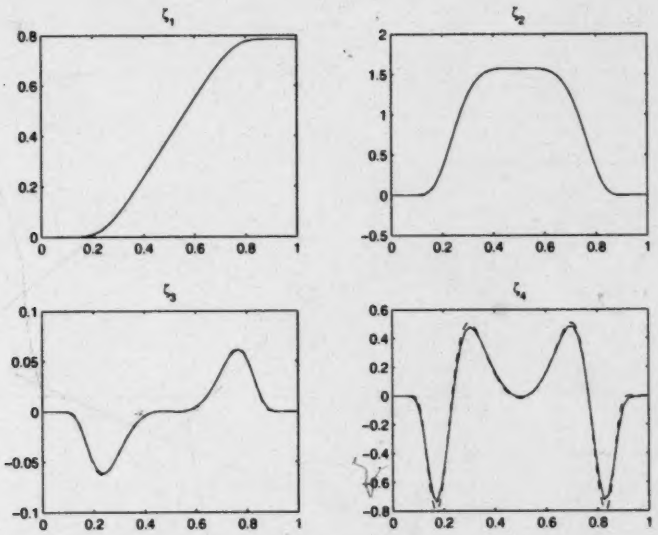

Figure 5.3: Observer (—) versus actual (---) states, $N = 2$.

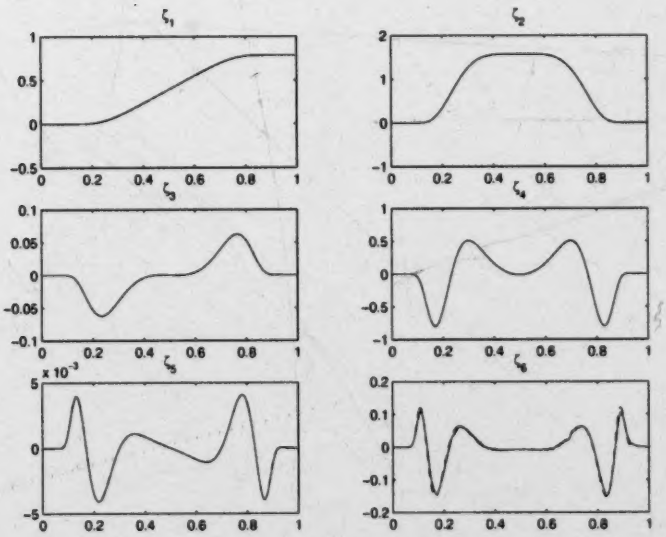

Figure 5.4: Observer (—) versus actual (---) states, $N = 3$.

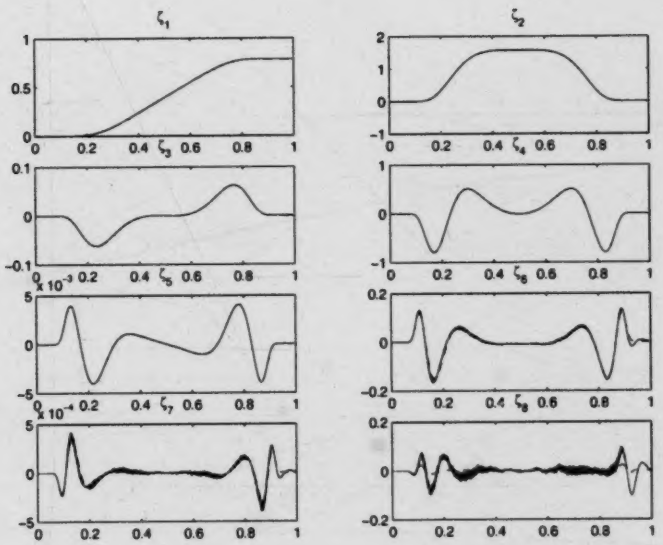

Figure 5.5: Observer (—) versus actual (- - -) states, $N = 4$.

5.3 FEA Model

The series expressions in the previous section can be used to calculate the system state $w(x,t)$ and input $\tau(t)$ for a given flat output trajectory. This approach does not provide a "real" simulation, in the sense that the system's response is not determined from the boundary input, but rather indirectly from $y(t)$. We require a method of obtaining $w(x,t)$ from $\tau(t)$ in order to validate both the open and closed-loop controls previously derived. In this section we develop a FEA simulation model following the work in [26, Section 8.3].

5.3.1 FEA Formulation of a Single Beam Element

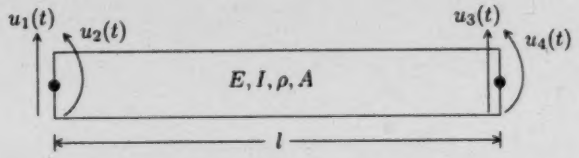

Figure 5.6: Single beam segment

We begin by looking at a single beam element, as illustrated in Figure 5.6, which will be used to assemble the complete beam model in Section 5.3.2. The segment has two *nodes*, each of which has two nodal coordinates, denoted by $u_k(t)$. The beam element has a length l and physical parameters E, I, ρ and A. The beam element is governed by the Euler-Bernoulli PDE:

$$EI\frac{\partial^4 w(x,t)}{\partial x^4} + \rho A\frac{\partial^2 w(x,t)}{\partial t^2} = 0 \tag{5.3}$$

We assume that at any instant of time, the beam displacement $w(x,t)$ must satisfy a static beam deflection profile,

$$EI\frac{\partial^4 w(x,t)}{\partial x^4} = 0 \tag{5.4}$$

The beam displacement is a function of time, so the solution to (5.4) is written as

$$w(x,t) = c_1(t)x^3 + c_2(t)x^2 + c_3(t)x + c_4(t) \tag{5.5}$$

In order to find the functions $c_k(t)$, we use the four nodal coordinates as boundary conditions for $w(x,t)$:

$$\begin{aligned} w(0,t) &= u_1(t) \quad & w(l,t) &= u_3(t) \\ \frac{\partial w}{\partial x}(0,t) &= u_2(t) \quad & \frac{\partial w}{\partial x}(l,t) &= u_4(t) \end{aligned} \tag{5.6}$$

Using (5.5) in (5.6) results in a system of four equations:

$$\begin{aligned} c_4(t) &= u_1(t) \\ c_3(t) &= u_2(t) \\ l^3c_1(t) + l^2c_2(t) + lc_3(t) + c_4(t) &= u_3(t) \\ 3l^2c_1(t) + 2lc_2(t) + c_3(t) &= u_4(t) \end{aligned} \tag{5.7}$$

System (5.7) is solved and the results substituted into (5.5):

$$\begin{aligned} w(x,t) = &\left(1 - \frac{3x^2}{l^2} + \frac{2x^3}{l^3}\right)u_1(t) + \left(x - \frac{2x^2}{l} + \frac{x^3}{l^2}\right)u_2(t) \\ &+ \left(\frac{3x^2}{l^2} - \frac{2x^3}{l^3}\right)u_3(t) + \left(\frac{x^3}{l^2} - \frac{x^2}{l}\right)u_4(t) \end{aligned} \tag{5.8}$$

Solution (5.8) is used to derive the *modal equation* for the beam segment,

$$M\ddot{u} + Ku = F(t) \tag{5.9}$$

where u is the vector of nodal coordinates, $F(t)$ is the modal forcing vector, and M and K are the segment's mass and stiffness matrices.

The modal matrices are found from the expressions for potential and kinetic energy of the beam segment. The strain energy of the segment is given by [26, p.537]:

$$V(t) = \frac{1}{2}\int_0^l EI\left[\frac{\partial^2 w(x,t)}{\partial x^2}\right]^2 dx = \frac{1}{2}u^T K u \tag{5.10}$$

Expanding the integral using (5.8),

$$\frac{4EI}{l^3}\Big\{3u_1^2 + 3lu_1u_2 + l^2u_2^2 - 6u_1u_3 - 3lu_2u_3 + 3u_3^2 + 3lu_1u_4 + l^2u_2u_4 - 3lu_3u_4 + l^2u_4^2\Big\} = u^T K u$$

The stiffness matrix is therefore

$$K = \frac{EI}{l^3}\begin{bmatrix} 12 & 6l & -12 & 6l \\ 6l & 4l^2 & -6l & 2l^2 \\ -12 & -6l & 12 & -6l \\ 6l & 2l^2 & -6l & 4l^2 \end{bmatrix} \tag{5.11}$$

The segment's kinetic energy is [26, p.538]:

$$T(t) = \frac{1}{2}\int_0^l \rho A\left[\frac{\partial w(x,t)}{\partial t}\right]^2 dx = \frac{1}{2}\dot{u}^T M \dot{u} \tag{5.12}$$

Expanding (5.12) using (5.8),

$$\frac{l\rho A}{210}\Big\{78\dot{u}_1^2 + 22l\dot{u}_1\dot{u}_2 + 2l^2\dot{u}_2^2 + 54\dot{u}_1\dot{u}_3 + 13l\dot{u}_2\dot{u}_3 + 78\dot{u}_3^2 - 13l\dot{u}_1\dot{u}_4 - 3l^2\dot{u}_2\dot{u}_4 - 22l\dot{u}_3\dot{u}_4 + 2l^2\dot{u}_4^2\Big\} = \dot{u}^T M \dot{u}$$

The mass matrix is therefore

$$M = \frac{\rho Al}{420}\begin{bmatrix} 156 & 22l & 54 & -13l \\ 22l & 4l^2 & 13l & -3l^2 \\ 54 & 13l & 156 & -22l \\ -13l & -3l^2 & -22l & 4l^2 \end{bmatrix} \tag{5.13}$$

The modal forcing vector $F(t)$ in (5.9) contains the forces and moments acting on each nodal coordinate. In the most general case,

$$F(t) = \begin{bmatrix} F_1(t) \\ M_1(t) \\ F_2(t) \\ M_2(t) \end{bmatrix}$$

where $F_1(t)$ is the force acting on the left node, $M_1(t)$ is the moment acting on the left node, and $F_2(t)$, $M_2(t)$ are the force and moment acting on the right node, respectively. If the beam is unforced, then

$$F(t) = \begin{bmatrix} 0 \\ 0 \\ 0 \\ 0 \end{bmatrix}$$

5.3.2 Superposition of Beam Elements

The full beam model is constructed by superposition of the individual beam segment equations. Each modal equation (5.9) represents a system of 4 second-order linear ODEs with constant coefficients.

Consider a two-segment discretization of a beam shown in Figure 5.7.

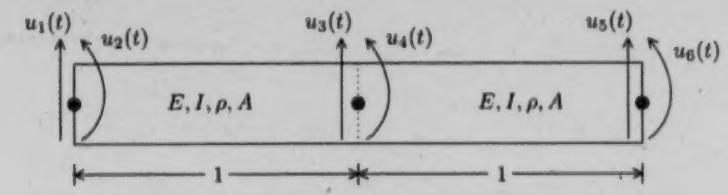

Figure 5.7: Two-segment beam example for superposition

In this particular case, the segments are identical in length and physical parameters. Using (5.11) and (5.13) gives:

$$K_1 = K_2 = EI \begin{bmatrix} 12 & 6 & -12 & 6 \\ 6 & 4 & -6 & 2 \\ -12 & -6 & 12 & -6 \\ 6 & 2 & -6 & 4 \end{bmatrix}$$

$$M_1 = M_2 = \frac{\rho A}{420} \begin{bmatrix} 156 & 22 & 54 & -13 \\ 22 & 4 & 13 & -3 \\ 54 & 13 & 156 & -22 \\ -13 & -3 & -22 & 4 \end{bmatrix}$$

The modal equations for each segment are:

$$\frac{\rho A}{420} \begin{bmatrix} 156 & 22 & 54 & -13 \\ 22 & 4 & 13 & -3 \\ 54 & 13 & 156 & -22 \\ -13 & -3 & -22 & 4 \end{bmatrix} \begin{bmatrix} \ddot{u}_1 \\ \ddot{u}_2 \\ \ddot{u}_3 \\ \ddot{u}_4 \end{bmatrix} + \begin{bmatrix} 12 & 6 & -12 & 6 \\ 6 & 4 & -6 & 2 \\ -12 & -6 & 12 & -6 \\ 6 & 2 & -6 & 4 \end{bmatrix} \begin{bmatrix} u_1 \\ u_2 \\ u_3 \\ u_4 \end{bmatrix} = \begin{bmatrix} 0 \\ 0 \\ 0 \\ 0 \end{bmatrix} \tag{5.14}$$

$$\frac{\rho A}{420} \begin{bmatrix} 156 & 22 & 54 & -13 \\ 22 & 4 & 13 & -3 \\ 54 & 13 & 156 & -22 \\ -13 & -3 & -22 & 4 \end{bmatrix} \begin{bmatrix} \ddot{u}_3 \\ \ddot{u}_4 \\ \ddot{u}_5 \\ \ddot{u}_6 \end{bmatrix} + \begin{bmatrix} 12 & 6 & -12 & 6 \\ 6 & 4 & -6 & 2 \\ -12 & -6 & 12 & -6 \\ 6 & 2 & -6 & 4 \end{bmatrix} \begin{bmatrix} u_3 \\ u_4 \\ u_5 \\ u_6 \end{bmatrix} = \begin{bmatrix} 0 \\ 0 \\ 0 \\ 0 \end{bmatrix} \tag{5.15}$$

The system above represents 8 LTI ODEs. Adding together the equations in u_3 and then in u_4 gives a system of 6 equations, expressed in modal form as:

$$\begin{aligned} &\frac{\rho A}{420} \begin{bmatrix} 156 & 22 & 54 & -13 & 0 & 0 \\ 22 & 4 & 13 & -3 & 0 & 0 \\ 54 & 13 & 156+156 & -22+22 & 54 & -13 \\ -13 & -3 & -22+22 & 4+4 & 13 & -3 \\ 0 & 0 & 54 & 13 & 156 & -22 \\ 0 & 0 & -13 & -3 & -22 & 4 \end{bmatrix} \begin{bmatrix} \ddot{u}_1 \\ \ddot{u}_2 \\ \ddot{u}_3 \\ \ddot{u}_4 \\ \ddot{u}_5 \\ \ddot{u}_6 \end{bmatrix} \\ &+ EI \begin{bmatrix} 12 & 6 & -12 & 6 & 0 & 0 \\ 6 & 4 & -6 & 2 & 0 & 0 \\ -12 & -6 & 12+12 & -6+6 & -12 & 6 \\ 6 & 2 & -6+6 & 4+4 & -6 & 2 \\ 0 & 0 & -12 & -6 & 12 & -6 \\ 0 & 0 & 6 & 2 & -6 & 4 \end{bmatrix} \begin{bmatrix} u_1 \\ u_2 \\ u_3 \\ u_4 \\ u_5 \\ u_6 \end{bmatrix} = \begin{bmatrix} 0 \\ 0 \\ 0 \\ 0 \\ 0 \\ 0 \end{bmatrix} \end{aligned} \tag{5.16}$$

which can be numerically integrated to obtain the nodal coordinates. The superposition approach is easily coded for an arbitrary number of beam segments.

In our application, a rotating beam is modeled as an N element system with torque input at the first node, as illustrated in Figure 5.8. Since the beam is uniform and all segments have equal length, the local mass and stiffness terms are calculated only once, then superimposed to form the global M and K matrices, similarly to the last example.

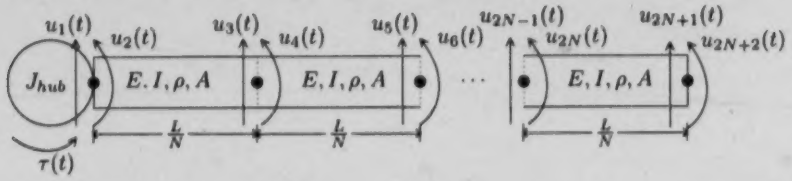

Figure 5.8: FEA model of rotating beam with N elements

Superposition is used to model the rigid hub attached to the beam. The global beam mass and stiffness matrices are assembled without a forcing vector. The hub's equation of motion,

$$J_{hub}\ddot{u}_2(t) = \tau(t)$$

is added to the global mass matrix and creates a modal forcing term $F(t)$.

5.3.3 Boundary Conditions in FEA

Boundary conditions on the original PDE are used to simplify the global mass and stiffness matrices by removing the corresponding $u_k(t)$ nodal coordinates. For example, if the beam from Figure 5.7 is clamped at the left and free at the right, then $u_1(t) = u_2(t) = 0$, although $u_5(t)$ and $u_6(t)$ remain unaltered.

The ODE corresponding to a $u_k(t) = 0$ term is trivial and is dropped from the system of equations. The nodal coordinate is also removed from the remaining equations. For the two-segment problem above, the system of 8 ODEs in 8 unknowns is simplified to 6 ODEs in 6 unknowns.

Removing equations and nodal coordinates is equivalent to deleting corresponding rows and columns in the modal M and K matrices. In our example, $u_1(t) = u_2(t) = 0$, which eliminates the top two rows, and the two left-most columns in the system's global matrices, and (5.16) becomes

$$\begin{aligned} \frac{\rho A}{420}\begin{bmatrix} 156+156 & -22+22 & 54 & -13 \\ -22+22 & 4+4 & 13 & -3 \\ 54 & 13 & 156 & -22 \\ -13 & -3 & -22 & 4 \end{bmatrix}\begin{bmatrix} \ddot{u}_3(t) \\ \ddot{u}_4(t) \\ \ddot{u}_5(t) \\ \ddot{u}_6(t) \end{bmatrix} \\ + EI\begin{bmatrix} 12+12 & -6+6 & -12 & 6 \\ -6+6 & 4+4 & -6 & 2 \\ -12 & -6 & 12 & -6 \\ 6 & 2 & -6 & 4 \end{bmatrix}\begin{bmatrix} u_3(t) \\ u_4(t) \\ u_5(t) \\ u_6(t) \end{bmatrix} = \begin{bmatrix} 0 \\ 0 \\ 0 \\ 0 \end{bmatrix} \end{aligned} \tag{5.17}$$

For the rotating beam in Figure 5.8, $u_1(t) = 0$, since the hub does not translate. No other simplifications are available.

5.3.4 State-space Representation of FEA model

Once the global M and K matrices are assembled and simplified using the BCs, a modal form (5.9) can be transformed into state-space form. For the rotating beam, we have

$$M\ddot{u}(t) + Ku(t) = F(t) = B\tau(t)$$

Where $B = [0 \quad 1 \quad 0 \quad \cdots \quad 0]^T$ due to the torque acting on the hub. Defining the variables $x_1 = u(t)$, $x_2 = \dot{u}(t)$,

$$\dot{x}_1 = \dot{u}(t) = x_2$$
$$\dot{x}_2 = \ddot{u}(t) = -M^{-1}Ku(t) + M^{-1}B\tau(t) = -M^{-1}Kx_1 + M^{-1}B\tau(t)$$
$$\begin{bmatrix}\dot{x}_1 \\ \dot{x}_2\end{bmatrix} = \begin{bmatrix}0 & I \\ -M^{-1}K & 0\end{bmatrix}\begin{bmatrix}x_1 \\ x_2\end{bmatrix} + \begin{bmatrix}0 \\ M^{-1}B\end{bmatrix}\tau(t)$$
$$y = [I \quad 0]\begin{bmatrix}x_1 \\ x_2\end{bmatrix}$$

we obtain the state-space representation of the system's modal equation, with the boundary torque $\tau(t)$ as the input and nodal displacements as the output y.

5.4 Validating the FEA Model

To validate the FEA model, an open-loop test is performed, using the series-computed $\tau(t)$ as the input. The simulated result will then be checked against the series-computed results in Section 5.1. The setup for this is shown in Figure 5.9.

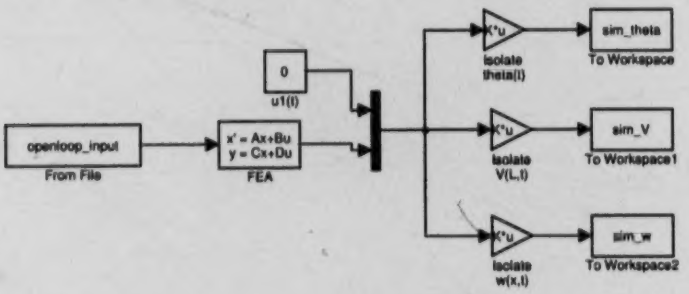

Figure 5.9: FEA open-loop testing, Simulink implementation

The physical beam parameters used to calculate the M and K matrices are taken from Table 2.1. We use $N = 20$ elements in the spatial discretization.

Since $u_1(t)$ is gets dropped as a zero boundary condition, $u_1(t) = 0$ is manually added into the FEA model output. The simulated nodal coordinates are arranged into the displacement field $w(x_i, t) = [u_1(t) \quad u_3(t) \quad \cdots \quad u_{2N+1}(t)]$, the hub angle $\theta(t) = u_2(t)$ and the tip elastic deflection $V(L,t) = u_{2N+1}(t) - Lu_2(t)$. The results are plotted in Figure 5.10.

Comparing the FEA model results in Figure 5.10 with the series-calculated in Figure 5.1, we see good agreement between the two, indicating the FEA model is a valid simulation tool. Based on informal testing, $N_{\text{FEA}} = 20$ elements gives results which are "sufficiently accurate" for simulating the closed-loop operation of the system. A large number of elements ($N_{\text{FEA}} = 150$) was used and no significant improvements in accuracy were observe.

5.5 Closed-loop Control Simulations

The closed-loop control Simulink diagram is shown in Figure 5.11. The FEA model is used as a state-space model of the plant and is connected to the tracking controller and observer systems derived in Chapter 4. The controller implementation is shown in Figure 5.12.

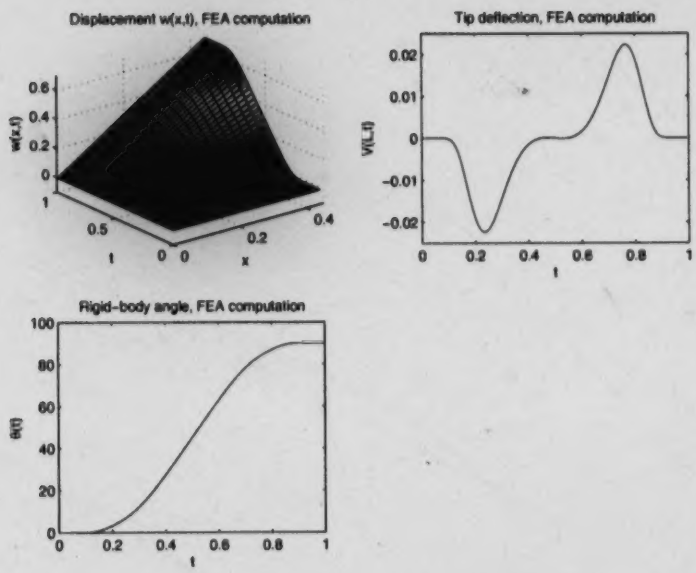

Figure 5.10: Results of FEA simulation

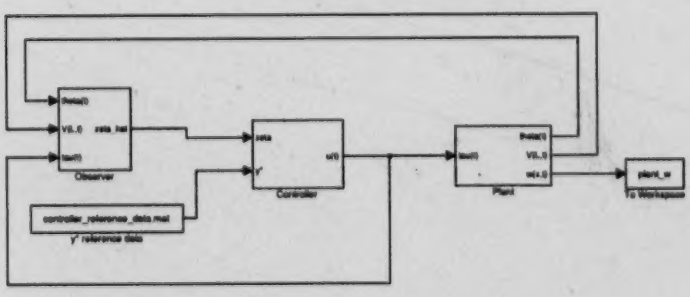

Figure 5.11: Closed-loop system Simulink diagram

To test control performance, we use a 90° rotation in one second as the control task, and give the beam an initial tracking error of $\theta(0) = -10°$. The open-loop operation is shown in Figure 5.13. The beam rotation is executed smoothly, but the beam undershoots the target and stops at $\theta(1) = 80°$ due to lack of feedback.

The same control task is now performed with a closed-loop control law. In the first run, $N = 2$ is used when deriving the controller and observer expressions. The observer eigenvalues are the same as for the $N = 2$ observer test in Figure 5.3, $\lambda_{obs} = \{-30, -35, -40, -45\}$. The controller uses $\lambda_{cont} = \{-5, -10, -15, -20, -25\}$. The results are shown in Figure 5.14. Due to the closed-loop control, the system is able to compensate for the initial downward deflection and move the system to the desired $\theta(1) = 90°$ ending configuration. The torque plot shows extra control effort at the beginning of the movement. The torque approaches the open-loop input profile in Figure 5.13 for the end of the motion, i.e., the open-loop control is doing most of the "work" at the end of the motion.

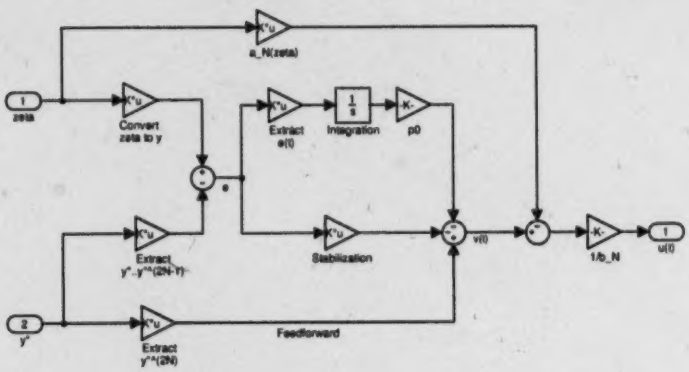

Figure 5.12: Controller subsystem Simulink implementation

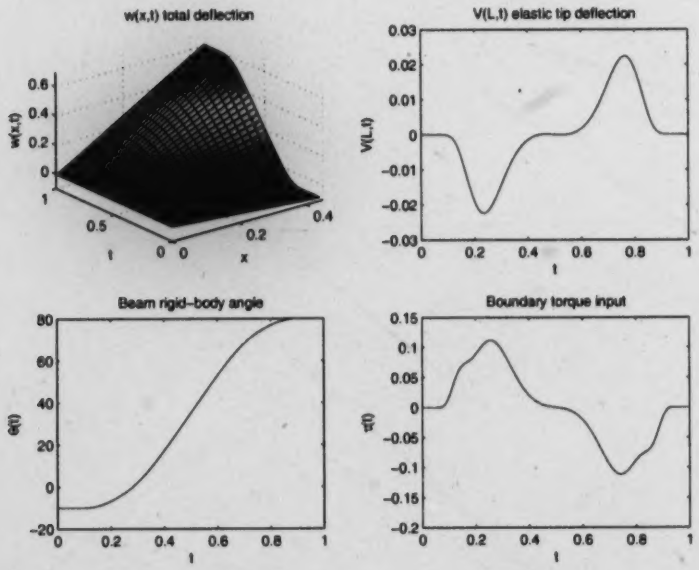

Figure 5.13: Open-loop steering of beam with $\theta(0) = -10°$

In a second run, we use $N = 3$ terms in the series truncation, producing a 6^{th} order state-space model. The closed-loop observer and controller eigenvalues are set to $\lambda_{obs} = \{-70, -75, -80, -85, -90, -95\}$ and $\lambda_{cont} = \{-40, -45, -50, -55, -60, -65, -70\}$, respectively. The results are plotted in Figure 5.15. The $N = 3$ plots show the controller does its job of moving the system to the desired final configuration, but the operation exhibits a high level of chatter, seen in the plot of $\theta(t)$. A more serious problem is with the system input $\tau(t)$ which exhibits increasingly large oscillations which would eventually destabilize the system.

For the last run, $N = 4$ is used, along with $\lambda_{obs} = \{-60, -65, -70, -75, -80, -85, -90, -95\}$

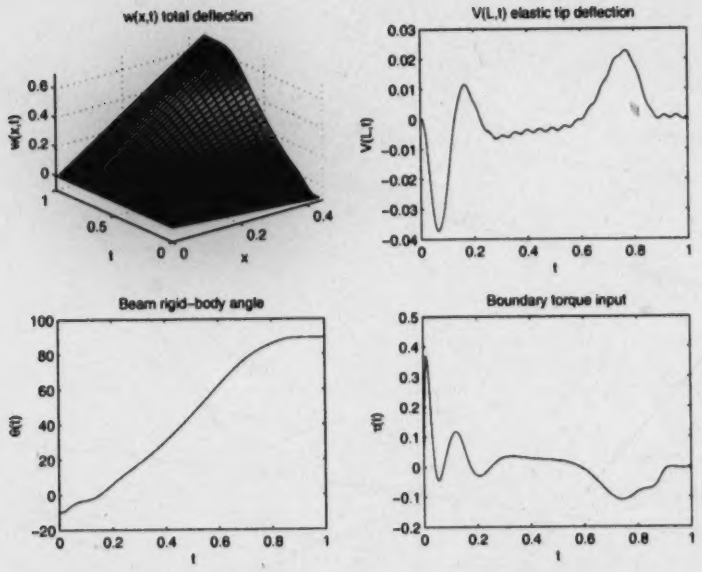

Figure 5.14: Closed-loop control of beam with $\theta(0) = -10°$, $N = 2$.

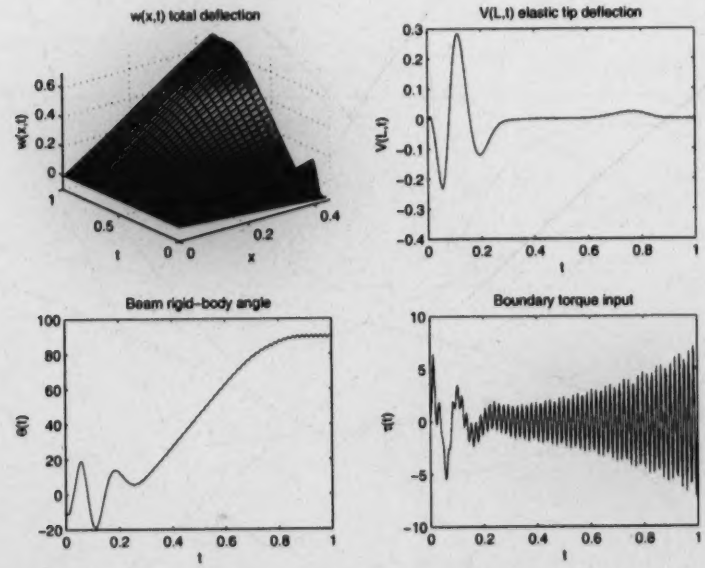

Figure 5.15: Closed-loop control of beam with $\theta(0) = -10°$, $N = 3$.

and $\lambda_{cont} = \{-10, -15, -20, -25, -30, -35, -40, -45, -50\}$. The system goes unstable, as shown in Figure 5.16.

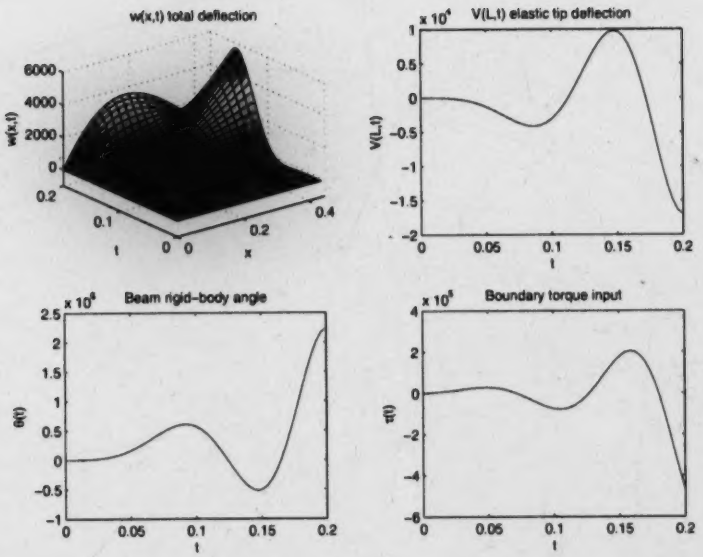

Figure 5.16: Closed-loop control of beam with $\theta(0) = -10°$, $N = 4$. Unstable operation.

Chapter 6

Experimental Validation

In this chapter, the control law designs from Chapters 3 and 4 are tested on the flexible beam experimental hardware.

6.1 Overview of Experimental Setup

The rotating beam plant, shown in Figure 2.1 on Page 6, was connected to a PC running Matlab/WinCon/RTX. The setup readily allows controller development in Simulink and generates real-time code taking care of implementation details such as discretization and data I/O.

6.2 Constant Gain Control

Before testing the flatness-based controllers we consider the performance of a simple proportional controller as shown in Figure 6.1.

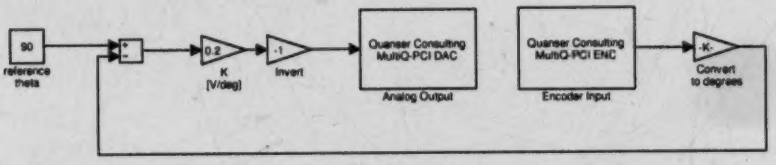

Figure 6.1: Proportional controller for rotating beam

We use $\theta = 90°$ as the reference input. The gain value is tuned to $K = 0.2$, giving a fast response without saturating the input. The experimental data is plotted in Figure 6.2.

The constant gain controller moves the beam to the end configuration without steady-state error. However, this solution exhibits poor transient performance, giving a large overshoot and long settling time.

6.3 Flatness-based Open-loop Control Experiment

The next test is the open-loop control using the input $\tau(t)$ computed from the Chapter 3 series. The Simulink setup is shown in Figure 6.3. The experimental results are plotted in Figure 6.4.

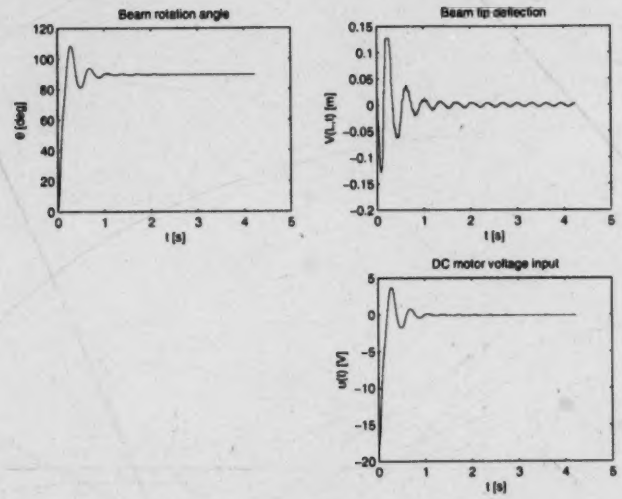

Figure 6.2: 90° transition using constant gain controller

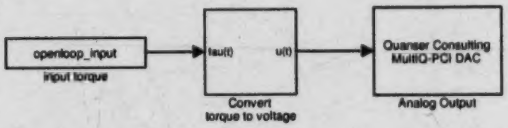

Figure 6.3: Open-loop experimental testing setup

For the open-loop operation, the target rotation of 90° is not met, with the final angle being about 75°. This is caused by the unmodeled friction present in the experiment. The system exhibits a discontinuous 'stiction' effect, where input torque below a certain level does not produce motion, since it is insufficient to overcome the static friction present. This effect is seen by looking at the $\tau(t)$ and $\theta(t)$ plots near the start time. The graph for $\tau(t)$ starts to increase smoothly at about $t = 0.05$ and yet the value for $\theta(t)$ only begins to move at $t = 0.15$.

We remark however, that the transient characteristics of the system's performance are better than the constant gain controller, with lower tip deflection amplitude and smaller overshoot. The settling time is the same or better.

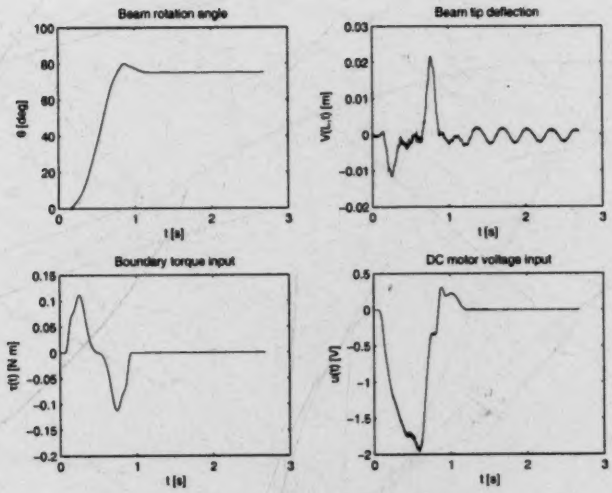

Figure 6.4: Experimental open-loop steering to 90°

6.4 Flatness-Based Closed-loop Control Experiment

The experimental setup for this section is shown in Figure 6.5. The control task is still a 90° transition in 1 second.

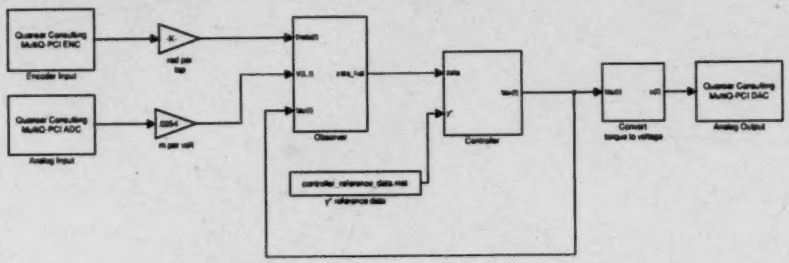

Figure 6.5: Closed-loop experiment Simulink model

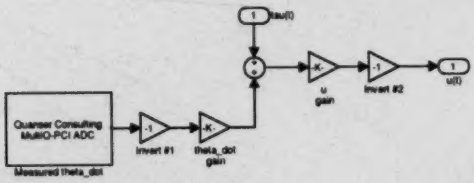

Figure 6.6: Closed-loop experiment, $\tau(t)$ to $u(t)$ conversion subsystem

6.4.1 Disturbance-Free Test, $N = 2$ Design

Using $N = 2$ gives a fourth order state-space system representation. The system eigenvalues are chosen as $\lambda_{cont} = \{-5, -10, -15, -20, -25\}$ and $\lambda_{obs} = \{-30, -35, -40, -45\}$. Based on the simulation results, we expect this system to function well. The experimental data is plotted in Figure 6.7.

In contrast to the open-loop experiment, the closed-loop control law meets the target of $\theta = 90°$. The transient characteristics of maximum overshoot and settling time are better than both the proportional controller and the open-loop control.

The beam tip exhibits some residual oscillations at the end of the transition. The controller attempts to compensate, as seen from the $\tau(t)$ and $u(t)$ input plots. However, the plant hardware contains a "dead zone", where actuator efforts below a certain threshold do not produce movement, caused by static friction.

6.4.2 External Disturbances Test, $N = 2$ Design

The controller from Section 6.4.1 is now run while manually interfering with its operation. The goal is to test the robustness of the controller. The disturbances applied are described as follows:

1. During transition, the ruler is stopped by hand, held briefly and released.
2. Once the system reaches its final endpoint, the beam is deflected in the counter-clockwise direction and released.

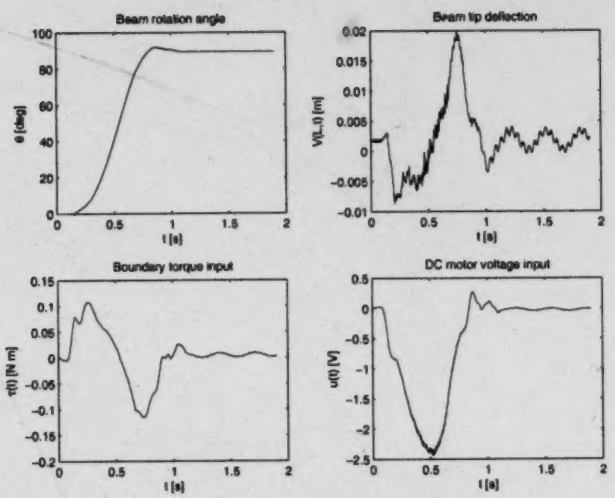

Figure 6.7: Experimental 1 second 90° transition, $N = 2$ controller

3. The deflection from the previous step is repeated in the opposite clockwise sense

The results are plotted in Figure 6.8. The controller remains stable and rejects disturbances, both during tracking and in stabilizing mode at the end of the transition.

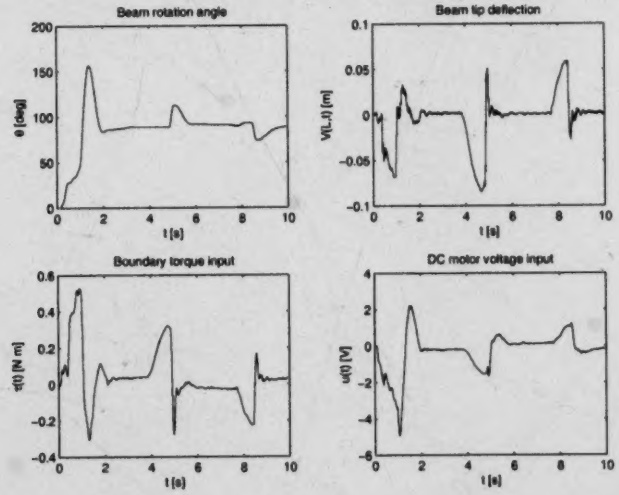

Figure 6.8: Attempted 1 second 90° transition, subjected to manual interference.

6.4.3 Disturbance-Free Run, $N = 3$ Design

The final experiment is to test the performance of a controller designed using $N = 3$, as done in simulation in Figure 5.15, which exhibited a large level of chatter. The parameters used are the same as before, $\lambda_{obs} = \{-70, -75, -80, -85, -90, -95\}$ and $\lambda_{cont} = \{-40, -45, -50, -55, -60, -65, -70\}$. The results are shown in Figure 6.9.

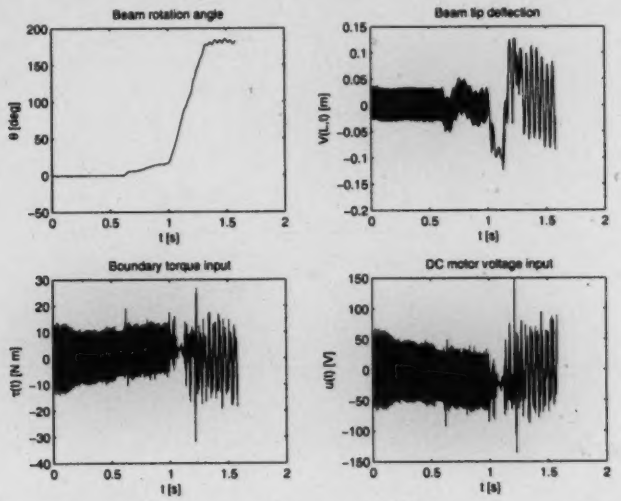

Figure 6.9: Attempted 90° transition, $N = 3$ controller. Unstable operation.

The $N = 3$ version of the controller is unstable. Note that the beam remains stationary for about one second while the gears chatter, then goes unstable.

Chapter 7

Generalization of the Rotating Beam Model

In this chapter, we generalize the previously used rotating beam model to include a tip payload, as studied in [2], for instance. Also to increase the level of generality, the system is initially modeled as a Rayleigh beam, which includes the Euler-Bernoulli beam as a special case.

7.1 Derivation of the Rayleigh Beam Model

7.1.1 Rayleigh Beam PDE

Consider the free-body diagram of an infinitesimal beam element, shown in Figure 7.1. The right-hand side force and moments have been converted to one-term Taylor series expansions, as in Section 2.2.2.

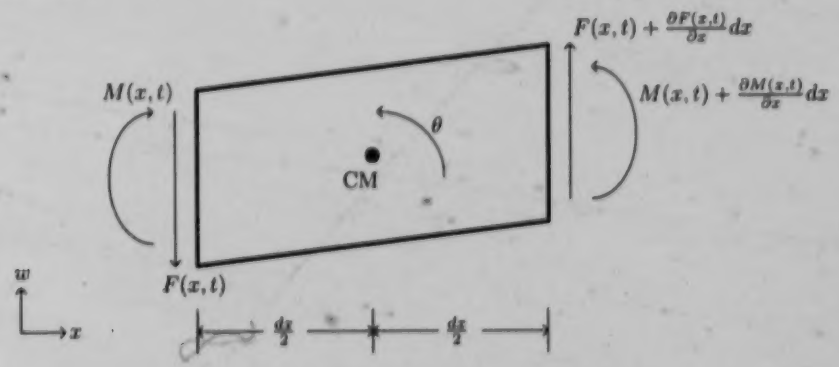

Figure 7.1: Free-body diagram of infinitesimal Rayleigh beam segment

Performing a force balance, taking upwards as positive

$$\sum F_w = m \frac{\partial^2 w(x,t)}{\partial t^2}$$

$$F(x,t) + \frac{\partial F(x,t)}{\partial x} dx - F(x,t) = \rho A dx \frac{\partial^2 w(x,t)}{\partial t^2}$$

$$\frac{\partial F(x,t)}{\partial x} = \rho A \frac{\partial^2 w(x,t)}{\partial t^2} \tag{7.1}$$

Next, performing a moment balance about the centre of mass, taking counter-clockwise as positive

$$\begin{aligned}
\sum M_{CM} &= J\frac{d^2\theta(t)}{dt^2} \\
M(x,t) + \frac{\partial M(x,t)}{\partial x}dx - M(x,t) + \left(F(x,t) + \frac{\partial F(x,t)}{\partial x}dx\right)\frac{dx}{2} + F(x,t)\frac{dx}{2} &= J\frac{\partial^3 w(x,t)}{\partial t^2 \partial x} \\
\frac{\partial M(x,t)}{\partial x}dx + F(x,t)dx + \underbrace{\frac{\partial F(x,t)}{\partial x}\frac{(dx)^2}{2}}_{\approx 0} &= J\frac{\partial^3 w(x,t)}{\partial t^2 \partial x}
\end{aligned} \tag{7.2}$$

The internal restoring moment is related to the curvature of the beam by

$$M(x,t) = EI\frac{\partial^2 w(x,t)}{\partial x^2} \tag{7.3}$$

which is exactly the same as for the Euler-Bernoulli model, see (2.7). With (7.3), (7.2) becomes

$$EI\frac{\partial^3 w(x,t)}{\partial x^3}dx + F(x,t)dx = J\frac{\partial^3 w(x,t)}{\partial t^2 \partial x} \tag{7.4}$$

Another fact that we use is the relationship between J, the *mass* moment of inertia, and I, the *area* of moment of inertia. Assuming the segment has a rectangular cross-section with base b and height h,

$$\begin{aligned}
J &= \frac{1}{12}m(h^2 + \underbrace{(dx)^2}_{\approx 0}) = \frac{1}{12}mh^2 \\
I &= \frac{1}{12}bh^3 \\
J &= \frac{Im}{bh} = \frac{I}{A}\rho A dx = \rho I dx
\end{aligned} \tag{7.5}$$

In fact, (7.5) can be shown to apply to *any* cross-section form, providing ρ and A are constants. Applying (7.5) to (7.4) gives

$$\begin{aligned}
EI\frac{\partial^3 w(x,t)}{\partial x^3}dx + F(x,t)dx &= \rho I dx \frac{\partial^3 w(x,t)}{\partial t^2 \partial x} \\
F(x,t) &= \rho I \frac{\partial^3 w(x,t)}{\partial t^2 \partial x} - EI\frac{\partial^3 w(x,t)}{\partial x^3}
\end{aligned} \tag{7.6}$$

Finally, substituting (7.6) into the force balance result (7.1) gives

$$\begin{aligned}
\frac{\partial}{\partial x}\left(\rho I \frac{\partial^3 w(x,t)}{\partial t^2 \partial x} - EI\frac{\partial^3 w(x,t)}{\partial x^3}\right) &= \rho A \frac{\partial^2 w(x,t)}{\partial t^2} \\
EI\frac{\partial^4 w(x,t)}{\partial x^4} - \rho I \frac{\partial^4 w(x,t)}{\partial x^2 \partial t^2} + \rho A \frac{\partial^2 w(x,t)}{\partial t^2} &= 0
\end{aligned} \tag{7.7}$$

The Rayleigh PDE (7.7) is found in [73] and [21], for example.

7.1.2 Force and Moment Boundary Conditions

In this section, we discuss how forces and moments acting on the beam edges can be translated into boundary conditions for the Rayleigh PDE.

For moment BCs, we use equation (7.3), so that

$$\frac{\partial^2 w(x,t)}{\partial x^2} = \frac{M(x,t)}{EI} \tag{7.8}$$

Result (7.8) is identical to the earlier Euler-Bernoulli case. It is important to use the sign convention of Section 2.2.3:

- Left side: clockwise external moment=positive M (and vice-versa)
- Right side: counter-clockwise external moment=positive M (and vice-versa)

If there is no moment applied (free or pinned end), $M = 0$, the sign gets canceled out and $\frac{\partial^2 w(x,t)}{\partial x^2} = 0$ applies.

For force BCs, we use Equation (7.6)

$$\frac{\partial^3 w(x,t)}{\partial x^3} - \frac{\rho}{E}\frac{\partial^3 w(x,t)}{\partial t^2 \partial x} = \frac{-F(x,t)}{EI} \tag{7.9}$$

Result (7.9) is *not* the same as for Euler-Bernoulli. We again need to observe the direction convention from Section 2.2.3:

- Left side: downward external force=positive F (and vice-versa)
- Right side: upward external force=positive F (and vice-verse)

If there is no force applied (free or sliding end), $F = 0$, the sign gets canceled and $\frac{\partial^3 w(x,t)}{\partial x^3} = \frac{\rho}{E}\frac{\partial^3 w}{\partial t^2 \partial x}$ for either side.

7.2 Rotating Beam Model

We now derive a model for a rotating beam system with tip payload using the Rayleigh beam equation for generality. The equations derived can be easily simplified to the Euler-Bernoulli case, as done in the next section.

The schematic diagram of the system is shown in Figure 7.2.

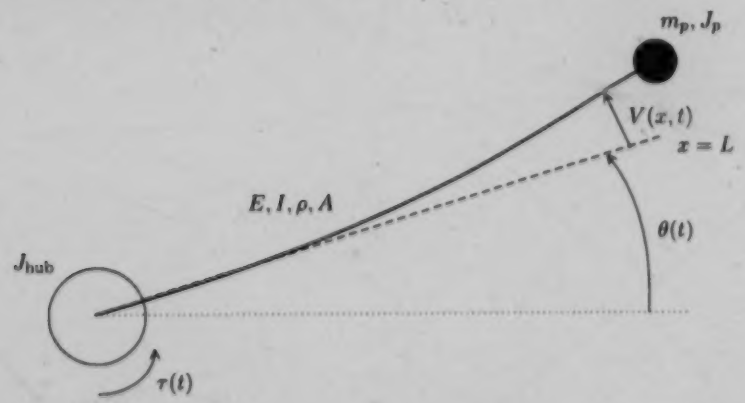

Figure 7.2: Rotating beam diagram

First, focus on the payload, as shown in Figure 7.3. Note $F_{\text{beam,payload}}$ and $M_{\text{beam,payload}}$ are the reaction forces *by* the beam *on* the payload.

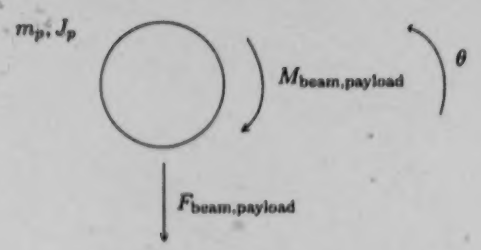

Figure 7.3: Free-body diagram of payload

Force balance

$$\begin{aligned}
\sum F &= m_p \frac{\partial^2}{\partial t^2}\Big(L\theta(t) + V(L,t)\Big) \\
-F_{\text{beam,payload}} &= m_p \frac{\partial^2}{\partial t^2}\Big(L\theta(t) + V(L,t)\Big) \\
F_{\text{beam,payload}} &= -m_p \frac{\partial^2}{\partial t^2}\Big(V(L,t) + L\theta(t)\Big)
\end{aligned} \tag{7.10}$$

Moment balance

$$\begin{aligned}
\sum M &= J_p \frac{\partial^2}{\partial t^2}\left(\theta(t) + \frac{\partial V(L,t)}{\partial x}\right) \\
-M_{\text{beam,payload}} &= J_p \frac{\partial^2}{\partial t^2}\left(\theta(t) + \frac{\partial V(L,t)}{\partial x}\right) \\
M_{\text{beam,payload}} &= -J_p \frac{\partial^2}{\partial t^2}\left(\frac{\partial V(L,t)}{\partial x} + \theta(t)\right)
\end{aligned} \tag{7.11}$$

Next, we look at the hub, shown in Figure 7.4, and perform a moment balance. The term $M_{\text{beam,hub}}$ represents the reaction *by* the beam *on* the hub.

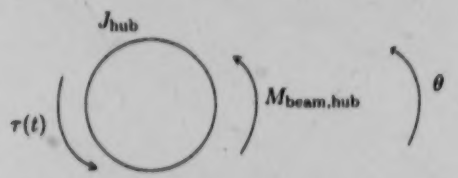

Figure 7.4: Free-body diagram of hub

$$\begin{aligned}
\sum M &= J_{\text{hub}} \frac{d^2\theta(t)}{dt^2} \\
M_{\text{beam,hub}} + \tau(t) &= J_{\text{hub}} \frac{d^2\theta(t)}{dt^2} \\
M_{\text{beam,hub}} &= J_{\text{hub}} \frac{d^2\theta}{dt^2} - \tau(t)
\end{aligned} \tag{7.12}$$

Finally, we consider the forces acting on the beam in Figure 7.5. Note the payload and hub reaction forces and moments are reversed in direction from Figures 7.3 and 7.4 by Newton's third law.

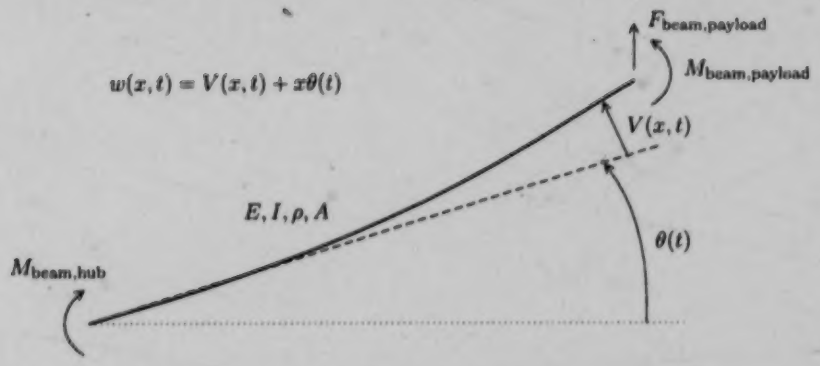

Figure 7.5: Forces and moments acting on Rayleigh beam

We now write down the Rayleigh beam equation, defining $w(x,t) = V(x,t) + x\theta(t)$ as the deflection field formulated in an inertial frame of reference; $V(x,t)$ is formulated in a rotating (non-inertial) frame, so it cannot be used by itself in the equations of motion. Recalling equation (7.7),

$$EI\frac{\partial^4 w(x,t)}{\partial x^4} - \rho I\frac{\partial^4 w(x,t)}{\partial x^2 \partial t^2} + \rho A\frac{\partial^2 w(x,t)}{\partial t^2} = 0 \tag{7.13}$$

We have the beam boundary conditions

$$\begin{aligned} w(0,t) &= 0 & \frac{\partial^2 w(L,t)}{\partial x^2} &= \frac{M_{\text{beam,payload}}}{EI} \\ \frac{\partial^2 w(0,t)}{\partial x^2} &= \frac{M_{\text{beam,hub}}}{EI} & \frac{\partial^3 w(L,t)}{\partial x^3} - \frac{\rho}{E}\frac{\partial^3 w(L,t)}{\partial t^2 \partial x} &= \frac{-F_{\text{beam,payload}}}{EI} \end{aligned} \tag{7.14}$$

Note (7.14) respect the directional convention for forces and moments discussed in Section 7.1.2.

For the hub side, using (7.12),

$$\frac{\partial^2 w(0,t)}{\partial x^2} = \frac{1}{EI}\left(J_{\text{hub}}\frac{d^2\theta(t)}{dt^2} - \tau(t)\right) \tag{7.15}$$

By the definition of $w(x,t)$,

$$\begin{aligned} \frac{\partial w(x,t)}{\partial x} &= \frac{\partial V(x,t)}{\partial x} + \theta(t) \\ \frac{\partial w(0,t)}{\partial x} &= \underbrace{\frac{\partial V(0,t)}{\partial x}}_{=0} + \theta(t) \\ \theta(t) &= \frac{\partial w(0,t)}{\partial x} \end{aligned} \tag{7.16}$$

Using (7.16) in (7.15), we obtain

$$\begin{aligned} \frac{\partial^2 w(0,t)}{\partial x^2} &= \frac{1}{EI}\left(J_{\text{hub}}\frac{\partial^3 w(0,t)}{\partial t^2 \partial x} - \tau(t)\right) \\ J_{\text{hub}}\frac{\partial^3 w(0,t)}{\partial t^2 \partial x} - EI\frac{\partial^2 w(0,t)}{\partial x^2} &= \tau(t) \end{aligned} \tag{7.17}$$

We now look at the right-hand side BCs. Using (7.11) and the definition of $w(x,t)$, we get

$$\frac{\partial^2 w(L,t)}{\partial x^2} = \frac{-J_p}{EI}\frac{\partial^2}{\partial t^2}\left(\frac{\partial w(L,t)}{\partial x}\right)$$
$$\frac{\partial^2 w(L,t)}{\partial x^2} = \frac{-J_p}{EI}\frac{\partial^3 w(L,t)}{\partial t^2 \partial x} \tag{7.18}$$

Using (7.10) in the fourth BC,

$$\frac{\partial^3 w(L,t)}{\partial x^3} - \frac{\rho}{E}\frac{\partial^3 w(L,t)}{\partial t^2 \partial x} = \frac{m_p}{EI}\frac{\partial^2 w(L,t)}{\partial t^2} \tag{7.19}$$

Putting (7.14), (7.17), (7.18) and (7.19) together with (7.13) gives us the PDE problem formulation for a Rayleigh beam with boundary torque input and tip payload:

$$EI\frac{\partial^4 w(x,t)}{\partial x^4} - \rho I\frac{\partial^4 w(x,t)}{\partial x^2 \partial t^2} + \rho A\frac{\partial^2 w(x,t)}{\partial t^2} = 0 \quad 0 < x < L \tag{7.20}$$

BCs:

$$w(0,t) = 0 \qquad \frac{\partial^2 w(L,t)}{\partial x^2} = \frac{-J_p}{EI}\frac{\partial^3 w(L,t)}{\partial t^2 \partial x}$$
$$J_{\text{hub}}\frac{\partial^3 w(0,t)}{\partial t^2 \partial x} - EI\frac{\partial^2 w(0,t)}{\partial x^2} = \tau(t) \quad \frac{\partial^3 w(L,t)}{\partial x^3} - \frac{\rho}{E}\frac{\partial^3 w(L,t)}{\partial t^2 \partial x} = \frac{m_p}{EI}\frac{\partial^2 w(L,t)}{\partial t^2} \tag{7.21}$$

The last step is to define the new term

$$S = \frac{I}{A}$$

Using S, (7.20) becomes

$$EI\frac{\partial^4 w(x,t)}{\partial x^4} - \rho AS\frac{\partial^4 w(x,t)}{\partial x^2 \partial t^2} + \rho A\frac{\partial^2 w(x,t)}{\partial t^2} = 0 \quad 0 < x < L \tag{7.22}$$

and (7.21) becomes

$$w(0,t) = 0 \qquad \frac{\partial^2 w(L,t)}{\partial x^2} = \frac{-J_p}{EI}\frac{\partial^3 w(L,t)}{\partial t^2 \partial x}$$
$$J_{\text{hub}}\frac{\partial^3 w(0,t)}{\partial t^2 \partial x} - EI\frac{\partial^2 w(0,t)}{\partial x^2} = \tau(t) \quad EI\frac{\partial^3 w(L,t)}{\partial x^3} - \rho AS\frac{\partial^3 w(L,t)}{\partial t^2 \partial x} = m_p\frac{\partial^2 w(L,t)}{\partial t^2} \tag{7.23}$$

The reason for introducing S is that it represents the rotary inertia effect; by setting $S = 0$, the PDE and BC terms simplify to the Euler-Bernoulli case [73]. For the flexible beam experiment, using Table 2.1, we calculate

$$S = 5.3333 \times 10^{-8}$$

meaning that the rotary inertia of the flexible beam is negligibly small for the experimental plant we are working with.

7.3 Alternative Series Solution

In this section we give the full details of the open-loop control using special basis functions. This calculation approach first appeared in [2], and is reprinted in [63, Section 5.4], although both references skip the calculation steps and only give the final solution.

7.4 Normalizing the Boundary-Value Problem

The example we will be working with is a rotating Euler-Bernoulli beam with a tip payload. The system model is immediately obtained by setting $S = 0$ in (7.22) and (7.23):

$$\begin{aligned} &EI\frac{\partial^4 w(x,t)}{\partial x^4} + \rho A\frac{\partial^2 w(x,t)}{\partial t^2} = 0 \qquad 0 < x < L \\ &w(0,t) = 0 \qquad\qquad \frac{\partial^2 w(L,t)}{\partial x^2} = \frac{-J_p}{EI}\frac{\partial^3 w(L,t)}{\partial t^2 \partial x} \\ &J_{\text{hub}}\frac{\partial^3 w(0,t)}{\partial t^2 \partial x} - EI\frac{\partial^2 w(0,t)}{\partial x^2} = \tau(t) \qquad EI\frac{\partial^3 w(L,t)}{\partial x^3} = m_p\frac{\partial^2 w(L,t)}{\partial t^2} \end{aligned} \tag{7.24}$$

A method to reduce the complexity of the series expressions is to replace the torque input boundary condition, by assuming $\theta(t)$ is the input and writing the torque relationship as a separate ODE. This gives the BVP

$$\begin{aligned} &EI\frac{\partial^4 w(x,t)}{\partial x^4} + \rho A\frac{\partial^2 w(x,t)}{\partial t^2} = 0 \qquad 0 < x < L \\ &w(0,t) = 0 \qquad\qquad \frac{\partial^2 w(L,t)}{\partial x^2} = \frac{-J_p}{EI}\frac{\partial^3 w(L,t)}{\partial t^2 \partial x} \\ &\frac{\partial w(0,t)}{\partial x} = \theta(t) \qquad EI\frac{\partial^3 w(L,t)}{\partial x^3} = m_p\frac{\partial^2 w(L,t)}{\partial t^2} \end{aligned} \tag{7.25}$$

with input equation

$$\tau(t) = J_{\text{hub}}\frac{\partial^3 w(0,t)}{\partial t^2 \partial x} - EI\frac{\partial^2 w(0,t)}{\partial x^2} \tag{7.26}$$

The BVP (7.25) is now normalized by introducing the change of variables

$$\tilde{x} = \frac{x}{L} \qquad \tilde{t} = \frac{t\sqrt{EI}}{L^2\sqrt{\rho A}} \qquad \tilde{w}(\tilde{x},\tilde{t}) = w(x,t) \tag{7.27}$$

transforming (7.25) into

$$\begin{aligned} &EI\frac{\partial^4 \tilde{w}(\tilde{x},\tilde{t})}{\partial x^4} + \rho A\frac{\partial^2 \tilde{w}(\tilde{x},\tilde{t})}{\partial t^2} = 0 \qquad 0 < \tilde{x} < 1 \\ &\tilde{w}(0,\tilde{t}) = 0 \qquad\qquad \frac{\partial^2 \tilde{w}(1,\tilde{t})}{\partial x^2} = \frac{-J_p}{EI}\frac{\partial^3 \tilde{w}(1,\tilde{t})}{\partial t^2 \partial x} \\ &\frac{\partial \tilde{w}(0,\tilde{t})}{\partial x} = \theta\left(\frac{\tilde{t}L^2\sqrt{\rho A}}{\sqrt{EI}}\right) \qquad EI\frac{\partial^3 \tilde{w}(1,\tilde{t})}{\partial x^3} = m_p\frac{\partial^2 \tilde{w}(1,\tilde{t})}{\partial t^2} \end{aligned} \tag{7.28}$$

Note that

$$\begin{aligned} &\frac{\partial \tilde{w}}{\partial x} = \frac{\partial \tilde{w}}{\partial \tilde{x}}\frac{d\tilde{x}}{dx} = \frac{1}{L}\frac{\partial \tilde{w}}{\partial \tilde{x}} \\ &\frac{\partial^2 \tilde{w}}{\partial x} = \frac{\partial}{\partial x}\left(\frac{\partial \tilde{w}}{\partial x}\right) = \frac{\partial}{\partial x}\left(\frac{1}{L}\frac{\partial \tilde{w}}{\partial \tilde{x}}\right) = \frac{1}{L}\frac{\partial}{\partial \tilde{x}}\left(\frac{\partial \tilde{w}}{\partial \tilde{x}}\right)\frac{d\tilde{x}}{dx} = \frac{1}{L^2}\frac{\partial^2 \tilde{w}}{\partial \tilde{x}^2} \\ &\frac{\partial^3 \tilde{w}}{\partial x^3} = \cdots = \frac{1}{L^3}\frac{\partial^3 \tilde{w}}{\partial \tilde{x}^3} \\ &\frac{\partial^4 \tilde{w}}{\partial x^4} = \cdots = \frac{1}{L^4}\frac{\partial^4 \tilde{w}}{\partial \tilde{x}^4} \end{aligned}$$

Also,

$$\begin{aligned} &\frac{\partial \tilde{w}}{\partial t} = \frac{\partial \tilde{w}}{\partial \tilde{t}}\frac{d\tilde{t}}{dt} = \frac{\sqrt{EI}}{L^2\sqrt{\rho A}}\frac{\partial \tilde{w}}{\partial \tilde{t}} \\ &\frac{\partial^2 \tilde{w}}{\partial t^2} = \frac{\partial}{\partial t}\left(\frac{\partial \tilde{w}}{\partial t}\right) = \frac{\partial}{\partial t}\left(\frac{\sqrt{EI}}{L^2\sqrt{\rho A}}\frac{\partial \tilde{w}}{\partial \tilde{t}}\right) = \frac{\partial}{\partial \tilde{t}}\left(\frac{\sqrt{EI}}{L^2\sqrt{\rho A}}\frac{\partial \tilde{w}}{\partial \tilde{t}}\right)\frac{d\tilde{t}}{dt} = \frac{EI}{L^4\rho A}\left(\frac{\partial^2 \tilde{w}}{\partial \tilde{t}^2}\right) \end{aligned}$$

Expression (7.28) becomes

$$EI\frac{1}{L^4}\frac{\partial^4\widetilde{w}(\widetilde{x},\widetilde{t})}{\partial\widetilde{x}^4}+\rho A\frac{EI}{L^4\rho A}\frac{\partial^2\widetilde{w}(\widetilde{x},\widetilde{t})}{\partial\widetilde{t}^2}=0 \qquad 0<\widetilde{x}<1$$

$$\widetilde{w}(0,\widetilde{t})=0 \qquad \frac{1}{L^2}\frac{\partial^2\widetilde{w}(1,\widetilde{t})}{\partial\widetilde{x}^2}=\frac{-J_p}{EI}\frac{EI}{L^5\rho A}\frac{\partial^3\widetilde{w}(1,\widetilde{t})}{\partial\widetilde{t}^2\partial\widetilde{x}}$$

$$\frac{1}{L}\frac{\partial\widetilde{w}(0,\widetilde{t})}{\partial\widetilde{x}}=\theta\left(\frac{\widetilde{t}L^2\sqrt{\rho A}}{\sqrt{EI}}\right) \qquad EI\frac{1}{L^3}\frac{\partial^3\widetilde{w}(1,\widetilde{t})}{\partial\widetilde{x}^3}=m_p\frac{EI}{L^4\rho A}\frac{\partial^2\widetilde{w}(1,\widetilde{t})}{\partial\widetilde{t}^2}$$

which simplifies to

$$\begin{aligned}
&\frac{\partial^4\widetilde{w}(\widetilde{x},\widetilde{t})}{\partial\widetilde{x}^4}+\frac{\partial^2\widetilde{w}(\widetilde{x},\widetilde{t})}{\partial\widetilde{t}^2}=0 \qquad 0<\widetilde{x}<1\\
&\widetilde{w}(0,\widetilde{t})=0 \qquad \frac{\partial^2\widetilde{w}(1,\widetilde{t})}{\partial\widetilde{x}^2}=-\lambda\frac{\partial^3\widetilde{w}(1,\widetilde{t})}{\partial\widetilde{t}^2\partial\widetilde{x}}\\
&\frac{\partial\widetilde{w}(0,\widetilde{t})}{\partial\widetilde{x}}=\widetilde{u}\left(\widetilde{t}\right) \qquad \frac{\partial^3\widetilde{w}(1,\widetilde{t})}{\partial\widetilde{x}^3}=\mu\frac{\partial^2\widetilde{w}(1,\widetilde{t})}{\partial\widetilde{t}^2}
\end{aligned} \tag{7.29}$$

where

$$\lambda=\frac{J_p}{L^3\rho A} \qquad \mu=\frac{m_p}{L\rho A} \qquad \widetilde{u}\left(\widetilde{t}\right)=L\theta\left(\frac{\widetilde{t}L^2\sqrt{\rho A}}{\sqrt{EI}}\right)$$

BVP (7.29) is the normalized version of the original expression (7.25). The normalization eliminates the leading constants from the PDE and sets the space interval to unit length, which makes the equations easier to work with. After an expression for the $\widetilde{w}(\widetilde{x},\widetilde{t})$ field is found, the normalization will be undone to produce $w(x,t)$ in the original coordinates, and equation (7.26) will be used to obtain $\tau(t)$, the boundary torque input expression.

7.5 Assumed Solution of Normalized BVP

For the purposes of this section, we will temporarily drop the $\widetilde{\ }$ superscripts from all variables. This is done because the operator s does not have any superscripts, and to avoid confusion with the $\bar{\ }$ superscript notation introduced soon. However, it must be remembered that we are still working with normalized variables, and the normalization will need to be undone after the series manipulations are carried out.

The Laplace transform is applied to BVP (7.29), leading to

$$\frac{\partial^4 W(x,s)}{\partial x^4}+s^2W(x,s)=0 \tag{7.30}$$

$$\begin{aligned}
&W(0,s)=0 \qquad \frac{\partial^2 W(1,s)}{\partial x^2}=-\lambda s^2\frac{\partial W(1,s)}{\partial x}\\
&\frac{\partial W(0,s)}{\partial x}=U(s) \qquad \frac{\partial^3 W(1,s)}{\partial x^3}=\mu s^2 W(1,s)
\end{aligned} \tag{7.31}$$

We previously expressed the solution to (7.30) as a linear combination of trigonometric functions, (3.7). Following [2], the solution takes the alternative form

$$W(x,s)=a(s)C^+(x)+b(s)C^-(x)+c(s)S^+(x)+d(s)S^-(x) \tag{7.32}$$

With basis functions

$$\begin{aligned} C^+(x) &= \frac{C(x)+\overline{C}(x)}{2} \\ C^-(x) &= \frac{C(x)-\overline{C}(x)}{2i} \\ S^+(x) &= \frac{\overline{S}(x)+iS(x)}{2h\sqrt{s}} \\ S^-(x) &= \frac{-\overline{S}(x)+iS(x)}{2\bar{h}\sqrt{s}} \end{aligned} \tag{7.33}$$

Where $\overline{\ }$ denotes the complex conjugate, and

$$\begin{aligned} C(x) &= \cosh[h\sqrt{s}(1-x)] & \overline{C}(x) &= \cosh[\bar{h}\sqrt{s}(1-x)] \\ S(x) &= \sinh[h\sqrt{s}(1-x)] & \overline{S}(x) &= \sinh[\bar{h}\sqrt{s}(1-x)] \\ h &= \sqrt{i} & \bar{h} &= \sqrt{-i} \end{aligned} \tag{7.34}$$

It can be verified that (7.32) satisfies the governing equation (7.30). Further, the basis functions (7.33) have properties which make the series manipulations easier, as will be seen shortly.

It can be verified that

$$\begin{aligned} \frac{\partial S^-(x)}{\partial x} &= C^+(x) \\ \frac{\partial S^+(x)}{\partial x} &= C^-(x) \\ \frac{\partial C^+(x)}{\partial x} &= -sS^+(x) \\ \frac{\partial C^-(x)}{\partial x} &= sS^-(x) \end{aligned}$$

Using the above when differentiating (7.32) gives

$$\begin{aligned} \frac{\partial W(x,s)}{\partial x} &= -a(s)sS^+(x) + b(s)sS^-(x) + c(s)C^-(x) + d(s)C^+(x) \\ \frac{\partial^2 W(x,s)}{\partial x^2} &= -a(s)sC^-(x) + b(s)sC^+(x) + c(s)sS^-(x) - d(s)sS^+(x) \\ \frac{\partial^3 W(x,s)}{\partial x^3} &= -a(s)s^2S^-(x) - b(s)s^2S^+(x) + c(s)sC^+(x) - d(s)sC^-(x) \end{aligned}$$

At $x = 1$, the expressions simplify considerably

$$\begin{aligned} C(1) &= \cosh(0) = 1 & S(1) &= \sinh(0) = 0 \\ \overline{C}(1) &= 1 & \overline{S}(1) &= 0 \\ C^+(1) &= \frac{1+1}{2} = 1 & C^-(1) &= \frac{1-1}{2i} = 0 \\ S^+(1) &= \frac{0+i0}{2h\sqrt{s}} = 0 & S^-(1) &= \frac{-0+i0}{2\bar{h}\sqrt{s}} = 0 \end{aligned}$$

At $x = 0$, the terms do not simplify, so we leave them unevaluated. For compactness, we will denote

$$\begin{aligned} C^+(0) &= C_0^+ & S^+(0) &= S_0^+ \\ C^-(0) &= C_0^- & S^-(0) &= S_0^- \end{aligned}$$

Making use of the BCs (7.31), we obtain a system of four equations in four unknowns $\{a(s), b(s), c(s), d(s)\}$. The (s) will be dropped at this point, again for compactness.

$$\begin{aligned} aC_0^+ + bC_0^- + cS_0^+ + dS_0^- &= 0 \\ -asS_0^+ + bsS_0^- + cC_0^- + dC_0^+ &= U(s) \\ b &= -\lambda sd \\ c &= \mu sa \end{aligned}$$

The system of linear equations is particularly easy to solve for this choice of basis. Subbing the expressions for b and c into the first two equations gives

$$\begin{aligned} aC_0^+ - \lambda sdC_0^- + \mu saS_0^+ + dS_0^- &= 0 \\ -asS_0^+ - \lambda s^2 dS_0^- + \mu saC_0^- + dC_0^+ &= U(s) \end{aligned}$$

Gathering terms,

$$\begin{aligned} a[C_0^+ + \mu sS_0^+] &= d[\lambda sC_0^- - S_0^-] \\ a[\mu sC_0^- - sS_0^+] + d[C_0^+ - \lambda s^2 S_0^-] &= U(s) \end{aligned}$$

The first equation above gives

$$a = d\frac{[\lambda sC_0^- - S_0^-]}{[C_0^+ + \mu sS_0^+]}$$

Subbing into the second expression gives

$$\begin{aligned} d\frac{[\lambda sC_0^- - S_0^-][\mu sC_0^- - sS_0^+]}{[C_0^+ + \mu sS_0^+]} + d[C_0^+ - \lambda s^2 S_0^-] &= U(s) \\ \frac{[\lambda sC_0^- - S_0^-][\mu sC_0^- - sS_0^+] + [C_0^+ - \lambda s^2 S_0^-][C_0^+ + \mu sS_0^+]}{[C_0^+ + \mu sS_0^+]} d &= U(s) \end{aligned}$$

$$\begin{aligned} d &= \frac{[C_0^+ + \mu sS_0^+]U(s)}{[\lambda sC_0^- - S_0^-][\mu sC_0^- - sS_0^+] + [C_0^+ - \lambda s^2 S_0^-][C_0^+ + \mu sS_0^+]} \\ a &= \frac{[\lambda sC_0^- - S_0^-]U(s)}{[\lambda sC_0^- - S_0^-][\mu sC_0^- - sS_0^+] + [C_0^+ - \lambda s^2 S_0^-][C_0^+ + \mu sS_0^+]} \\ c &= \frac{\mu s[\lambda sC_0^- - S_0^-]U(s)}{[\lambda sC_0^- - S_0^-][\mu sC_0^- - sS_0^+] + [C_0^+ - \lambda s^2 S_0^-][C_0^+ + \mu sS_0^+]} \\ b &= \frac{-\lambda s[C_0^+ + \mu sS_0^+]U(s)}{[\lambda sC_0^- - S_0^-][\mu sC_0^- - sS_0^+] + [C_0^+ - \lambda s^2 S_0^-][C_0^+ + \mu sS_0^+]} \end{aligned}$$

Returning to (7.32), dropping (x) for compactness, leads to

$$\begin{aligned} & W(x,s) \\ &= \frac{[\lambda sC_0^- - S_0^-]C^+ - \lambda s[C_0^+ + \mu sS_0^+]C^- + \mu s[\lambda sC_0^- - S_0^-]S^+ + [C_0^+ + \mu sS_0^+]S^-}{[\lambda sC_0^- - S_0^-][\mu sC_0^- - sS_0^+] + [C_0^+ - \lambda s^2 S_0^-][C_0^+ + \mu sS_0^+]} U(s) \\ &= \frac{[\lambda sC_0^- - S_0^-][C^+ + \mu sS^+] + [C_0^+ + \mu sS_0^+][S^- - \lambda sC^-]}{[\lambda sC_0^- - S_0^-][\mu sC_0^- - sS_0^+] + [C_0^+ - \lambda s^2 S_0^-][C_0^+ + \mu sS_0^+]} U(s) \\ &= \frac{P(x,s)}{Q(x,s)} U(s) \end{aligned} \tag{7.35}$$

Where (7.35) is equivalent to the form (3.9), obtained during the earlier series manipulations using trigonometric basis functions. The system is parameterized as before,

$$\begin{aligned} W(x,s) &= P(x,s)Y(s) \\ U(s) &= Q(x,s)Y(s) \end{aligned} \tag{7.36}$$

where $Y(s)$ is the transformed flat output.

7.6 Series Manipulations

We now need to manipulate the s-domain expressions (7.36) to factor out the s operator, which will allow us to perform an inverse Laplace transform. We only need to work with the $P(x,s)$ term, because once $w(x,t)$ is found and returned to the original coordinates, the system input $\tau(t)$ will be given by (7.26), so inverting the $Q(x,s)Y(s)$ term in unnecessary.

Starting from (7.35), we expand $P(x,s)$ and express it in terms of C and S components according to (7.33):

$$
\begin{aligned}
P(x,s) &= \lambda s C_0^- C^+ + \lambda\mu s^2 C_0^- S^+ - S_0^- C^+ - \mu s S_0^- S^+ + C_0^+ S^- - \lambda s C_0^+ C^- + \mu s S_0^+ S^- \\
&\quad - \lambda\mu s^2 S_0^+ C^- \\
&= \lambda s\left(\frac{C_0-\overline{C}_0}{2i}\right)\left(\frac{C+\overline{C}}{2}\right) + \lambda\mu s^2\left(\frac{C_0-\overline{C}_0}{2i}\right)\left(\frac{\overline{S}+iS}{2h\sqrt{s}}\right) \\
&\quad - \left(\frac{-\overline{S}_0+iS_0}{2h\sqrt{s}}\right)\left(\frac{C+\overline{C}}{2}\right) - \mu s\left(\frac{-\overline{S}_0+iS_0}{2h\sqrt{s}}\right)\left(\frac{\overline{S}+iS}{2h\sqrt{s}}\right) \\
&\quad + \left(\frac{C_0+\overline{C}_0}{2}\right)\left(\frac{-\overline{S}+iS}{2h\sqrt{s}}\right) - \lambda s\left(\frac{C_0+\overline{C}_0}{2}\right)\left(\frac{C-\overline{C}}{2i}\right) \\
&\quad + \mu s\left(\frac{\overline{S}_0+iS_0}{2h\sqrt{s}}\right)\left(\frac{-\overline{S}+iS}{2h\sqrt{s}}\right) - \lambda\mu s^2\left(\frac{\overline{S}_0+iS_0}{2h\sqrt{s}}\right)\left(\frac{C-\overline{C}}{2i}\right) \\
&= \frac{\lambda s}{4i}\Big(C_0C + C_0\overline{C} - \overline{C}_0C - \overline{C}_0\overline{C}\Big) + \frac{\lambda\mu s^2}{4ih\sqrt{s}}\Big(C_0\overline{S} + iC_0S - \overline{C}_0\overline{S} - i\overline{C}_0S\Big) \\
&\quad - \frac{1}{4h\sqrt{s}}\Big(-\overline{S}_0C - \overline{S}_0\overline{C} + iS_0C + iS_0\overline{C}\Big) - \frac{\mu}{4}\Big(-\overline{S}_0\overline{S} - i\overline{S}_0S + iS_0\overline{S} - S_0S\Big) \\
&\quad + \frac{1}{4h\sqrt{s}}\Big(-C_0\overline{S} + iC_0S - \overline{C}_0\overline{S} + i\overline{C}_0S\Big) - \frac{\lambda s}{4i}\Big(C_0C - C_0\overline{C} + \overline{C}_0C - \overline{C}_0\overline{C}\Big) \\
&\quad + \frac{\mu}{4}\Big(-\overline{S}_0\overline{S} + i\overline{S}_0S - iS_0\overline{S} - S_0S\Big) - \frac{\lambda\mu s^2}{4ih\sqrt{s}}\Big(\overline{S}_0C - \overline{S}_0\overline{C} + iS_0C - iS_0\overline{C}\Big) \\
&= \frac{\lambda s}{2i}\Big(C_0\overline{C} - \overline{C}_0C\Big) - \frac{\mu}{2}\Big(-i\overline{S}_0S + iS_0\overline{S}\Big) \\
&\quad + \frac{\lambda\mu s^2}{4ih\sqrt{s}}\Big(C_0\overline{S} + iC_0S - \overline{C}_0\overline{S} - i\overline{C}_0S - \overline{S}_0C + \overline{S}_0\overline{C} - iS_0C + iS_0\overline{C}\Big) \\
&\quad - \frac{1}{4h\sqrt{s}}\Big(-\overline{S}_0C - \overline{S}_0\overline{C} + iS_0C + iS_0\overline{C} + C_0\overline{S} - iC_0S + \overline{C}_0\overline{S} - i\overline{C}_0S\Big) \\
&= \frac{\lambda s}{2i}\Big(C_0\overline{C} - \overline{C}_0C\Big) - \frac{\mu}{2}\Big(-i\overline{S}_0S + iS_0\overline{S}\Big) \\
&\quad + \frac{\lambda\mu s^2}{4h\sqrt{s}}\Big(-C_0\overline{S} - iC_0S + \overline{C}_0\overline{S} + i\overline{C}_0S + \overline{S}_0C - \overline{S}_0\overline{C} + iS_0C - iS_0\overline{C}\Big) \\
&\quad - \frac{1}{4h\sqrt{s}}\Big(-\overline{S}_0C - \overline{S}_0\overline{C} + iS_0C + iS_0\overline{C} + C_0\overline{S} - iC_0S + \overline{C}_0\overline{S} - i\overline{C}_0S\Big) \\
P(x,s) &= \underbrace{\frac{\lambda s}{2i}\Big(C_0\overline{C} - \overline{C}_0C\Big)}_{I} + \underbrace{\left(\frac{\lambda\mu s^2-1}{4h\sqrt{s}}\right)\Big(-iC_0S + \overline{C}_0\overline{S} - \overline{S}_0\overline{C} + iS_0C\Big)}_{II} \\
&\quad + \underbrace{\left(\frac{\lambda\mu s^2+1}{4h\sqrt{s}}\right)\Big(-C_0\overline{S} + i\overline{C}_0S + \overline{S}_0C - iS_0\overline{C}\Big)}_{III} - \underbrace{\frac{\mu}{2}\Big(-i\overline{S}_0S + iS_0\overline{S}\Big)}_{IV}
\end{aligned}
$$

The $P(x,s)$ expression has been split into four sub-groups in the last line above. These will be analyzed separately in the following subsections.

7.6.1 Part I of $P(x,s)$

$$
\begin{aligned}
&= \frac{\lambda s}{2i}\left[C_0\overline{C} - \overline{C}_0 C\right] \\
&= \frac{\lambda s}{2i}\left[\cosh(h\sqrt{s})\cosh[\bar{h}\sqrt{s}(1-x)] - \cosh[\bar{h}\sqrt{s}]\cosh[h\sqrt{s}(1-x)]\right] \\
&= \frac{\lambda s}{2i}\left[\left(\frac{e^{h\sqrt{s}}+e^{-h\sqrt{s}}}{2}\right)\left(\frac{e^{\bar{h}\sqrt{s}(1-x)}+e^{-\bar{h}\sqrt{s}(1-x)}}{2}\right)\right. \\
&\qquad \left. - \left(\frac{e^{\bar{h}\sqrt{s}}+e^{-\bar{h}\sqrt{s}}}{2}\right)\left(\frac{e^{h\sqrt{s}(1-x)}+e^{-h\sqrt{s}(1-x)}}{2}\right)\right] \\
&= \frac{\lambda s}{8i}\left[e^{h\sqrt{s}+\bar{h}\sqrt{s}(1-x)} + e^{h\sqrt{s}-\bar{h}\sqrt{s}(1-x)} + e^{-h\sqrt{s}+\bar{h}\sqrt{s}(1-x)} + e^{-h\sqrt{s}-\bar{h}\sqrt{s}(1-x)}\right. \\
&\qquad \left. - e^{\bar{h}\sqrt{s}+h\sqrt{s}(1-x)} - e^{\bar{h}\sqrt{s}-h\sqrt{s}(1-x)} - e^{-\bar{h}\sqrt{s}+h\sqrt{s}(1-x)} - e^{-\bar{h}\sqrt{s}-h\sqrt{s}(1-x)}\right] \\
&= \frac{\lambda s}{8i}\left[e^{i\bar{h}\sqrt{s}+h\sqrt{s}(1-x)} + e^{i\bar{h}\sqrt{s}-h\sqrt{s}(1-x)} + e^{-i\bar{h}\sqrt{s}+h\sqrt{s}(1-x)} + e^{-i\bar{h}\sqrt{s}-h\sqrt{s}(1-x)}\right. \\
&\qquad \left. - e^{-i\bar{h}\sqrt{s}+h\sqrt{s}(1-x)} - e^{-i\bar{h}\sqrt{s}-h\sqrt{s}(1-x)} - e^{i\bar{h}\sqrt{s}+h\sqrt{s}(1-x)} - e^{i\bar{h}\sqrt{s}-h\sqrt{s}(1-x)}\right] \\
&= \frac{\lambda s}{8i}\left[e^{\bar{h}\sqrt{s}(1+i-x)} + e^{\bar{h}\sqrt{s}(i-1+x)} + e^{\bar{h}\sqrt{s}(-i+1-x)} + e^{\bar{h}\sqrt{s}(-i-1+x)}\right. \\
&\qquad \left. - e^{h\sqrt{s}(1-i-x)} - e^{h\sqrt{s}(-i-1+x)} - e^{h\sqrt{s}(i+1-x)} - e^{h\sqrt{s}(i-1+x)}\right] \\
&= \frac{\lambda s}{4i}\left[\frac{e^{\bar{h}\sqrt{s}(1+i-x)}+e^{-\bar{h}\sqrt{s}(i+1-x)}}{2} + \frac{e^{\bar{h}\sqrt{s}(1-i-x)}+e^{-\bar{h}\sqrt{s}(1-i-x)}}{2}\right. \\
&\qquad \left. - \left(\frac{e^{h\sqrt{s}(1-i-x)}+e^{-h\sqrt{s}(1-i-x)}}{2}\right) - \left(\frac{e^{h\sqrt{s}(1+i-x)}+e^{-h\sqrt{s}(1+i-x)}}{2}\right)\right] \\
&= \frac{\lambda s}{4i}\left[\cosh[\bar{h}\sqrt{s}(1+i-x)] + \cosh[\bar{h}\sqrt{s}(1-i-x)]\right. \\
&\qquad \left. - \cosh[h\sqrt{s}(1-i-x)] - \cosh[h\sqrt{s}(1+i-x)]\right] \\
&= \frac{-\lambda s}{2}\left[\frac{\cosh[h\sqrt{s}(1+i-x)] - \cosh[\bar{h}\sqrt{s}(1+i-x)]}{2i}\right. \\
&\qquad \left. + \frac{\cosh[h\sqrt{s}(1-i-x)] - \cosh[\bar{h}\sqrt{s}(1-i-x)]}{2i}\right] \\
&= \frac{-\lambda s}{2}\left[\underbrace{C_x^-(1+i-x) + C_x^-(1-i-x)}_{\text{conjugates}}\right] \\
&= -\lambda s\,\mathrm{Re}\left\{C_x^-(1+i-x)\right\}
\end{aligned}
$$

Where we have introduced a new term for compactness,

$$C_x^-(x) \equiv \frac{\cosh[h\sqrt{s}\,x] - \cosh[\bar{h}\sqrt{s}\,x]}{2i} \tag{7.37}$$

which is very similar, *but not identical to*, the $C^-(x)$ term in (7.33); the x subscript is used to differentiate between the two. The fact that

$$C_x^-(z) = \overline{C_x^-(\bar{z})} \qquad z \in \mathbf{C}$$

can be directly verified.

7.6.2 Part II of $P(x,s)$

$$
\begin{aligned}
&= \frac{\lambda\mu s^2-1}{4\bar{h}\sqrt{s}}\Big[-iC_0S+\overline{C}_0\overline{S}-\overline{S}_0\overline{C}+iS_0C\Big]\\
&= \frac{\lambda\mu s^2-1}{4\bar{h}\sqrt{s}}\Big[-i\cosh[h\sqrt{s}]\sinh[h\sqrt{s}(1-x)]+\cosh[\bar{h}\sqrt{s}]\sinh[\bar{h}\sqrt{s}(1-x)]\\
&\qquad -\sinh[\bar{h}\sqrt{s}]\cosh[\bar{h}\sqrt{s}(1-x)]+i\sinh[h\sqrt{s}]\cosh[h\sqrt{s}(1-x)]\Big]\\
&= \frac{\lambda\mu s^2-1}{4\bar{h}\sqrt{s}}\Big[-i\left(\frac{e^{h\sqrt{s}}+e^{-h\sqrt{s}}}{2}\right)\left(\frac{e^{h\sqrt{s}(1-x)}-e^{-h\sqrt{s}(1-x)}}{2}\right)\\
&\qquad +\left(\frac{e^{\bar{h}\sqrt{s}}+e^{-\bar{h}\sqrt{s}}}{2}\right)\left(\frac{e^{\bar{h}\sqrt{s}(1-x)}-e^{-\bar{h}\sqrt{s}(1-x)}}{2}\right)\\
&\qquad -\left(\frac{e^{\bar{h}\sqrt{s}}-e^{-\bar{h}\sqrt{s}}}{2}\right)\left(\frac{e^{\bar{h}\sqrt{s}(1-x)}+e^{-\bar{h}\sqrt{s}(1-x)}}{2}\right)\\
&\qquad +i\left(\frac{e^{h\sqrt{s}}-e^{-h\sqrt{s}}}{2}\right)\left(\frac{e^{h\sqrt{s}(1-x)}+e^{-h\sqrt{s}(1-x)}}{2}\right)\Big]\\
&= \frac{\lambda\mu s^2-1}{16\bar{h}\sqrt{s}}\Big[-i\Big(e^{h\sqrt{s}+\bar{h}\sqrt{s}(1-x)}-e^{h\sqrt{s}-\bar{h}\sqrt{s}(1-x)}+e^{-h\sqrt{s}+\bar{h}\sqrt{s}(1-x)}-e^{-h\sqrt{s}-\bar{h}\sqrt{s}(1-x)}\Big)\\
&\qquad +e^{\bar{h}\sqrt{s}+\bar{h}\sqrt{s}(1-x)}-e^{\bar{h}\sqrt{s}-\bar{h}\sqrt{s}(1-x)}+e^{-\bar{h}\sqrt{s}+\bar{h}\sqrt{s}(1-x)}-e^{-\bar{h}\sqrt{s}-\bar{h}\sqrt{s}(1-x)}\\
&\qquad -\Big(e^{\bar{h}\sqrt{s}+\bar{h}\sqrt{s}(1-x)}+e^{\bar{h}\sqrt{s}-\bar{h}\sqrt{s}(1-x)}-e^{-\bar{h}\sqrt{s}+\bar{h}\sqrt{s}(1-x)}-e^{-\bar{h}\sqrt{s}-\bar{h}\sqrt{s}(1-x)}\Big)\\
&\qquad +i\Big(e^{h\sqrt{s}+h\sqrt{s}(1-x)}+e^{h\sqrt{s}-h\sqrt{s}(1-x)}-e^{-h\sqrt{s}+h\sqrt{s}(1-x)}-e^{-h\sqrt{s}-h\sqrt{s}(1-x)}\Big)\Big]\\
&= \frac{\lambda\mu s^2-1}{16\bar{h}\sqrt{s}}\Big[-2e^{\bar{h}\sqrt{s}x}+2e^{-\bar{h}\sqrt{s}x}+2ie^{h\sqrt{s}x}-2ie^{-h\sqrt{s}x}\Big]\\
&= \frac{\lambda\mu s^2-1}{4\bar{h}\sqrt{s}}\Big[-\left(\frac{e^{\bar{h}\sqrt{s}x}-e^{-\bar{h}\sqrt{s}x}}{2}\right)+i\left(\frac{e^{h\sqrt{s}x}-e^{-h\sqrt{s}x}}{2}\right)\Big]\\
&= \frac{\lambda\mu s^2-1}{4\bar{h}\sqrt{s}}\Big[-\sinh(\bar{h}\sqrt{s}\,x)+i\sinh(h\sqrt{s}\,x)\Big]\\
&= \frac{\lambda\mu s^2-1}{2}\Big[\frac{-\sinh(\bar{h}\sqrt{s}\,x)+i\sinh(h\sqrt{s}\,x)}{2\bar{h}\sqrt{s}}\Big]\\
&= \frac{\lambda\mu s^2-1}{2}S_x^-(x)
\end{aligned}
$$

Where

$$S_x^-(x) \equiv \frac{-\sinh(\bar{h}\sqrt{s}\,x)+i\sinh(h\sqrt{s}\,x)}{2\bar{h}\sqrt{s}} \tag{7.38}$$

is a new definition, similar but not identical to $S^-(x)$ in (7.33).

7.6.3 Part III of $P(x,s)$

$$= \frac{\lambda\mu s^2+1}{4\bar{h}\sqrt{s}}\Big[-C_0\overline{S}+i\overline{C}_0S+\overline{S}_0C-iS_0\overline{C}\Big]$$

$$= \frac{\lambda\mu s^2+1}{4h\sqrt{s}}\Big[-\cosh[h\sqrt{s}]\sinh[\bar{h}\sqrt{s}(1-x)] + i\cosh[\bar{h}\sqrt{s}]\sinh[h\sqrt{s}(1-x)]$$
$$+\sinh[\bar{h}\sqrt{s}]\cosh[h\sqrt{s}(1-x)] - i\sinh[h\sqrt{s}]\cosh[\bar{h}\sqrt{s}(1-x)]$$

$$= \frac{\lambda\mu s^2+1}{4h\sqrt{s}}\Big[-\left(\frac{e^{h\sqrt{s}}+e^{-h\sqrt{s}}}{2}\right)\left(\frac{e^{\bar{h}\sqrt{s}(1-x)}-e^{-\bar{h}\sqrt{s}(1-x)}}{2}\right)$$
$$+i\left(\frac{e^{\bar{h}\sqrt{s}}+e^{-\bar{h}\sqrt{s}}}{2}\right)\left(\frac{e^{h\sqrt{s}(1-x)}-e^{-h\sqrt{s}(1-x)}}{2}\right)$$
$$+\left(\frac{e^{\bar{h}\sqrt{s}}-e^{-\bar{h}\sqrt{s}}}{2}\right)\left(\frac{e^{h\sqrt{s}(1-x)}+e^{-h\sqrt{s}(1-x)}}{2}\right)$$
$$-i\left(\frac{e^{h\sqrt{s}}-e^{-h\sqrt{s}}}{2}\right)\left(\frac{e^{\bar{h}\sqrt{s}(1-x)}+e^{-\bar{h}\sqrt{s}(1-x)}}{2}\right)\Big]$$

$$= \frac{\lambda\mu s^2+1}{16h\sqrt{s}}\Big[-\left(e^{h\sqrt{s}+\bar{h}\sqrt{s}(1-x)} - e^{h\sqrt{s}-\bar{h}\sqrt{s}(1-x)} + e^{-h\sqrt{s}+\bar{h}\sqrt{s}(1-x)} - e^{-h\sqrt{s}-\bar{h}\sqrt{s}(1-x)}\right)$$
$$+i\left(e^{\bar{h}\sqrt{s}+h\sqrt{s}(1-x)} - e^{\bar{h}\sqrt{s}-h\sqrt{s}(1-x)} + e^{-\bar{h}\sqrt{s}+h\sqrt{s}(1-x)} - e^{-\bar{h}\sqrt{s}-h\sqrt{s}(1-x)}\right)$$
$$+e^{\bar{h}\sqrt{s}+h\sqrt{s}(1-x)} + e^{\bar{h}\sqrt{s}-h\sqrt{s}(1-x)} - e^{-\bar{h}\sqrt{s}+h\sqrt{s}(1-x)} - e^{-\bar{h}\sqrt{s}-h\sqrt{s}(1-x)}$$
$$-i\left(e^{h\sqrt{s}+\bar{h}\sqrt{s}(1-x)} + e^{h\sqrt{s}-\bar{h}\sqrt{s}(1-x)} - e^{-h\sqrt{s}+\bar{h}\sqrt{s}(1-x)} - e^{-h\sqrt{s}-\bar{h}\sqrt{s}(1-x)}\right)\Big]$$

$$= \frac{\lambda\mu s^2+1}{16h\sqrt{s}}\Big[-\left(e^{i\bar{h}\sqrt{s}+\bar{h}\sqrt{s}(1-x)} - e^{i\bar{h}\sqrt{s}-\bar{h}\sqrt{s}(1-x)} + e^{-i\bar{h}\sqrt{s}+\bar{h}\sqrt{s}(1-x)} - e^{-i\bar{h}\sqrt{s}-\bar{h}\sqrt{s}(1-x)}\right)$$
$$+i\left(e^{-ih\sqrt{s}+h\sqrt{s}(1-x)} - e^{-ih\sqrt{s}-h\sqrt{s}(1-x)} + e^{ih\sqrt{s}+h\sqrt{s}(1-x)} - e^{ih\sqrt{s}-h\sqrt{s}(1-x)}\right)$$
$$+e^{-ih\sqrt{s}+h\sqrt{s}(1-x)} + e^{-ih\sqrt{s}-h\sqrt{s}(1-x)} - e^{ih\sqrt{s}+h\sqrt{s}(1-x)} - e^{ih\sqrt{s}-h\sqrt{s}(1-x)}$$
$$-i\left(e^{i\bar{h}\sqrt{s}+\bar{h}\sqrt{s}(1-x)} + e^{i\bar{h}\sqrt{s}-\bar{h}\sqrt{s}(1-x)} - e^{-i\bar{h}\sqrt{s}+\bar{h}\sqrt{s}(1-x)} - e^{-i\bar{h}\sqrt{s}-\bar{h}\sqrt{s}(1-x)}\right)\Big]$$

$$= \frac{\lambda\mu s^2+1}{16h\sqrt{s}}\Big[-\left(e^{\bar{h}\sqrt{s}(i+1-x)} - e^{\bar{h}\sqrt{s}(i-1+x)} + e^{\bar{h}\sqrt{s}(-i+1-x)} - e^{\bar{h}\sqrt{s}(-i-1+x)}\right)$$
$$+i\left(e^{h\sqrt{s}(-i+1-x)} - e^{h\sqrt{s}(-i-1+x)} + e^{h\sqrt{s}(i+1-x)} - e^{h\sqrt{s}(i-1+x)}\right)$$
$$+e^{h\sqrt{s}(-i+1-x)} + e^{h\sqrt{s}(-i-1+x)} - e^{h\sqrt{s}(i+1-x)} - e^{h\sqrt{s}(i-1+x)}$$
$$-i\left(e^{\bar{h}\sqrt{s}(i+1-x)} + e^{\bar{h}\sqrt{s}(i-1+x)} - e^{\bar{h}\sqrt{s}(-i+1-x)} - e^{\bar{h}\sqrt{s}(-i-1+x)}\right)\Big]$$

$$= \frac{\lambda\mu s^2+1}{8h\sqrt{s}}\Big[-\left(\frac{e^{\bar{h}\sqrt{s}(i+1-x)}-e^{-\bar{h}\sqrt{s}(i+1-x)}}{2} + \frac{e^{\bar{h}\sqrt{s}(-i+1-x)}-e^{-\bar{h}\sqrt{s}(-i+1-x)}}{2}\right)$$
$$+i\left(\frac{e^{h\sqrt{s}(-i+1-x)}-e^{-h\sqrt{s}(-i+1-x)}}{2} + \frac{e^{h\sqrt{s}(i+1-x)}-e^{-h\sqrt{s}(i+1-x)}}{2}\right)$$
$$+\frac{e^{h\sqrt{s}(-i+1-x)}-e^{-h\sqrt{s}(-i+1-x)}}{2} - \frac{e^{\bar{h}\sqrt{s}(i+1-x)}-e^{-\bar{h}\sqrt{s}(i+1-x)}}{2}$$
$$-i\left(\frac{e^{\bar{h}\sqrt{s}(i+1-x)}-e^{-\bar{h}\sqrt{s}(i+1-x)}}{2} - \frac{e^{\bar{h}\sqrt{s}(-i+1-x)}-e^{-\bar{h}\sqrt{s}(-i+1-x)}}{2}\right)\Big]$$

$$= \frac{\lambda\mu s^2+1}{8h\sqrt{s}}\Big[-\sinh[\bar{h}\sqrt{s}(1+i-x)] - \sinh[\bar{h}\sqrt{s}(1-i-x)]$$

$$
\begin{aligned}
&+ i\sinh[h\sqrt{s}(1-i-x)] + i\sinh[h\sqrt{s}(1+i-x)] \\
&+ \sinh[h\sqrt{s}(1-i-x)] - \sinh[h\sqrt{s}(1+i-x)] \\
&- i\sinh[h\sqrt{s}(1+i-x)] + i\sinh[h\sqrt{s}(1-i-x)]\Big] \\
= \frac{\lambda\mu s^2+1}{4}\Bigg[&\frac{-\sinh[h\sqrt{s}(1+i-x)] + i\sinh[h\sqrt{s}(1+i-x)]}{2h\sqrt{s}} \\
&+ \frac{-\sinh[h\sqrt{s}(1-i-x)] + i\sinh[h\sqrt{s}(1-i-x)]}{2h\sqrt{s}} \\
&+ i\left(\frac{-\sinh[h\sqrt{s}(1+i-x)] + i\sinh[h\sqrt{s}(1+i-x)]}{2h\sqrt{s}}\right) \\
&- i\left(\frac{-\sinh[h\sqrt{s}(1-i-x)] + i\sinh[h\sqrt{s}(1-i-x)]}{2h\sqrt{s}}\right)\Bigg] \\
= \frac{\lambda\mu s^2+1}{4}\Bigg[&\underbrace{S_x^-(1+i-x) + S_x^-(1-i-x)}_{\text{conjugates}} + i\Big(\underbrace{S_x^-(1+i-x) - S_x^-(1-i-x)}_{\text{conjugates}}\Big)\Bigg] \\
= \frac{\lambda\mu s^2+1}{4}&\Big[2\,\mathrm{Re}\left\{S_x^-(1+i-x)\right\} + i2i\,\mathrm{Im}\left\{S_x^-(1+i-x)\right\}\Big] \\
= \frac{\lambda\mu s^2+1}{2}&\Big[\mathrm{Re}\left\{S_x^-(1+i-x)\right\} - \mathrm{Im}\left\{S_x^-(1+i-x)\right\}\Big]
\end{aligned}
$$

Where $S_x^-(x)$ was defined in (7.38). It can be verified that

$$S_x^-(z) = \overline{S_x^-(\bar{z})} \qquad z \in \mathbf{C}$$

7.6.4 Part IV of $P(x,s)$

$$
\begin{aligned}
&= \frac{-\mu}{2}\Big[-i\overline{S}_0 S + iS_0\overline{S}\Big] \\
&= \frac{-\mu i}{2}\Big[-\sinh[\bar{h}\sqrt{\bar{s}}]\sinh[h\sqrt{s}(1-x)] + \sinh[h\sqrt{s}]\sinh[\bar{h}\sqrt{\bar{s}}(1-x)]\Big] \\
&= \frac{-\mu i}{2}\Bigg[-\left(\frac{e^{\bar{h}\sqrt{\bar{s}}} - e^{-\bar{h}\sqrt{\bar{s}}}}{2}\right)\left(\frac{e^{h\sqrt{s}(1-x)} - e^{-h\sqrt{s}(1-x)}}{2}\right) \\
&\qquad + \left(\frac{e^{h\sqrt{s}} - e^{-h\sqrt{s}}}{2}\right)\left(\frac{e^{\bar{h}\sqrt{\bar{s}}(1-x)} - e^{-\bar{h}\sqrt{\bar{s}}(1-x)}}{2}\right)\Bigg] \\
&= \frac{-\mu i}{8}\Big[-\left(e^{\bar{h}\sqrt{\bar{s}}+h\sqrt{s}(1-x)} - e^{\bar{h}\sqrt{\bar{s}}-h\sqrt{s}(1-x)} - e^{-\bar{h}\sqrt{\bar{s}}+h\sqrt{s}(1-x)} + e^{-\bar{h}\sqrt{\bar{s}}-h\sqrt{s}(1-x)}\right) \\
&\qquad + e^{h\sqrt{s}+\bar{h}\sqrt{\bar{s}}(1-x)} - e^{h\sqrt{s}-\bar{h}\sqrt{\bar{s}}(1-x)} - e^{-h\sqrt{s}+\bar{h}\sqrt{\bar{s}}(1-x)} + e^{-h\sqrt{s}-\bar{h}\sqrt{\bar{s}}(1-x)}\Big] \\
&= \frac{-\mu i}{8}\Big[-\left(e^{-i\bar{h}\sqrt{\bar{s}}+h\sqrt{s}(1-x)} - e^{-i\bar{h}\sqrt{\bar{s}}-h\sqrt{s}(1-x)} - e^{i\bar{h}\sqrt{\bar{s}}+h\sqrt{s}(1-x)} + e^{i\bar{h}\sqrt{\bar{s}}-h\sqrt{s}(1-x)}\right) \\
&\qquad + e^{i\bar{h}\sqrt{\bar{s}}+h\sqrt{s}(1-x)} - e^{i\bar{h}\sqrt{\bar{s}}-h\sqrt{s}(1-x)} - e^{-i\bar{h}\sqrt{\bar{s}}+h\sqrt{s}(1-x)} + e^{-i\bar{h}\sqrt{\bar{s}}-h\sqrt{s}(1-x)}\Big] \\
&= \frac{-\mu i}{8}\Big[-\left(e^{h\sqrt{s}(1-i-x)} - e^{h\sqrt{s}(-1-i+x)} - e^{h\sqrt{s}(1+i-x)} + e^{h\sqrt{s}(-1+i+x)}\right) \\
&\qquad + e^{h\sqrt{s}(1+i-x)} - e^{h\sqrt{s}(-1+i+x)} - e^{h\sqrt{s}(1-i-x)} + e^{h\sqrt{s}(-1-i+x)}\Big]
\end{aligned}
$$

$$
\begin{aligned}
&= \frac{-\mu i}{8}\left[-\frac{e^{h\sqrt{s}(1-i-x)}+e^{-h\sqrt{s}(1-i-x)}}{2} + \frac{e^{h\sqrt{s}(1+i-x)}+e^{-h\sqrt{s}(1+i-x)}}{2} \right.\\
&\qquad \left. + \left(\frac{e^{h\sqrt{s}(1+i-x)}+e^{-h\sqrt{s}(1+i-x)}}{2}\right) - \left(\frac{e^{h\sqrt{s}(1-i-x)}+e^{-h\sqrt{s}(1-i-x)}}{2}\right)\right]\\
&= \frac{-\mu i}{8}\Big[-\cosh[h\sqrt{s}(1-i-x)] + \cosh[h\sqrt{s}(1+i-x)]\\
&\qquad + \cosh[\bar{h}\sqrt{s}(1+i-x)] - \cosh[\bar{h}\sqrt{s}(1-i-x)]\Big]\\
&= \frac{-\mu i}{4}\left[\frac{\cosh[h\sqrt{s}(1+i-x)]+\cosh[\bar{h}\sqrt{s}(1+i-x)]}{2}\right.\\
&\qquad \left. - \frac{\cosh[h\sqrt{s}(1-i-x)]+\cosh[\bar{h}\sqrt{s}(1-i-x)]}{2}\right]\\
&= \frac{-\mu i}{4}\Big[\underbrace{C_x^+(1+i-x) - C_x^+(1-i-x)}_{\text{conjugates}}\Big]\\
&= \frac{-\mu i}{4} 2i \operatorname{Im}\left\{C_x^+(1+i-x)\right\}\\
&= \mu \operatorname{Im}\left\{C_x^+(1+i-x)\right\}
\end{aligned}
$$

where we introduced

$$C_x^+(x) \equiv \frac{\cosh[h\sqrt{s}\,x]+\cosh[\bar{h}\sqrt{s}\,x]}{2} \tag{7.39}$$

by analogy to (7.33), and

$$C_x^+(z) = \overline{C_x^+(\bar{z})} \qquad z \in \mathbb{C}$$

can be verified.

7.7 Conversion to Infinite Series

Returning to the $P(x,s)$ expression on Page 72, and making use of the expressions from Parts I, II, III and IV,

$$
\begin{aligned}
P(x,s) = &-\lambda s \operatorname{Re}\left\{C_x^-(1+i-x)\right\} + \left(\frac{\lambda\mu s^2-1}{2}\right) S_x^-(x)\\
&+ \frac{\lambda\mu s^2+1}{2}\Big[\operatorname{Re}\left\{S_x^-(1+i-x)\right\} - \operatorname{Im}\left\{S_x^-(1+i-x)\right\}\Big] + \mu \operatorname{Im}\left\{C_x^+(1+i-x)\right\}
\end{aligned} \tag{7.40}
$$

where C_x^-, S_x^- and C_x^+ were introduced in (7.37), (7.38) and (7.39), respectively.

The individual terms of $P(x,s)$ are now converted into their infinite-series representations, referenced in Section 3.4.1.

$$
\begin{aligned}
&\operatorname{Re}\left\{C_x^-(1+i-x)\right\}\\
&= \operatorname{Re}\left\{\frac{\cosh[h\sqrt{s}(1+i-x)] - \cosh[\bar{h}\sqrt{s}(1+i-x)]}{2i}\right\}\\
&= \operatorname{Re}\left\{\frac{1}{2i}\left[\sum_{k=0}^{\infty}\frac{\sqrt{is}^{2k}(1+i-x)^{2k}}{(2k)!} - \sum_{k=0}^{\infty}\frac{(i)^{2k}\sqrt{is}^{-2k}(1+i-x)^{2k}}{(2k)!}\right]\right\}
\end{aligned}
$$

$$= \mathrm{Re}\left\{ \frac{1}{2i} \sum_{k=0}^{\infty} \frac{(is)^k (1+i-x)^{2k}}{(2k)!} \underbrace{\left(1-(-1)^k\right)}_{\substack{=2, k=1,3,5,\ldots \\ =0, k=0,2,4,\ldots \\ \text{let } k=2n+1}} \right\}$$

$$= \mathrm{Re}\left\{ \frac{1}{2i} \sum_{n=0}^{\infty} \frac{(is)(is)^{2n} (1+i-x)^{4n+2}}{(4n+2)!} 2 \right\}$$

$$= \mathrm{Re}\left\{ \sum_{n=0}^{\infty} \frac{(-1)^n (1+i-x)^{4n+2} s^{2n+1}}{(4n+2)!} \right\}$$

$$= \sum_{n=0}^{\infty} \frac{(-1)^n \,\mathrm{Re}\left\{(1+i-x)^{4n+2}\right\} s^{2n+1}}{(4n+2)!}$$

$$\begin{aligned}
&S_x^-(x) \\
&= \frac{-\sinh[\bar{h}\sqrt{\bar{s}}\,x] + i\sinh[h\sqrt{\bar{s}}\,x]}{2h\sqrt{s}} \\
&= \frac{-\sinh[\bar{h}\sqrt{\bar{s}}\,x] + i\sinh[i\bar{h}\sqrt{\bar{s}}\,x]}{2h\sqrt{s}} \\
&= \frac{1}{2\sqrt{-is}} \left[-\sum_{k=0}^{\infty} \frac{\sqrt{-is}^{2k+1} x^{2k+1}}{(2k+1)!} + i \sum_{k=0}^{\infty} \frac{i^{2k+1} \sqrt{-is}^{2k+1} x^{2k+1}}{(2k+1)!} \right] \\
&= \frac{1}{2} \sum_{k=0}^{\infty} \frac{(-is)^k x^{2k+1}}{(2k+1)!} \left[-1 + i^{2k+2} \right] \\
&= \frac{1}{2} \sum_{k=0}^{\infty} \frac{(-is)^k x^{2k+1}}{(2k+1)!} \underbrace{\left[-1 + (-1)^{k+1} \right]}_{\substack{=-2, k=0,2,4,\ldots \\ = 0, k=1,3,5,\ldots \\ \text{let } k=2n}} \\
&= \frac{1}{2} \sum_{n=0}^{\infty} \frac{(-is)^{2n} x^{4n+1}}{(4n+1)!} (-2) \\
&= -\sum_{n=0}^{\infty} \frac{(-1)^{2n} (-1)^n s^{2n} x^{4n+1}}{(4n+1)!} \\
&= -\sum_{n=0}^{\infty} \frac{(-1)^n x^{4n+1} s^{2n}}{(4n+1)!}
\end{aligned}$$

The next two terms use the $S_x^-(x)$ infinite series result from the previous line

$$\begin{aligned}
&\mathrm{Re}\left\{S_x^-(1+i-x)\right\} \\
&= \mathrm{Re}\left\{ -\sum_{n=0}^{\infty} \frac{(-1)^n (1+i-x)^{4n+1} s^{2n}}{(4n+1)!} \right\} \\
&= -\sum_{n=0}^{\infty} \frac{(-1)^n \,\mathrm{Re}\left\{(1+i-x)^{4n+1}\right\} s^{2n}}{(4n+1)!}
\end{aligned}$$

$$\begin{aligned}
&\mathrm{Im}\left\{S_x^-(1+i-x)\right\} \\
&= -\sum_{n=0}^{\infty} \frac{(-1)^n \,\mathrm{Im}\left\{(1+i-x)^{4n+1}\right\} s^{2n}}{(4n+1)!}
\end{aligned}$$

The last term is

$$
\begin{aligned}
&\operatorname{Im}\left\{C_x^+(1+i-x)\right\} \\
&= \operatorname{Im}\left\{\frac{\cosh[h\sqrt{s}(1+i-x)] + \cosh[\bar{h}\sqrt{s}(1+i-x)]}{2}\right\} \\
&= \operatorname{Im}\left\{\frac{1}{2}\left(\sum_{k=0}^{\infty}\frac{\sqrt{is}^{2k}(1+i-x)^{2k}}{(2k)!} + \sum_{k=0}^{\infty}\frac{\sqrt{-is}^{2k}(1+i-x)^{2k}}{(2k)!}\right)\right\} \\
&= \operatorname{Im}\left\{\frac{1}{2}\sum_{k=0}^{\infty}\frac{(is)^k(1+i-x)^{2k}}{(2k)!}\underbrace{\left[1+(-1)^k\right]}_{\substack{=2,k=0,2,4,\ldots \\ =0,k=1,3,5,\ldots \\ \text{let } k=2n}}\right\} \\
&= \operatorname{Im}\left\{\frac{1}{2}\sum_{n=0}^{\infty}\frac{(is)^{2n}(1+i-x)^{4n}}{(4n)!}2\right\} \\
&= \operatorname{Im}\left\{\sum_{n=0}^{\infty}\frac{(-1)^n(1+i-x)^{4n}s^{2n}}{(4n)!}\right\} \\
&= \sum_{n=0}^{\infty}\frac{(-1)^n \operatorname{Im}\left\{(1+i-x)^{4n}\right\}s^{2n}}{(4n)!}
\end{aligned}
$$

With these expressions worked out, (7.40) becomes

$$
\begin{aligned}
P(x,s) = &-\lambda s\sum_{n=0}^{\infty}\frac{(-1)^n \operatorname{Re}\left\{(1+i-x)^{4n+2}\right\}s^{2n+1}}{(4n+2)!} - \left(\frac{\lambda\mu s^2-1}{2}\right)\sum_{n=0}^{\infty}\frac{(-1)^n x^{4n+1}s^{2n}}{(4n+1)!} \\
&+ \frac{\lambda\mu s^2+1}{2}\left[-\sum_{n=0}^{\infty}\frac{(-1)^n \operatorname{Re}\left\{(1+i-x)^{4n+1}\right\}s^{2n}}{(4n+1)!}\right. \\
&\left.+\sum_{n=0}^{\infty}\frac{(-1)^n \operatorname{Im}\left\{(1+i-x)^{4n+1}\right\}s^{2n}}{(4n+1)!}\right] + \mu\sum_{n=0}^{\infty}\frac{(-1)^n \operatorname{Im}\left\{(1+i-x)^{4n}\right\}s^{2n}}{(4n)!}
\end{aligned}
$$

expanding out,

$$
\begin{aligned}
&= \frac{1}{2}\sum_{n=0}^{\infty}\frac{(-1)^n x^{4n+1}s^{2n}}{(4n+1)!} + \frac{1}{2}\sum_{n=0}^{\infty}\frac{(-1)^n \operatorname{Im}\left\{(1+i-x)^{4n+1}\right\}s^{2n}}{(4n+1)!} \\
&- \frac{1}{2}\sum_{n=0}^{\infty}\frac{(-1)^n \operatorname{Re}\left\{(1+i-x)^{4n+1}\right\}s^{2n}}{(4n+1)!} + \mu\sum_{n=0}^{\infty}\frac{(-1)^n \operatorname{Im}\left\{(1+i-x)^{4n}\right\}s^{2n}}{(4n)!} \\
&- \frac{\lambda\mu s^2}{2}\sum_{n=0}^{\infty}\frac{(-1)^n x^{4n+1}s^{2n}}{(4n+1)!} - \frac{\lambda\mu s^2}{2}\sum_{n=0}^{\infty}\frac{(-1)^n \operatorname{Re}\left\{(1+i-x)^{4n+1}\right\}s^{2n}}{(4n+1)!} \\
&+ \frac{\lambda\mu s^2}{2}\sum_{n=0}^{\infty}\frac{(-1)^n \operatorname{Im}\left\{(1+i-x)^{4n+1}\right\}s^{2n}}{(4n+1)!} - \lambda s\sum_{n=0}^{\infty}\frac{(-1)^n \operatorname{Re}\left\{(1+i-x)^{4n+2}\right\}s^{2n+1}}{(4n+2)!}
\end{aligned}
$$

leading to the final form

$$
\begin{aligned}
P(x,s) = \sum_{n=0}^{\infty} \Bigg[& \frac{x^{4n+1} + \operatorname{Im}\left\{(1+i-x)^{4n+1}\right\} - \operatorname{Re}\left\{(1+i-x)^{4n+1}\right\}}{2(4n+1)} \\
& + \mu \operatorname{Im}\left\{(1+i-x)^{4n}\right\} \Bigg] \frac{(-1)^n s^{2n}}{(4n)!} \\
+ \sum_{n=0}^{\infty} \Bigg[& \frac{\lambda\mu}{2} \left(\operatorname{Im}\left\{(1+i-x)^{4n+1}\right\} - \operatorname{Re}\left\{(1+i-x)^{4n+1}\right\} - x^{4n+1} \right) \\
& - \frac{\lambda \operatorname{Re}\left\{(1+i-x)^{4n+2}\right\}}{(4n+2)} \Bigg] \frac{(-1)^n s^{2n+2}}{(4n+1)!}
\end{aligned}
\tag{7.41}
$$

7.8 Parameterizing the System Trajectories

From (7.36), the system state was parameterized by the flat output as

$$W(x,s) = P(x,s)Y(s)$$

The $P(x,s)$ expression (7.41) has the s operator factored out, so the inverse Laplace transform can be obtained by inspection.

In Section 7.5, we dropped the $\tilde{}$ notation after transforming into the s-domain, for compactness. However, we are still working with the *normalized* BVP, (7.29). Following the inverse transform, the superscript notation is restored, to indicate the solution is expressed in the normalized variables (7.27):

$$\widetilde{w}(\widetilde{x},\widetilde{t}) = P(\widetilde{x},\widetilde{t})\widetilde{y}(\widetilde{t}) \tag{7.42}$$

where $P(\widetilde{x},\widetilde{t})$ is the inverse transform of (7.41) acting on $\widetilde{y}(\widetilde{t})$,

$$
\begin{aligned}
P(\widetilde{x},\widetilde{t}) = \sum_{n=0}^{\infty} \Bigg[& \frac{\widetilde{x}^{4n+1} + \operatorname{Im}\left\{(1+i-\widetilde{x})^{4n+1}\right\} - \operatorname{Re}\left\{(1+i-\widetilde{x})^{4n+1}\right\}}{2(4n+1)} \\
& + \mu \operatorname{Im}\left\{(1+i-\widetilde{x})^{4n}\right\} \Bigg] \frac{(-1)^n}{(4n)!} \frac{d^{2n}}{d\widetilde{t}^{2n}} \\
+ \sum_{n=0}^{\infty} \Bigg[& \frac{\lambda\mu}{2} \left(\operatorname{Im}\left\{(1+i-\widetilde{x})^{4n+1}\right\} - \operatorname{Re}\left\{(1+i-\widetilde{x})^{4n+1}\right\} - \widetilde{x}^{4n+1} \right) \\
& - \frac{\lambda \operatorname{Re}\left\{(1+i-\widetilde{x})^{4n+2}\right\}}{(4n+2)} \Bigg] \frac{(-1)^n}{(4n+1)!} \frac{d^{2n+2}}{d\widetilde{t}^{2n+2}}
\end{aligned}
\tag{7.43}
$$

7.9 Undoing the Normalization

The variable normalizations in (7.27) were introduced to simplify the PDE and make the series manipulations easier. However, we want to obtain a control law in terms of the original independent variables, (7.25). Hence, (7.42) must be changed into the original, non-normalized variables.

By definition in (7.27), $\widetilde{w}(\widetilde{x},\widetilde{t}) = w(x,t)$. By the same reasoning, $\widetilde{y}(\widetilde{t}) = y(t)$, because $\widetilde{y}(\widetilde{t})$ is the time-scaled version of the flat output steering the original system. All that remains to be done is to replace $\widetilde{x}$ and $\widetilde{t}$ in (7.43) by their x and t equivalents. Using (7.27),

$$\widetilde{x} = \frac{x}{L} \tag{7.44}$$

and

$$\frac{d}{d\tilde{t}} = \frac{d}{dt}\frac{dt}{d\tilde{t}} = \frac{L^2\sqrt{\rho A}}{\sqrt{EI}}\frac{d}{dt}$$
$$\frac{d^2}{d\tilde{t}^2} = \frac{d}{d\tilde{t}}\left(\frac{L^2\sqrt{\rho A}}{\sqrt{EI}}\frac{d}{dt}\right) = \frac{d}{dt}\left(\frac{L^2\sqrt{\rho A}}{\sqrt{EI}}\frac{d}{dt}\right)\frac{dt}{d\tilde{t}} = \left(\frac{L^2\sqrt{\rho A}}{\sqrt{EI}}\right)^2\frac{d^2}{dt^2}$$
$$\vdots \qquad (7.45)$$
$$\frac{d^{2n}}{d\tilde{t}^{2n}} = \left(\frac{L^2\sqrt{\rho A}}{\sqrt{EI}}\right)^{2n}\frac{d^{2n}}{dt^{2n}} = L^{4n}\left(\frac{\rho A}{EI}\right)^n\frac{d^{2n}}{dt^{2n}} = L^{4n}\kappa^n\frac{d^{2n}}{dt^{2n}}$$
$$\frac{d^{2n+2}}{d\tilde{t}^{2n+2}} = \left(\frac{L^2\sqrt{\rho A}}{\sqrt{EI}}\right)^{2n+2}\frac{d^{2n+2}}{dt^{2n+2}} = L^{4n+4}\left(\frac{\rho A}{EI}\right)^{n+1}\frac{d^{2n+2}}{dt^{2n+2}} = L^{4n+4}\kappa^{n+1}\frac{d^{2n+2}}{dt^{2n+2}}$$

where $\kappa = \left(\frac{\rho A}{EI}\right)$ was introduced for compactness during the earlier series manipulations, Section 3.4.4. Using (7.44) and (7.45) in (7.43) gives

$$\begin{aligned}
P(x,t) = \sum_{n=0}^{\infty}\Bigg[&\frac{\left(\frac{x}{L}\right)^{4n+1} + \operatorname{Im}\left\{\left(1+i-\frac{x}{L}\right)^{4n+1}\right\} - \operatorname{Re}\left\{\left(1+i-\frac{x}{L}\right)^{4n+1}\right\}}{2(4n+1)} \\
&+ \mu\operatorname{Im}\left\{\left(1+i-\frac{x}{L}\right)^{4n}\right\}\Bigg]\frac{(-1)^n}{(4n)!}L^{4n}\kappa^n\frac{d^{2n}}{dt^{2n}} \\
+\sum_{n=0}^{\infty}\Bigg[&\frac{\lambda\mu}{2}\left(\operatorname{Im}\left\{\left(1+i-\frac{x}{L}\right)^{4n+1}\right\} - \operatorname{Re}\left\{\left(1+i-\frac{x}{L}\right)^{4n+1}\right\} - \left(\frac{x}{L}\right)^{4n+1}\right) \\
&- \frac{\lambda\operatorname{Re}\left\{\left(1+i-\frac{x}{L}\right)^{4n+2}\right\}}{(4n+2)}\Bigg]\frac{(-1)^n}{(4n+1)!}L^{4n+4}\kappa^{n+1}\frac{d^{2n+2}}{dt^{2n+2}} \\
= \sum_{n=0}^{\infty}\Bigg[&\frac{x^{4n+1} + \operatorname{Im}\left\{(L+iL-x)^{4n+1}\right\} - \operatorname{Re}\left\{(L+iL-x)^{4n+1}\right\}}{2(4n+1)L^{4n+1}} \\
&+ \frac{\mu\operatorname{Im}\left\{(L+iL-x)^{4n}\right\}}{L^{4n}}\Bigg]\frac{(-1)^n}{(4n)!}L^{4n}\kappa^n\frac{d^{2n}}{dt^{2n}} \\
+\sum_{n=0}^{\infty}\Bigg[&\frac{\lambda\mu}{2L^{4n+1}}\left(\operatorname{Im}\left\{(L+iL-x)^{4n+1}\right\} - \operatorname{Re}\left\{(L+iL-x)^{4n+1}\right\} - x^{4n+1}\right) \\
&- \frac{\lambda\operatorname{Re}\left\{(L+iL-x)^{4n+2}\right\}}{L^{4n+2}(4n+2)}\Bigg]\frac{(-1)^n}{(4n+1)!}L^{4n+4}\kappa^{n+1}\frac{d^{2n+2}}{dt^{2n+2}} \\
= \sum_{n=0}^{\infty}\Bigg[&\frac{x^{4n+1} + \operatorname{Im}\left\{(L+iL-x)^{4n+1}\right\} - \operatorname{Re}\left\{(L+iL-x)^{4n+1}\right\}}{2L(4n+1)!} \\
&+ \frac{\mu\operatorname{Im}\left\{(L+iL-x)^{4n}\right\}}{(4n)!}\Bigg](-\kappa)^n\frac{d^{2n}}{dt^{2n}} \\
-\sum_{n=0}^{\infty}\Bigg[&\frac{\lambda\mu L^3}{2}\left(\frac{\operatorname{Im}\left\{(L+iL-x)^{4n+1}\right\} - \operatorname{Re}\left\{(L+iL-x)^{4n+1}\right\} - x^{4n+1}}{(4n+1)!}\right) \\
&- \frac{\lambda L^2\operatorname{Re}\left\{(L+iL-x)^{4n+2}\right\}}{(4n+2)!}\Bigg](-\kappa)^{n+1}\frac{d^{2n+2}}{dt^{2n+2}}
\end{aligned}$$

Leading to the final form of the state parametrization,

$$
\begin{aligned}
w(x,t) = \sum_{n=0}^{\infty}\Bigg[& \frac{x^{4n+1} + \operatorname{Im}\left\{(L+iL-x)^{4n+1}\right\} - \operatorname{Re}\left\{(L+iL-x)^{4n+1}\right\}}{2L(4n+1)!} \\
& + \frac{\mu \operatorname{Im}\left\{(L+iL-x)^{4n}\right\}}{(4n)!}\Bigg](-\kappa)^n y^{(2n)}(t) \\
- \sum_{n=0}^{\infty}\Bigg[& \frac{\lambda\mu L^3}{2}\left(\frac{\operatorname{Im}\left\{(L+iL-x)^{4n+1}\right\} - \operatorname{Re}\left\{(L+iL-x)^{4n+1}\right\} - x^{4n+1}}{(4n+1)!}\right) \\
& - \frac{\lambda L^2 \operatorname{Re}\left\{(L+iL-x)^{4n+2}\right\}}{(4n+2)!}\Bigg](-\kappa)^{n+1} y^{(2n+2)}(t)
\end{aligned}
\tag{7.46}
$$

where, from before,

$$
\kappa = \frac{\rho A}{EI} \qquad \lambda = \frac{J_p}{L^3 \rho A} \qquad \mu = \frac{m_p}{L\rho A}
$$

7.10 Boundary Input Torque

Referring back to (7.26), the input boundary torque

$$
\tau(t) = J_{\text{hub}} \frac{\partial^3 w(0,t)}{\partial t^2 \partial x} - EI \frac{\partial^2 w(0,t)}{\partial x^2}
$$

is expressed in terms of the derivatives of $w(x,t)$, given by (7.46). We now work out $\tau(t)$ explicitly.

$$
\begin{aligned}
\frac{\partial w(x,t)}{\partial x} = \sum_{n=0}^{\infty}\Bigg[& \frac{(4n+1)x^{4n} + \operatorname{Im}\left\{(4n+1)(L+iL-x)^{4n}(-1)\right\}}{2L(4n+1)!} \\
& - \frac{\operatorname{Re}\left\{(4n+1)(L+iL-x)^{4n}(-1)\right\}}{2L(4n+1)!} \\
& + \frac{\mu \operatorname{Im}\left\{(4n)(L+iL-x)^{4n-1}(-1)\right\}}{(4n)!}\Bigg](-\kappa)^n y^{(2n)}(t) \\
- \sum_{n=0}^{\infty}\Bigg[& \frac{\lambda\mu L^3}{2}\Bigg(\frac{\operatorname{Im}\left\{(4n+1)(L+iL-x)^{4n}(-1)\right\}}{(4n+1)!} \\
& + \frac{-\operatorname{Re}\left\{(4n+1)(L+iL-x)^{4n}(-1)\right\} - (4n+1)x^{4n}}{(4n+1)!}\Bigg) \\
& - \frac{\lambda L^2 \operatorname{Re}\left\{(4n+2)(L+iL-x)^{4n+1}(-1)\right\}}{(4n+2)!}\Bigg](-\kappa)^{n+1} y^{(2n+2)}(t)
\end{aligned}
\tag{7.47}
$$

$$\frac{\partial^2 w(x,t)}{\partial x^2} = \sum_{n=0}^{\infty}\Bigg[\frac{(4n+1)(4n)x^{4n-1} + \operatorname{Im}\left\{(4n+1)(4n)(L+iL-x)^{4n-1}\right\}}{2L(4n+1)!}$$
$$- \frac{\operatorname{Re}\left\{(4n+1)(4n)(L+iL-x)^{4n-1}\right\}}{2L(4n+1)!}$$
$$+ \frac{\mu \operatorname{Im}\left\{(4n)(4n-1)(L+iL-x)^{4n-2}\right\}}{(4n)!}\Bigg](-\kappa)^n y^{(2n)}(t)$$
$$- \sum_{n=0}^{\infty}\Bigg[\frac{\lambda\mu L^3}{2}\Bigg(\frac{\operatorname{Im}\left\{(4n+1)(4n)(L+iL-x)^{4n-1}\right\}}{(4n+1)!}$$
$$+ \frac{-\operatorname{Re}\left\{(4n+1)(4n)(L+iL-x)^{4n-1}\right\} - (4n+1)(4n)x^{4n-1}}{(4n+1)!}\Bigg)$$
$$- \frac{\lambda L^2 \operatorname{Re}\left\{(4n+2)(4n+1)(L+iL-x)^{4n}\right\}}{(4n+2)!}\Bigg](-\kappa)^{n+1} y^{(2n+2)}(t) \tag{7.48}$$

Evaluating (7.47) at $x = 0$,

$$\frac{\partial w(0,t)}{\partial x} = \left[\frac{0^0 + \operatorname{Im}\{-1\} - \operatorname{Re}\{(-1)\}}{2L} + \mu \operatorname{Im}\{0\}\right] y(t)$$
$$- \left[\frac{\lambda\mu L^3}{2}\left(\operatorname{Im}\{-1\} - \operatorname{Re}\{-1\} - 0^0\right) - \frac{\lambda L^2 \operatorname{Re}\{2(L+iL)(-1)\}}{2!}\right](-\kappa) y^{(2)}(t)$$
$$+ \sum_{n=1}^{\infty}\Bigg[\frac{\operatorname{Im}\left\{(4n+1)(L+iL)^{4n}(-1)\right\} - \operatorname{Re}\left\{(4n+1)(L+iL)^{4n}(-1)\right\}}{2L(4n+1)!}$$
$$+ \frac{\mu \operatorname{Im}\left\{4n(L+iL)^{4n-1}(-1)\right\}}{(4n)!}\Bigg](-\kappa)^n y^{(2n)}(t)$$
$$- \sum_{n=1}^{\infty}\Bigg[\frac{\lambda\mu L^3}{2}\left(\frac{\operatorname{Im}\left\{(4n+1)(L+iL)^{4n}(-1)\right\} - \operatorname{Re}\left\{(4n+1)(L+iL)^{4n}(-1)\right\}}{(4n+1)!}\right)$$
$$- \frac{\lambda L^2 \operatorname{Re}\left\{(4n+2)(L+iL)^{4n+1}(-1)\right\}}{(4n+2)!}\Bigg](-\kappa)^{n+1} y^{(2n+2)}(t)$$
$$= \frac{1}{L} y(t) + \lambda L^3 \kappa y^{(2)}(t)$$
$$+ \sum_{n=1}^{\infty}\Bigg[\frac{-\operatorname{Im}\left\{(L+iL)^{4n}\right\} + \operatorname{Re}\left\{(L+iL)^{4n}\right\}}{2L(4n)!} - \frac{\mu \operatorname{Im}\left\{(L+iL)^{4n-1}\right\}}{(4n-1)!}\Bigg](-\kappa)^n y^{(2n)}(t)$$
$$- \sum_{n=1}^{\infty}\Bigg[\frac{\lambda\mu L^3}{2}\left(\frac{-\operatorname{Im}\left\{(L+iL)^{4n}\right\} + \operatorname{Re}\left\{(L+iL)^{4n}\right\}}{(4n)!}\right)$$
$$+ \frac{\lambda L^2 \operatorname{Re}\left\{(L+iL)^{4n+1}\right\}}{(4n+1)!}\Bigg](-\kappa)^{n+1} y^{(2n+2)}(t)$$
$$= \frac{1}{L} y(t) + \lambda L^3 \kappa y^{(2)}(t)$$
$$+ \sum_{n=1}^{\infty}\Bigg[\frac{\operatorname{Re}\left\{(1+i)^{4n}\right\} - \operatorname{Im}\left\{(1+i)^{4n}\right\}}{2(4n)!} - \frac{\mu \operatorname{Im}\left\{(1+i)^{4n-1}\right\}}{(4n-1)!}\Bigg] L^{4n-1}(-\kappa)^n y^{(2n)}(t)$$
$$- \sum_{n=1}^{\infty}\Bigg[\frac{\lambda\mu}{2}\left(\frac{\operatorname{Re}\left\{(1+i)^{4n}\right\} - \operatorname{Im}\left\{(1+i)^{4n}\right\}}{(4n)!}\right)$$
$$+ \frac{\lambda \operatorname{Re}\left\{(1+i)^{4n+1}\right\}}{(4n+1)!}\Bigg] L^{4n+3}(-\kappa)^{n+1} y^{(2n+2)}(t)$$

It can be verified that for all positive n values,

$$\operatorname{Re}\left\{(1+i)^{4n}\right\} - \operatorname{Im}\left\{(1+i)^{4n}\right\} = (-4)^n$$

$$\operatorname{Im}\left\{(1+i)^{4n-1}\right\} = -\frac{1}{2}(-4)^n$$

$$\operatorname{Re}\left\{(1+i)^{4n+1}\right\} = (-4)^n$$

Returning to the preceding expression,

$$\begin{aligned}\frac{\partial w(0,t)}{\partial x} &= \frac{1}{L}y(t) + \lambda L^3\kappa y^{(2)}(t) + \sum_{n=1}^{\infty}\left[\frac{(-4)^n}{2(4n)!} + \frac{\mu(-4)^n}{2(4n-1)!}\right]L^{4n-1}(-\kappa)^n y^{(2n)}(t)\\ &\quad - \sum_{n=1}^{\infty}\left[\frac{\lambda\mu}{2}\frac{(-4)^n}{(4n)!} + \frac{\lambda(-4)^n}{(4n+1)!}\right]L^{4n+3}(-\kappa)^{n+1}y^{(2n+2)}(t)\\ &= \frac{1}{L}y(t) + \lambda L^3\kappa y^{(2)}(t) + \sum_{n=1}^{\infty}\frac{(4\kappa)^n L^{4n-1}}{2}\left[\frac{1}{(4n)!} + \frac{\mu}{(4n-1)!}\right]y^{(2n)}(t)\\ &\quad - \sum_{n=1}^{\infty}\frac{\lambda(4\kappa)^{n+1}L^{4n+3}}{(-4)}\left[\frac{\mu}{2(4n)!} + \frac{1}{(4n+1)!}\right]y^{(2n+2)}(t)\end{aligned}$$

It immediately follows that

$$\begin{aligned}\frac{\partial^3 w(0,t)}{\partial t^2\partial x} &= \frac{1}{L}y^{(2)}(t) + \lambda L^3\kappa y^{(4)}(t) + \sum_{n=1}^{\infty}\frac{(4\kappa)^n L^{4n-1}}{2}\left[\frac{1}{(4n)!} + \frac{\mu}{(4n-1)!}\right]y^{(2n+2)}(t)\\ &\quad - \sum_{n=1}^{\infty}\frac{\lambda(4\kappa)^{n+1}L^{4n+3}}{(-4)}\left[\frac{\mu}{2(4n)!} + \frac{1}{(4n+1)!}\right]y^{(2n+4)}(t)\end{aligned} \tag{7.49}$$

Turning to expression (7.48) and substituting $x = 0$,

$$\begin{aligned}\frac{\partial^2 w(0,t)}{\partial x^2} &= \frac{\lambda L^2\operatorname{Re}\{(2)(1)\}}{2}(-\kappa)y^{(2)}(t)\\ &\quad + \sum_{n=1}^{\infty}\left[\frac{\operatorname{Im}\left\{(4n+1)(4n)(L+iL)^{4n-1}\right\} - \operatorname{Re}\left\{(4n+1)(4n)(L+iL)^{4n-1}\right\}}{2L(4n+1)!}\right.\\ &\qquad \left. + \frac{\mu\operatorname{Im}\left\{4n(4n-1)(L+iL)^{4n-2}\right\}}{(4n)!}\right](-\kappa)^n y^{(2n)}(t)\\ &\quad - \sum_{n=1}^{\infty}\left[\frac{\lambda\mu L^3}{2}\left(\frac{\operatorname{Im}\left\{(4n+1)(4n)(L+iL)^{4n-1}\right\} - \operatorname{Re}\left\{(4n+1)(4n)(L+iL)^{4n-1}\right\}}{(4n+1)!}\right)\right.\\ &\qquad \left. - \frac{\lambda L^2\operatorname{Re}\left\{(4n+2)(4n+1)(L+iL)^{4n}\right\}}{(4n+2)!}\right](-\kappa)^{n+1}y^{(2n+2)}(t)\\ &= -\lambda L^2\kappa y^{(2)}(t)\\ &\quad + \sum_{n=1}^{\infty}\left[\frac{L^{4n-2}\left(\operatorname{Im}\left\{(1+i)^{4n-1}\right\} - \operatorname{Re}\left\{(1+i)^{4n-1}\right\}\right)}{2(4n-1)!}\right.\\ &\qquad \left. + \frac{\mu L^{4n-2}\operatorname{Im}\left\{(1+i)^{4n-2}\right\}}{(4n-2)!}\right](-\kappa)^n y^{(2n)}(t)\\ &\quad - \sum_{n=1}^{\infty}\left[\frac{\lambda\mu L^{4n+2}\left(\operatorname{Im}\left\{(1+i)^{4n-1}\right\} - \operatorname{Re}\left\{(1+i)^{4n-1}\right\}\right)}{2(4n-1)!}\right.\\ &\qquad \left. - \frac{\lambda L^{4n+2}\operatorname{Re}\left\{(1+i)^{4n}\right\}}{(4n)!}\right](-\kappa)^{n+1}y^{(2n+2)}(t)\end{aligned}$$

as before, it can be verified that for $n > 0$,

$$\begin{aligned}\mathrm{Im}\left\{(1+i)^{4n-1}\right\} - \mathrm{Re}\left\{(1+i)^{4n-1}\right\} &= -(-4)^n \\ \mathrm{Im}\left\{(1+i)^{4n-2}\right\} &= -\frac{1}{2}(-4)^n \\ \mathrm{Re}\left\{(1+i)^{4n}\right\} &= (-4)^n\end{aligned}$$

returning to the preceding expression,

$$\begin{aligned}\frac{\partial^2 w(0,t)}{\partial x^2} &= -\lambda L^2 \kappa y^{(2)}(t) + \sum_{n=1}^{\infty}\left[\frac{-L^{4n-2}(-4)^n}{2(4n-1)!} - \frac{\mu L^{4n-2}(-4)^n}{2(4n-2)!}\right](-\kappa)^n y^{(2n)}(t) \\ &\quad - \sum_{n=1}^{\infty}\left[\frac{-\lambda\mu L^{4n+2}(-4)^n}{2(4n-1)!} - \frac{\lambda L^{4n+2}(-4)^n}{(4n)!}\right](-\kappa)^{n+1} y^{(2n+2)}(t)\end{aligned}$$

giving

$$\begin{aligned}\frac{\partial^2 w(0,t)}{\partial x^2} &= -\lambda L^2 \kappa y^{(2)}(t) - \sum_{n=1}^{\infty}\frac{(4\kappa)^n L^{4n-2}}{2}\left[\frac{1}{(4n-1)!} + \frac{\mu}{(4n-2)!}\right] y^{(2n)}(t) \\ &\quad + \sum_{n=1}^{\infty}\frac{\lambda(4\kappa)^{n+1}L^{4n+2}}{(-4)}\left[\frac{\mu}{2(4n-1)!} + \frac{1}{(4n)!}\right] y^{(2n+2)}(t)\end{aligned} \tag{7.50}$$

Using (7.49) and (7.50) in the input expression (7.26) gives the final input expression,

$$\begin{aligned}\tau(t) &= \frac{J_{\mathrm{hub}}}{L} y^{(2)}(t) + J_{\mathrm{hub}}\lambda L^3 \kappa y^{(4)}(t) + \sum_{n=1}^{\infty}\frac{J_{\mathrm{hub}}(4\kappa)^n L^{4n-1}}{2}\left[\frac{1}{(4n)!} + \frac{\mu}{(4n-1)!}\right] y^{(2n+2)}(t) \\ &\quad + \sum_{n=1}^{\infty}\frac{J_{\mathrm{hub}}\lambda(4\kappa)^{n+1}L^{4n+3}}{4}\left[\frac{\mu}{2(4n)!} + \frac{1}{(4n+1)!}\right] y^{(2n+4)}(t) \\ &\quad + EI\lambda L^2 \kappa y^{(2)}(t) + \sum_{n=1}^{\infty}\frac{EI(4\kappa)^n L^{4n-2}}{2}\left[\frac{1}{(4n-1)!} + \frac{\mu}{(4n-2)!}\right] y^{(2n)}(t) \\ &\quad + \sum_{n=1}^{\infty}\frac{EI\lambda(4\kappa)^{n+1}L^{4n+2}}{4}\left[\frac{\mu}{2(4n-1)!} + \frac{1}{(4n)!}\right] y^{(2n+2)}(t)\end{aligned} \tag{7.51}$$

where, from before,

$$\kappa = \frac{\rho A}{EI} \qquad \lambda = \frac{J_p}{L^3 \rho A} \qquad \mu = \frac{m_p}{L\rho A}$$

The expressions (7.46) and (7.51) give the state and input for the rotating beam system with tip payload in terms of the flat output and its time derivatives. These expressions reduce to the no-payload expressions (3.20) and (3.21) by setting $\lambda = 0$ and $\mu = 0$. To obtain the same expressions it is necessary to multiply both $P(x,s)$ and $Q(x,s)$ by $2L$. This is possible due to the non-uniqueness of state and input parametrization, as discussed in Section 3.3.

Chapter 8

Levitating Flexible Beam and Superposition

This chapter investigates the controlled levitation of a flexible beam with multiple force inputs. We present the system model and derive the open-loop control using the principle of superposition.

8.1 Introduction

The original motivation for this investigation comes from an active magnetic bearing system shown in Figure 8.1. The rotor is supported by two magnetic bearings and driven via a flexible coupling by a DC motor seen on the far right of the figure. Since the rotor is long and slender, it experiences lateral deformation during high-speed rotation. Here we design an open-loop control for the system using the flatness-based approach described in Chapter 3.

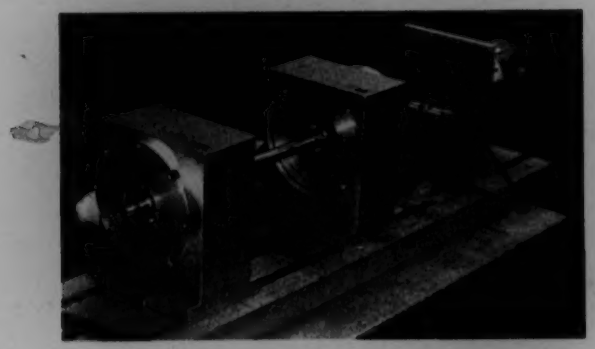

Figure 8.1: Active magnetic bearing

To keep things simple, we assume no beam rotation and only consider the problem of levitation in a vertical plane. This situation is encountered during system start-up when the rotor is lifted from its supports to a centered configuration. The two bearings are assumed to exert point forces on the rotor. The system is shown schematically in Figure 8.2.

In order to use the flatness-based techniques, the system must be expressed in BVP form with inputs appearing in the BCs. The system model consists of 3 coupled PDEs in $w_1(x,t)$, $w_2(x,t)$ and $w_3(x,t)$ and 12 BCs (4 BCs for each PDE). While modeling such a system is

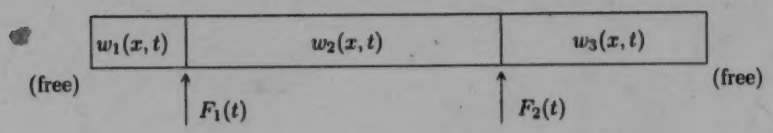

Figure 8.2: 3-input system with 3 displacement fields

straightforward, deriving its control is difficult due to the large complexity in the expressions that result. We manage this complexity by applying the principle of superposition.

8.2 Input Superposition

As the governing Euler-Bernoulli PDEs are *linear*, we can apply the principle of superposition. This technique appears in [64, 65]. The idea is shown graphically in Figure 8.3: to obtain the response of a multi-input model, we calculate the response to individual forces, then sum up the results. As will be seen shortly, this approach requires carrying out the symbolic calculations only once, leaving the location of where the force is applied as a parameter.

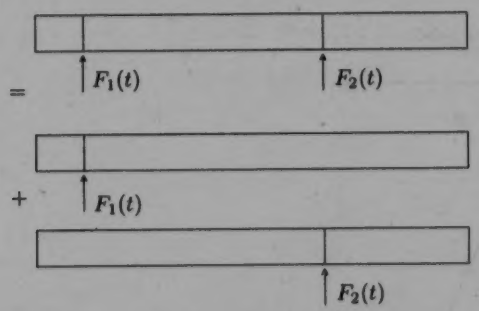

Figure 8.3: Graphical interpretation of superposition

8.3 Boundary Conditions and Input Forces

As mentioned before, the system inputs appear in the BCs. We will work out the expressions for these BCs using results in Section 2.2.2. We focus on a common boundary between two segments of the beam at $x = l$, where the external force F_{ext} and moment M_{ext} are being applied. Internal forces and moments are present in both segments. This is shown in Figure 8.4.

Performing a force balance at the inner boundary in Figure 8.4, taking upwards as positive, and using (2.8) for the internal force expression,

$$F_1 - F_2 = F_{ext}$$

$$-EI\frac{\partial^3 w_1(l,t)}{\partial x^3} - \left(-EI\frac{\partial^3 w_2(l,t)}{\partial x^3}\right) = F_{ext}$$

$$-\frac{\partial^3 w_1(l,t)}{\partial x^3} + \frac{\partial^3 w_2(l,t)}{\partial x^3} = \frac{F_{ext}}{EI}$$

Figure 8.4: Internal and external forces at inner beam boundary, $x = l$

If no external force is applied at the boundary, $F_{ext} = 0$ and the BC becomes

$$\frac{\partial^3 w_1(l,t)}{\partial x^3} = \frac{\partial^3 w_2(l,t)}{\partial x^3}$$

A moment balance at the inner boundary in Figure 8.4, taking counter-clockwise as positive and using (2.7) for the internal moment expression,

$$\begin{aligned} M_1 - M_2 &= M_{ext} \\ EI\frac{\partial^2 w_1(l,t)}{\partial x^2} - EI\frac{\partial^2 w_2(l,t)}{\partial x^2} &= M_{ext} \\ \frac{\partial^2 w_1(l,t)}{\partial x^2} - \frac{\partial^2 w_2(l,t)}{\partial x^2} &= \frac{M_{ext}}{EI} \end{aligned}$$

If no external moment is present, $M_{ext} = 0$, so the BC is

$$\frac{\partial^2 w_1(l,t)}{\partial x^2} = \frac{\partial^2 w_2(l,t)}{\partial x^2}$$

The above discussion provides two BCs. We have four more from the beam ends. We need a total of eight BCs, four per PDE. The remaining two BCs are due to the beam being continuous at the inner boundary:

$$\begin{aligned} w_1(l,t) &= w_2(l,t) \\ \frac{\partial w_1(l,t)}{\partial x} &= \frac{\partial w_2(l,t)}{\partial x} \end{aligned}$$

8.4 Problem Formulation for Single-input System

We work with the system shown in Figure 8.5: a two-segment, one-input flexible beam modeled by the Euler-Bernoulli PDE. The results obtained will be used to treat the multi-input case by superposition.

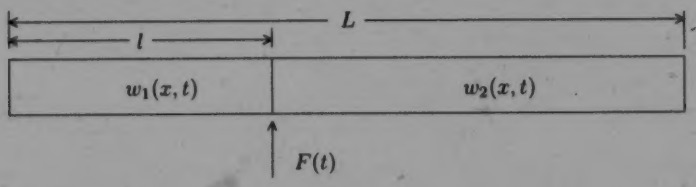

Figure 8.5: Two-segment beam with input at $x = l$

The beam is governed by the system of PDEs

$$\begin{aligned} EI\frac{\partial^4 w_1(x,t)}{\partial x^4} + \rho A\frac{\partial^2 w_1(x,t)}{\partial t^2} &= 0 \\ EI\frac{\partial^4 w_2(x,t)}{\partial x^4} + \rho A\frac{\partial^2 w_2(x,t)}{\partial t^2} &= 0 \end{aligned} \tag{8.1}$$

with BCs

$$\begin{aligned} \frac{\partial^2 w_1(0,t)}{\partial x^2} &= 0 & w_1(l,t) &= w_2(l,t) \\ \frac{\partial^3 w_1(0,t)}{\partial x^3} &= 0 & \frac{\partial w_1(l,t)}{\partial x} &= \frac{\partial w_2(l,t)}{\partial x} \\ \frac{\partial^2 w_1(l,t)}{\partial x^2} &= \frac{\partial^2 w_2(l,t)}{\partial x^2} & \frac{\partial^2 w_2(L,t)}{\partial x^2} &= 0 \\ -\frac{\partial^3 w_1(l,t)}{\partial x^3} + \frac{\partial^3 w_2(l,t)}{\partial x^3} &= \frac{F(t)}{EI} & \frac{\partial^3 w_2(L,t)}{\partial x^3} &= 0 \end{aligned} \tag{8.2}$$

and ICs

$$\begin{aligned} w_1(x,0) &= 0 & w_2(x,0) &= 0 \\ \frac{\partial w_1(x,0)}{\partial t} &= 0 & \frac{\partial w_2(x,0)}{\partial t} &= 0 \end{aligned} \tag{8.3}$$

To simplify the series manipulations, we normalize the x and t variables, as was done in Section 7.4. Let

$$\begin{aligned} \tilde{x} &= \frac{x}{L} & a &= \frac{l}{L} & \tilde{t} &= \frac{\sqrt{EI}}{L^2\sqrt{\rho A}}\,t \\ \tilde{w}_1(\tilde{x},\tilde{t}) &= w_1(x,t) & \tilde{w}_2(\tilde{x},\tilde{t}) &= w_2(x,t) \end{aligned} \tag{8.4}$$

Using (8.4), (8.1) becomes:

$$\begin{aligned} EI\frac{\partial^4 \tilde{w}_1(\tilde{x},\tilde{t})}{\partial x^4} + \rho A\frac{\partial^2 \tilde{w}_1(\tilde{x},\tilde{t})}{\partial t^2} &= 0 \\ EI\frac{\partial^4 \tilde{w}_2(\tilde{x},\tilde{t})}{\partial x^4} + \rho A\frac{\partial^2 \tilde{w}_2(\tilde{x},\tilde{t})}{\partial t^2} &= 0 \end{aligned} \tag{8.5}$$

Note that

$$\begin{aligned} \frac{\partial \tilde{w}}{\partial x} &= \frac{\partial \tilde{w}}{\partial \tilde{x}}\frac{d\tilde{x}}{dx} = \frac{\partial \tilde{w}}{\partial \tilde{x}}\left(\frac{1}{L}\right) \\ \frac{\partial^2 \tilde{w}}{\partial x^2} &= \frac{\partial}{\partial x}\left(\frac{\partial \tilde{w}}{\partial x}\right) = \frac{\partial}{\partial x}\left(\frac{\partial \tilde{w}}{\partial \tilde{x}}\frac{1}{L}\right) = \frac{1}{L}\frac{\partial}{\partial \tilde{x}}\left(\frac{\partial \tilde{w}}{\partial \tilde{x}}\right)\frac{d\tilde{x}}{dx} = \frac{1}{L^2}\frac{\partial^2 \tilde{w}}{\partial \tilde{x}^2} \\ \frac{\partial^3 \tilde{w}}{\partial x^3} &= \frac{1}{L^3}\frac{\partial^3 \tilde{w}}{\partial \tilde{x}^3} \\ \frac{\partial^4 \tilde{w}}{\partial x^4} &= \frac{1}{L^4}\frac{\partial^4 \tilde{w}}{\partial \tilde{x}^4} \end{aligned}$$

Also,

$$\begin{aligned} \frac{\partial \tilde{w}}{\partial t} &= \frac{\partial \tilde{w}}{\partial \tilde{t}}\frac{d\tilde{t}}{dt} = \frac{\sqrt{EI}}{L^2\sqrt{\rho A}}\frac{\partial \tilde{w}}{\partial \tilde{t}} \\ \frac{\partial^2 \tilde{w}}{\partial t^2} &= \frac{\partial}{\partial t}\left(\frac{\partial \tilde{w}}{\partial t}\right) = \frac{\partial}{\partial \tilde{t}}\left(\frac{\partial \tilde{w}}{\partial t}\right)\frac{d\tilde{t}}{dt} = \frac{\partial}{\partial \tilde{t}}\left(\frac{\sqrt{EI}}{L^2\sqrt{\rho A}}\frac{\partial \tilde{w}}{\partial \tilde{t}}\right)\frac{\sqrt{EI}}{L^2\sqrt{\rho A}} = \frac{EI}{L^4\rho A}\left(\frac{\partial^2 \tilde{w}}{\partial \tilde{t}^2}\right) \end{aligned}$$

Substituting the above expressions into (8.5):

$$EI\left(\frac{1}{L^4}\frac{\partial^4\tilde{w}_1}{\partial\tilde{x}^4}\right)+\rho A\left(\frac{EI}{L^4\rho A}\frac{\partial^2\tilde{w}_1}{\partial\tilde{t}^2}\right)=0$$

$$EI\left(\frac{1}{L^4}\frac{\partial^4\tilde{w}_2}{\partial\tilde{x}^4}\right)+\rho A\left(\frac{EI}{L^4\rho A}\frac{\partial^2\tilde{w}_2}{\partial\tilde{t}^2}\right)=0$$

$$\frac{\partial^4\tilde{w}_1}{\partial\tilde{x}^4}+\frac{\partial^2\tilde{w}_1}{\partial\tilde{t}^2}=0 \qquad 0<\tilde{x}<a \qquad \tilde{t}\geq 0$$

$$\frac{\partial^4\tilde{w}_2}{\partial\tilde{x}^4}+\frac{\partial^2\tilde{w}_2}{\partial\tilde{t}^2}=0 \qquad a<\tilde{x}<1 \qquad \tilde{t}\geq 0$$

Now normalizing BCs in (8.2):

$$0=\frac{\partial^2 w_1(0,t)}{\partial x^2}=\frac{\partial^2\tilde{w}_1(0,\tilde{t})}{\partial x^2}=\frac{1}{L^2}\frac{\partial^2\tilde{w}_1(0,\tilde{t})}{\partial\tilde{x}^2} \qquad \frac{\partial^2\tilde{w}_1(0,\tilde{t})}{\partial\tilde{x}^2}=0$$

$$0=\frac{\partial^3 w_1(0,t)}{\partial x^3}=\frac{\partial^3\tilde{w}_1(0,\tilde{t})}{\partial x^3}=\frac{1}{L^3}\frac{\partial^3\tilde{w}_1(0,\tilde{t})}{\partial\tilde{x}^3} \qquad \frac{\partial^3\tilde{w}_1(0,\tilde{t})}{\partial\tilde{x}^3}=0$$

$$0=\frac{\partial^2 w_2(L,t)}{\partial x^2}=\frac{\partial^2\tilde{w}_2(1,\tilde{t})}{\partial x^2}=\frac{1}{L^2}\frac{\partial^2\tilde{w}_2(1,\tilde{t})}{\partial\tilde{x}^2} \qquad \frac{\partial^2\tilde{w}_2(1,\tilde{t})}{\partial\tilde{x}^2}=0$$

$$0=\frac{\partial^3 w_2(L,t)}{\partial x^3}=\frac{\partial^3\tilde{w}_2(1,\tilde{t})}{\partial x^3}=\frac{1}{L^3}\frac{\partial^3\tilde{w}_2(1,\tilde{t})}{\partial\tilde{x}^3} \qquad \frac{\partial^3\tilde{w}_2(1,\tilde{t})}{\partial\tilde{x}^3}=0$$

$$w_1(l,t)=w_2(l,t) \qquad \tilde{w}_1(a,\tilde{t})=\tilde{w}_2(a,\tilde{t})$$

$$\frac{\partial w_1(l,t)}{\partial x}=\frac{\partial w_2(l,t)}{\partial x}$$

$$\frac{\partial\tilde{w}_1(a,\tilde{t})}{\partial x}=\frac{\partial\tilde{w}_2(a,\tilde{t})}{\partial x}$$

$$\frac{1}{L}\frac{\partial\tilde{w}_1(a,\tilde{t})}{\partial\tilde{x}}=\frac{1}{L}\frac{\partial\tilde{w}_2(a,\tilde{t})}{\partial\tilde{x}} \qquad \frac{\partial\tilde{w}_1(a,\tilde{t})}{\partial\tilde{x}}=\frac{\partial\tilde{w}_2(a,\tilde{t})}{\partial\tilde{x}}$$

$$\frac{\partial^2 w_1(l,t)}{\partial x^2}=\frac{\partial^2 w_2(l,t)}{\partial x^2}$$

$$\frac{\partial^2\tilde{w}_1(a,\tilde{t})}{\partial x^2}=\frac{\partial^2\tilde{w}_2(a,\tilde{t})}{\partial x^2}$$

$$\frac{1}{L^2}\frac{\partial^2\tilde{w}_1(a,\tilde{t})}{\partial\tilde{x}^2}=\frac{1}{L^2}\frac{\partial^2\tilde{w}_2(a,\tilde{t})}{\partial\tilde{x}^2} \qquad \frac{\partial^2\tilde{w}_1(a,\tilde{t})}{\partial\tilde{x}^2}=\frac{\partial^2\tilde{w}_2(a,\tilde{t})}{\partial\tilde{x}^2}$$

And for the input term,

$$-\frac{\partial^3 w_1(l,t)}{\partial x^3}+\frac{\partial^3 w_2(l,t)}{\partial x^3}=\frac{F(t)}{EI}$$

$$-\frac{\partial^3\tilde{w}_1(a,\tilde{t})}{\partial x^3}+\frac{\partial^3\tilde{w}_2(a,\tilde{t})}{\partial x^3}=\frac{F\left(\frac{L^2\sqrt{\rho A}}{\sqrt{EI}}\tilde{t}\right)}{EI}$$

$$-\frac{1}{L^3}\frac{\partial^3\tilde{w}_1(a,\tilde{t})}{\partial\tilde{x}^3}+\frac{1}{L^3}\frac{\partial^3\tilde{w}_2(a,\tilde{t})}{\partial\tilde{x}^3}=\frac{F\left(\frac{L^2\sqrt{\rho A}}{\sqrt{EI}}\tilde{t}\right)}{EI}$$

$$-\frac{\partial^3\tilde{w}_1(a,\tilde{t})}{\partial\tilde{x}^3}+\frac{\partial^3\tilde{w}_2(a,\tilde{t})}{\partial\tilde{x}^3}=\frac{L^3F\left(\frac{L^2\sqrt{\rho A}}{\sqrt{EI}}\tilde{t}\right)}{EI}=u(\tilde{t})$$

where $u(\tilde{t})$ is introduced for compactness. Normalizing the ICs in (8.3),

$$0=w_1(x,0) \qquad \tilde{w}_1(\tilde{x},0)=0$$

$$0=\frac{\partial w_1(x,0)}{\partial t}=\frac{\partial\tilde{w}_1(\tilde{x},0)}{\partial t}=\frac{\sqrt{EI}}{L^2\sqrt{\rho A}}\frac{\partial\tilde{w}_1(\tilde{x},0)}{\partial\tilde{t}} \qquad \frac{\partial\tilde{w}_1(\tilde{x},0)}{\partial\tilde{t}}=0$$

$$0 = w_2(x,0) \qquad \tilde{w}_2(\tilde{x},0) = 0$$
$$0 = \frac{\partial w_2(x,0)}{\partial t} = \frac{\partial \tilde{w}_2(\tilde{x},0)}{\partial t} = \frac{\sqrt{EI}}{L^2\sqrt{\rho A}} \frac{\partial \tilde{w}_2(\tilde{x},0)}{\partial \tilde{t}} \qquad \frac{\partial \tilde{w}_2(\tilde{x},0)}{\partial \tilde{t}} = 0$$

8.5 Normalized Problem Formulation: Single-input

Following normalization, the original problem (8.1), (8.2) and (8.3) becomes transformed into that shown in Figure 8.6. Dropping the ~ notation for compactness, the normalized

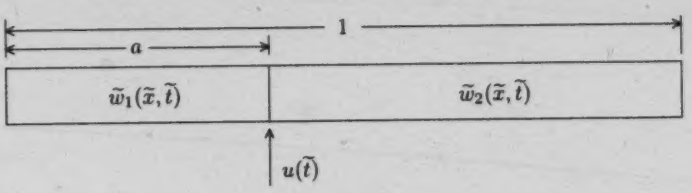

Figure 8.6: Normalized 1-input 2-segment beam problem

system of PDEs is

$$\begin{aligned} \frac{\partial^4 w_1(x,t)}{\partial x^4} + \frac{\partial^2 w_1(x,t)}{\partial t^2} &= 0 \\ \frac{\partial^4 w_2(x,t)}{\partial x^4} + \frac{\partial^2 w_2(x,t)}{\partial t^2} &= 0 \end{aligned} \tag{8.6}$$

with BCs

$$\begin{aligned} \frac{\partial^2 w_1(0,t)}{\partial x^2} &= 0 & w_1(a,t) &= w_2(a,t) \\ \frac{\partial^3 w_1(0,t)}{\partial x^3} &= 0 & \frac{\partial w_1(a,t)}{\partial x} &= \frac{\partial w_2(a,t)}{\partial x} \\ \frac{\partial^2 w_1(a,t)}{\partial x^2} &= \frac{\partial^2 w_2(a,t)}{\partial x^2} & \frac{\partial^2 w_2(1,t)}{\partial x^2} &= 0 \\ -\frac{\partial^3 w_1(a,t)}{\partial x^3} + \frac{\partial^3 w_2(a,t)}{\partial x^3} &= u(t) & \frac{\partial^3 w_2(1,t)}{\partial x^3} &= 0 \end{aligned} \tag{8.7}$$

and ICs

$$\begin{aligned} w_1(x,0) &= 0 & w_2(x,0) &= 0 \\ \frac{\partial w_1(x,0)}{\partial t} &= 0 & \frac{\partial w_2(x,0)}{\partial t} &= 0 \end{aligned} \tag{8.8}$$

Applying the Laplace transform to (8.6) and (8.7),

$$\begin{aligned} \frac{\partial^4 W_1(x,s)}{\partial x^4} + s^2 W_1(x,s) &= 0 \\ \frac{\partial^4 W_2(x,s)}{\partial x^4} + s^2 W_2(x,s) &= 0 \end{aligned}$$

$$\begin{aligned} \frac{\partial^2 W_1(0,s)}{\partial x^2} &= 0 & W_1(a,s) &= W_2(a,s) \\ \frac{\partial^3 W_1(0,s)}{\partial x^3} &= 0 & \frac{\partial W_1(a,s)}{\partial x} &= \frac{\partial W_2(a,s)}{\partial x} \\ \frac{\partial^2 W_1(a,s)}{\partial x^2} &= \frac{\partial^2 W_2(a,s)}{\partial x^2} & \frac{\partial^2 W_2(1,s)}{\partial x^2} &= 0 \\ -\frac{\partial^3 W_1(a,s)}{\partial x^3} + \frac{\partial^3 W_2(a,s)}{\partial x^3} &= U(s) & \frac{\partial^3 W_2(1,s)}{\partial x^3} &= 0 \end{aligned}$$

From (3.7), the solution is known to be

$$\begin{aligned} W_1(x,s) &= A(s)\cosh(\sqrt{is}x) + B(s)\sinh(\sqrt{is}x) + C(s)\cos(\sqrt{is}x) + D(s)\sin(\sqrt{is}x) \\ W_2(x,s) &= E(s)\cosh(\sqrt{is}x) + F(s)\sinh(\sqrt{is}x) + G(s)\cos(\sqrt{is}x) + H(s)\sin(\sqrt{is}x) \end{aligned} \tag{8.9}$$

Taking the derivatives of $W_1(x,s)$ and $W_2(x,s)$ with respect to x, dropping the argument of s for compactness,

$$\begin{aligned} \frac{\partial W_1(x,s)}{\partial x} &= A\sqrt{is}\sinh(\sqrt{is}x) + B\sqrt{is}\cosh(\sqrt{is}x) - C\sqrt{is}\sin(\sqrt{is}x) + D\sqrt{is}\cos(\sqrt{is}x) \\ \frac{\partial^2 W_1(x,s)}{\partial x^2} &= Ais\cosh(\sqrt{is}x) + Bis\sinh(\sqrt{is}x) - Cis\cos(\sqrt{is}x) - Dis\sin(\sqrt{is}x) \\ \frac{\partial^3 W_1(x,s)}{\partial x^3} &= A(is)^{3/2}\sinh(\sqrt{is}x) + B(is)^{3/2}\cosh(\sqrt{is}x) + C(is)^{3/2}\sin(\sqrt{is}x) \\ &\quad - D(is)^{3/2}\cos(\sqrt{is}x) \\ \frac{\partial W_2(x,s)}{\partial x} &= E\sqrt{is}\sinh(\sqrt{is}x) + F\sqrt{is}\cosh(\sqrt{is}x) - G\sqrt{is}\sin(\sqrt{is}x) + H\sqrt{is}\cos(\sqrt{is}x) \\ \frac{\partial^2 W_2(x,s)}{\partial x^2} &= Eis\cosh(\sqrt{is}x) + Fis\sinh(\sqrt{is}x) - Gis\cos(\sqrt{is}x) - His\sin(\sqrt{is}x) \\ \frac{\partial^3 W_2(x,s)}{\partial x^3} &= E(is)^{3/2}\sinh(\sqrt{is}x) + F(is)^{3/2}\cosh(\sqrt{is}x) + G(is)^{3/2}\sin(\sqrt{is}x) \\ &\quad - H(is)^{3/2}\cos(\sqrt{is}x) \end{aligned}$$

Using the above expressions with the transformed BCs gives a linear system of 8 equations in 8 unknowns $\{A \ldots H\}$:

$$\begin{aligned} Ais - Cis &= 0 \\ B(is)^{3/2} - D(is)^{3/2} &= 0 \\ Eis\cosh(\sqrt{is}) + Fis\sinh(\sqrt{is}) - G(s)is\cos(\sqrt{is}) - H(s)is\sin(\sqrt{is}) &= 0 \\ E(is)^{3/2}\sinh(\sqrt{is}) + F(is)^{3/2}\cosh(\sqrt{is}) + G(s)(is)^{3/2}\sin(\sqrt{is}) - H(s)(is)^{3/2}\cos(\sqrt{is}) &= 0 \\ A\cosh(a\sqrt{is}) + B\sinh(a\sqrt{is}) + C\cos(a\sqrt{is}) + D\sin(a\sqrt{is}) &= \\ E\cosh(a\sqrt{is}) + F\sinh(a\sqrt{is}) + G(s)\cos(a\sqrt{is}) + H(s)\sin(a\sqrt{is}) & \\ A\sqrt{is}\sinh(a\sqrt{is}) + B\sqrt{is}\cosh(a\sqrt{is}) - C\sqrt{is}\sin(a\sqrt{is}) + D\sqrt{is}\cos(a\sqrt{is}) &= \\ E\sqrt{is}\sinh(a\sqrt{is}) + F\sqrt{is}\cosh(a\sqrt{is}) - G(s)\sqrt{is}\sin(a\sqrt{is}) + H(s)\sqrt{is}\cos(a\sqrt{is}) & \\ Ais\cosh(a\sqrt{is}) + Bis\sinh(a\sqrt{is}) - Cis\cos(a\sqrt{is}) - Dis\sin(a\sqrt{is}) &= \\ Eis\cosh(a\sqrt{is}) + Fis\sinh(a\sqrt{is}) - G(s)is\cos(a\sqrt{is}) - H(s)is\sin(a\sqrt{is}) & \\ -A(is)^{3/2}\sinh(a\sqrt{is}) - B(is)^{3/2}\cosh(a\sqrt{is}) - C(is)^{3/2}\sin(a\sqrt{is}) & \\ +D(is)^{3/2}\cos(a\sqrt{is}) + E(is)^{3/2}\sinh(a\sqrt{is}) + F(is)^{3/2}\cosh(a\sqrt{is}) & \\ +G(s)(is)^{3/2}\sin(a\sqrt{is}) - H(s)(is)^{3/2}\cos(a\sqrt{is}) &= U(s) \end{aligned}$$

Simplifying,

$$\begin{aligned} A - C &= 0 \\ B - D &= 0 \\ E\cosh(\sqrt{is}) + F\sinh(\sqrt{is}) - G(s)\cos(\sqrt{is}) - H\sin(\sqrt{is}) &= 0 \\ E\sinh(\sqrt{is}) + F\cosh(\sqrt{is}) + G(s)\sin(\sqrt{is}) - H\cos(\sqrt{is}) &= 0 \\ (A-E)\cosh(a\sqrt{is}) + (B-F)\sinh(a\sqrt{is}) & \end{aligned}$$

$$
\begin{aligned}
&+(C-G)\cos(a\sqrt{is})+(D-H)\sin(a\sqrt{is})=0\\
&(A-E)\sinh(a\sqrt{is})+(B-F)\cosh(a\sqrt{is})\\
&+(-C+G)\sin(a\sqrt{is})+(D-H)\cos(a\sqrt{is})=0\\
&(A-E)\cosh(a\sqrt{is})+(B-F)\sinh(a\sqrt{is})\\
&+(-C+G)\cos(a\sqrt{is})+(-D+H)\sin(a\sqrt{is})=0\\
&(-A+E)\sinh(a\sqrt{is})+(-B+F)\cosh(a\sqrt{is})\\
&+(-C+G)\sin(a\sqrt{is})+(D-H)\cos(a\sqrt{is})=\frac{U(s)}{(is)^{3/2}}
\end{aligned}
$$

The above linear system of equations is solved and substituted into (8.9), giving

$$
W_1(x,s)=\frac{P(x,s)}{Q(x,s)}U(s) \qquad\qquad W_2(x,s)=\frac{R(x,s)}{Q(x,s)}U(s) \tag{8.10}
$$

where

$$
\begin{aligned}
&P(x,s)=(is)^{-3/2}\\
&\Big\{\cosh[\sqrt{is}(a+x-1)]\sin(\sqrt{is})-\cosh[\sqrt{is}(x-1)]\sin[\sqrt{is}(a-1)]+\cosh(\sqrt{is}\,x)\sin(\sqrt{is}\,a)\\
&-\cosh(\sqrt{is})\sin[\sqrt{is}(a-x-1)]+\sin[\sqrt{is}(a-x)]-\cosh[\sqrt{is}(a-1)]\sin[\sqrt{is}(x-1)]\\
&+\cosh(\sqrt{is}\,a)\sin(\sqrt{is}\,x)-\cos[\sqrt{is}(a+x-1)]\sinh(\sqrt{is})+\cos[\sqrt{is}(x-1)]\sinh[\sqrt{is}(a-1)]\\
&-\cos(\sqrt{is}\,x)\sinh(\sqrt{is}\,a)+\cos(\sqrt{is})\sinh[\sqrt{is}(a-x-1)]-\sinh[\sqrt{is}(a-x)]\\
&+\cos[\sqrt{is}(a-1)]\sinh[\sqrt{is}(x-1)]-\cos(\sqrt{is}\,a)\sinh(\sqrt{is}\,x)\Big\}
\end{aligned}
\tag{8.11}
$$

$$
Q(x,s)=4\Big\{-1+\cos(\sqrt{is})\cosh(\sqrt{is})\Big\} \tag{8.12}
$$

$$
\begin{aligned}
&R(x,s)=(is)^{(-3/2)}\\
&\quad\Big\{\cosh[\sqrt{is}(a+x-1)]\sin(\sqrt{is})-\cosh[\sqrt{is}(x-1)]\sin[\sqrt{is}(a-1)]\\
&\quad+\cosh(\sqrt{is}\,x)\sin(\sqrt{is}\,a)-\sin[\sqrt{is}(a-x)]+\cosh(\sqrt{is})\sin[\sqrt{is}(a-x+1)]\\
&\quad-\cosh[\sqrt{is}(a-1)]\sin[\sqrt{is}(x-1)]+\cosh(\sqrt{is}\,a)\sin(\sqrt{is}\,x)\\
&\quad-\cos[\sqrt{is}(a+x-1)]\sinh(\sqrt{is})+\cos[\sqrt{is}(x-1)]\sinh[\sqrt{is}(a-1)]\\
&\quad-\cos(\sqrt{is}\,x)\sinh(\sqrt{is}\,a)+\sinh[\sqrt{is}(a-x)]-\cos(\sqrt{is})\sinh[\sqrt{is}(a-x+1)]\\
&\quad+\cos[\sqrt{is}(a-1)]\sinh[\sqrt{is}(x-1)]-\cos(\sqrt{is}\,a)\sinh(\sqrt{is}\,x)\Big\}
\end{aligned}
\tag{8.13}
$$

8.6 Infinite Series Representation: Single-input

Expressions (8.11), (8.12) and (8.13) need to be converted into their infinite series representations, in order to perform an inverse Laplace transform.

For compactness, we introduce the definitions:

$$
\begin{aligned}
A&=\sqrt{is}\\
B&=\sqrt{is}(a+x-1)\\
C&=\sqrt{is}(x-1)\\
D&=\sqrt{is}(a-1)
\end{aligned}
$$

$$
\begin{aligned}
E &= \sqrt{is}\,x \\
F &= \sqrt{is}\,a \\
G &= \sqrt{is}(a-x-1) \\
H &= \sqrt{is}(a-x) \\
I &= \sqrt{is}(a-x+1)
\end{aligned}
$$

We also need the trigonometric function power series from Section 3.4.1,

$$
\cosh x = \sum_{k=0}^{\infty} \frac{x^{2k}}{(2k)!} \qquad \cos x = \sum_{k=0}^{\infty} \frac{(-1)^k x^{2k}}{(2k)!}
$$

$$
\sinh x = \sum_{k=0}^{\infty} \frac{x^{2k+1}}{(2k+1)!} \qquad \sin x = \sum_{k=0}^{\infty} \frac{(-1)^k x^{2k+1}}{(2k+1)!}
$$

And the identities

$$
\begin{aligned}
\cosh A \cos B &= \frac{\cosh(A+iB) + \cosh(A-iB)}{2} \\
\sinh A \cos B &= \frac{\sinh(A+iB) + \sinh(A-iB)}{2} \\
\sinh A \sin B &= \frac{\cosh(A+iB) - \cosh(A-iB)}{2i} \\
\cosh A \sin B &= \frac{\sinh(A+iB) - \sinh(A-iB)}{2i}
\end{aligned}
$$

8.6.1 Series Representation of $P(x,s)$

Starting from (8.11),

$$
\begin{aligned}
&P(x,s) \\
&= \frac{1}{A^3}\Big\{ \cosh B \sin A - \cosh C \sin D + \cosh E \sin F - \cosh A \sin G + \sin H - \cosh D \sin C \\
&+ \cosh F \sin E - \cos B \sinh A + \cos C \sinh D - \cos E \sinh F + \cos A \sinh G - \sinh H \\
&+ \cos D \sinh C - \cos F \sinh E \Big\} \\
&= \frac{1}{A^3}\Big\{ \frac{\sinh(B+iA) - \sinh(B-iA)}{2i} - \frac{\sinh(C+iD) - \sinh(C-iD)}{2i} \\
&+ \frac{\sinh(E+iF) - \sinh(E-iF)}{2i} - \frac{\sinh(A+iG) - \sinh(A-iG)}{2i} + \sin H \\
&- \frac{\sinh(D+iC) - \sinh(D-iC)}{2i} + \frac{\sinh(F+iE) - \sinh(F-iE)}{2i} \\
&- \frac{\sinh(A+iB) + \sinh(A-iB)}{2} + \frac{\sinh(D+iC) + \sinh(D-iC)}{2} \\
&- \frac{\sinh(F+iE) + \sinh(F-iE)}{2} + \frac{\sinh(G+iA) + \sinh(G-iA)}{2} - \sinh H \\
&+ \frac{\sinh(C+iD) + \sinh(C-iD)}{2} - \frac{\sinh(E+iF) + \sinh(E-iF)}{2} \Big\} \\
&= \frac{1}{A^3}\Big\{ \frac{i}{2}\Big[\sinh(B-iA) - \sinh(B+iA)\Big] + \frac{i}{2}\Big[\sinh(C+iD) - \sinh(C-iD)\Big] \\
&+ \frac{i}{2}\Big[\sinh(E-iF) - \sinh(E+iF)\Big] + \frac{i}{2}\Big[\sinh(A+iG) - \sinh(A-iG)\Big] + \sin H \\
&+ \frac{i}{2}\Big[\sinh(D+iC) - \sinh(D-iC)\Big] + \frac{i}{2}\Big[\sinh(F-iE) - \sinh(F+iE)\Big]
\end{aligned}
$$

$$
\begin{aligned}
&-\frac{1}{2}\Big[\sinh(A+iB)+\sinh(A-iB)\Big]+\frac{1}{2}\Big[\sinh(D+iC)+\sinh(D-iC)\Big]\\
&-\frac{1}{2}\Big[\sinh(F+iE)+\sinh(F-iE)\Big]+\frac{1}{2}\Big[\sinh(G+iA)+\sinh(G-iA)\Big]-\sinh H\\
&+\frac{1}{2}\Big[\sinh(C+iD)+\sinh(C-iD)\Big]-\frac{1}{2}\Big[\sinh(E+iF)+\sinh(E-iF)\Big]\Big\}\\
&=\frac{1}{A^3}\Big\{\frac{i}{2}\sinh(B-iA)-\frac{i}{2}\sinh(B+iA)+\left(\frac{1+i}{2}\right)\sinh(C+iD)+\left(\frac{1-i}{2}\right)\sinh(C-iD)\\
&-\left(\frac{1+i}{2}\right)\sinh(E+iF)-\left(\frac{1-i}{2}\right)\sinh(E-iF)+\frac{i}{2}\sinh(A+iG)-\frac{i}{2}\sinh(A-iG)\\
&+\sin H+\left(\frac{1+i}{2}\right)\sinh(D+iC)+\left(\frac{1-i}{2}\right)\sinh(D-iC)-\left(\frac{1+i}{2}\right)\sinh(F+iE)\\
&-\left(\frac{1-i}{2}\right)\sinh(F-iE)-\frac{1}{2}\sinh(A+iB)-\frac{1}{2}\sinh(A-iB)+\frac{1}{2}\sinh(G+iA)\\
&+\frac{1}{2}\sinh(G-iA)-\sinh H\Big\}
\end{aligned}
$$

Introducing power series representations, placing the sin and sinh terms first:

$$
\begin{aligned}
&P(x,s)\\
&=\frac{1}{A^3}\Big\{\sum_{k=0}^{\infty}\frac{(-1)^kH^{2k+1}}{(2k+1)!}-\sum_{k=0}^{\infty}\frac{H^{2k+1}}{(2k+1)!}+\frac{i}{2}\sum_{k=0}^{\infty}\frac{(B-iA)^{2k+1}}{(2k+1)!}-\frac{i}{2}\sum_{k=0}^{\infty}\frac{(B+iA)^{2k+1}}{(2k+1)!}\\
&+\left(\frac{1+i}{2}\right)\sum_{k=0}^{\infty}\frac{(C+iD)^{2k+1}}{(2k+1)!}+\left(\frac{1-i}{2}\right)\sum_{k=0}^{\infty}\frac{(C-iD)^{2k+1}}{(2k+1)!}-\left(\frac{1+i}{2}\right)\sum_{k=0}^{\infty}\frac{(E+iF)^{2k+1}}{(2k+1)!}\\
&-\left(\frac{1-i}{2}\right)\sum_{k=0}^{\infty}\frac{(E-iF)^{2k+1}}{(2k+1)!}+\frac{i}{2}\sum_{k=0}^{\infty}\frac{(A+iG)^{2k+1}}{(2k+1)!}-\frac{i}{2}\sum_{k=0}^{\infty}\frac{(A-iG)^{2k+1}}{(2k+1)!}\\
&+\left(\frac{1+i}{2}\right)\sum_{k=0}^{\infty}\frac{(D+iC)^{2k+1}}{(2k+1)!}+\left(\frac{1-i}{2}\right)\sum_{k=0}^{\infty}\frac{(D-iC)^{2k+1}}{(2k+1)!}-\left(\frac{1+i}{2}\right)\sum_{k=0}^{\infty}\frac{(F+iE)^{2k+1}}{(2k+1)!}\\
&-\left(\frac{1-i}{2}\right)\sum_{k=0}^{\infty}\frac{(F-iE)^{2k+1}}{(2k+1)!}-\frac{1}{2}\sum_{k=0}^{\infty}\frac{(A+iB)^{2k+1}}{(2k+1)!}-\frac{1}{2}\sum_{k=0}^{\infty}\frac{(A-iB)^{2k+1}}{(2k+1)!}\\
&+\frac{1}{2}\sum_{k=0}^{\infty}\frac{(G+iA)^{2k+1}}{(2k+1)!}+\frac{1}{2}\sum_{k=0}^{\infty}\frac{(G-iA)^{2k+1}}{(2k+1)!}\Big\}\\
&=\frac{1}{\sqrt{is}^3}\Big\{\sum_{k=0}^{\infty}\frac{(-1)^k\sqrt{is}^{2k+1}(a-x)^{2k+1}}{(2k+1)!}-\sum_{k=0}^{\infty}\frac{\sqrt{is}^{2k+1}(a-x)^{2k+1}}{(2k+1)!}\\
&+\frac{i}{2}\sum_{k=0}^{\infty}\frac{[\sqrt{is}(a+x-1)-i\sqrt{is}]^{2k+1}}{(2k+1)!}-\frac{i}{2}\sum_{k=0}^{\infty}\frac{[\sqrt{is}(a+x-1)+i\sqrt{is}]^{2k+1}}{(2k+1)!}\\
&+\left(\frac{1+i}{2}\right)\sum_{k=0}^{\infty}\frac{[\sqrt{is}(x-1)+i\sqrt{is}(a-1)]^{2k+1}}{(2k+1)!}+\left(\frac{1-i}{2}\right)\sum_{k=0}^{\infty}\frac{[\sqrt{is}(x-1)-i\sqrt{is}(a-1)]^{2k+1}}{(2k+1)!}\\
&-\left(\frac{1+i}{2}\right)\sum_{k=0}^{\infty}\frac{[\sqrt{is}\,x+i\sqrt{is}\,a]^{2k+1}}{(2k+1)!}-\left(\frac{1-i}{2}\right)\sum_{k=0}^{\infty}\frac{[\sqrt{is}\,x-i\sqrt{is}\,a]^{2k+1}}{(2k+1)!}\\
&+\frac{i}{2}\sum_{k=0}^{\infty}\frac{[\sqrt{is}+i\sqrt{is}(a-x-1)]^{2k+1}}{(2k+1)!}-\frac{i}{2}\sum_{k=0}^{\infty}\frac{[\sqrt{is}-i\sqrt{is}(a-x-1)]^{2k+1}}{(2k+1)!}\\
&+\left(\frac{1+i}{2}\right)\sum_{k=0}^{\infty}\frac{[\sqrt{is}(a-1)+i\sqrt{is}(x-1)]^{2k+1}}{(2k+1)!}+\left(\frac{1-i}{2}\right)\sum_{k=0}^{\infty}\frac{[\sqrt{is}(a-1)-i\sqrt{is}(x-1)]^{2k+1}}{(2k+1)!}
\end{aligned}
$$

$$
\begin{aligned}
&-\left(\frac{1+i}{2}\right)\sum_{k=0}^{\infty}\frac{[\sqrt{is}\,a+i\sqrt{is}\,x]^{2k+1}}{(2k+1)!}-\left(\frac{1-i}{2}\right)\sum_{k=0}^{\infty}\frac{[\sqrt{is}\,a-i\sqrt{is}\,x]^{2k+1}}{(2k+1)!}\\
&-\frac{1}{2}\sum_{k=0}^{\infty}\frac{[\sqrt{is}+i\sqrt{is}(a+x-1)]^{2k+1}}{(2k+1)!}-\frac{1}{2}\sum_{k=0}^{\infty}\frac{[\sqrt{is}-i\sqrt{is}(a+x-1)]^{2k+1}}{(2k+1)!}\\
&+\frac{1}{2}\sum_{k=0}^{\infty}\frac{[\sqrt{is}(a-x-1)+i\sqrt{is}]^{2k+1}}{(2k+1)!}+\frac{1}{2}\sum_{k=0}^{\infty}\frac{[\sqrt{is}(a-x-1)-i\sqrt{is}]^{2k+1}}{(2k+1)!}\Bigg\}\\
&=\frac{1}{\sqrt{is}^3}\sum_{k=0}^{\infty}\frac{\sqrt{is}^{2k+1}}{(2k+1)!}\Bigg[(-1)^k(a-x)^{2k+1}-(a-x)^{2k+1}+\frac{i}{2}(a+x-1-i)^{2k+1}\\
&-\frac{i}{2}(a+x-1+i)^{2k+1}+\left(\frac{1+i}{2}\right)[x-1+i(a-1)]^{2k+1}+\left(\frac{1-i}{2}\right)[x-1-i(a-1)]^{2k+1}\\
&-\left(\frac{1+i}{2}\right)(x+ia)^{2k+1}-\left(\frac{1-i}{2}\right)(x-ia)^{2k+1}+\frac{i}{2}[1+i(a-x-1)]^{2k+1}\\
&-\frac{i}{2}[1-i(a-x-1)]^{2k+1}+\left(\frac{1+i}{2}\right)[a-1+i(x-1)]^{2k+1}+\left(\frac{1-i}{2}\right)[a-1-i(x-1)]^{2k+1}\\
&-\left(\frac{1+i}{2}\right)(a+ix)^{2k+1}-\left(\frac{1-i}{2}\right)(a-ix)^{2k+1}-\frac{1}{2}[1+i(a+x-1)]^{2k+1}\\
&-\frac{1}{2}[1-i(a+x-1)]^{2k+1}+\frac{1}{2}(a-x-1+i)^{2k+1}+\frac{1}{2}(a-x-1-i)^{2k+1}\Bigg]\\
&=\frac{1}{\sqrt{is}^3}\sum_{k=0}^{\infty}\frac{\sqrt{is}^{2k+1}}{(2k+1)!}\Big[f_P(a,x,k)\Big]
\end{aligned}
$$

It can be verified that

$$
\begin{aligned}
f_P(a,x,k)&=0 && k=0,2,4,\ldots\\
f_P(a,x,k)&\neq 0\in\mathbb{R} && k=1,3,5,\ldots
\end{aligned}
$$

Letting $k=2m+1$ to eliminate the zero terms, we obtain the following substitutions:

$$
\begin{aligned}
2k+1&\to 4m+3\\
\frac{\sqrt{is}^{2k+1}}{\sqrt{is}^3}&=(is)^{k-1}\to(is)^{2m}=(-1)^m s^{2m}\\
\left[(-1)^k-1\right](a-x)^{2k+1}&\to\left[(-1)^{2m+1}-1\right](a-x)^{4m+3}=-2(a-x)^{4m+3}
\end{aligned}
$$

The expression becomes

$$
\begin{aligned}
&P(x,s)\\
&=\sum_{m=0}^{\infty}\frac{(-1)^m s^{2m}}{(4m+3)!}\Bigg[-2(a-x)^{4m+3}+\frac{i}{2}(a+x-1-i)^{4m+3}-\frac{i}{2}(a+x-1+i)^{4m+3}\\
&+\left(\frac{1+i}{2}\right)[x-1+i(a-1)]^{4m+3}+\left(\frac{1-i}{2}\right)[x-1-i(a-1)]^{4m+3}-\left(\frac{1+i}{2}\right)(x+ia)^{4m+3}\\
&-\left(\frac{1-i}{2}\right)(x-ia)^{4m+3}+\frac{i}{2}[1+i(a-x-1)]^{4m+3}-\frac{i}{2}[1-i(a-x-1)]^{4m+3}\\
&+\left(\frac{1+i}{2}\right)[a-1+i(x-1)]^{4m+3}+\left(\frac{1-i}{2}\right)[a-1-i(x-1)]^{4m+3}-\left(\frac{1+i}{2}\right)(a+ix)^{4m+3}\\
&-\left(\frac{1-i}{2}\right)(a-ix)^{4m+3}-\frac{1}{2}[1+i(a+x-1)]^{4m+3}-\frac{1}{2}[1-i(a+x-1)]^{4m+3}\\
&+\frac{1}{2}(a-x-1+i)^{4m+3}+\frac{1}{2}(a-x-1-i)^{4m+3}\Bigg]
\end{aligned}
$$

It can be verified that

$$\frac{i}{2}(a+x-1-i)^{4m+3}-\frac{i}{2}(a+x-1+i)^{4m+3}-\frac{1}{2}[1+i(a+x-1)]^{4m+3}$$
$$-\frac{1}{2}[1-i(a+x-1)]^{4m+3}=-2\,\mathrm{Im}\left\{(a+x-1-i)^{4m+3}\right\}$$
$$\left(\frac{1+i}{2}\right)[x-1+i(a-1)]^{4m+3}+\left(\frac{1-i}{2}\right)[x-1-i(a-1)]^{4m+3}$$
$$+\left(\frac{1+i}{2}\right)[a-1+i(x-1)]^{4m+3}+\left(\frac{1-i}{2}\right)[a-1-i(x-1)]^{4m+3}$$
$$=2\,\mathrm{Re}\left\{[a-1+i(x-1)]^{4m+3}\right\}+2\,\mathrm{Im}\left\{[a-1-i(x-1)]^{4m+3}\right\}$$
$$-\left(\frac{1+i}{2}\right)(x+ia)^{4m+3}-\left(\frac{1-i}{2}\right)(x-ia)^{4m+3}-\left(\frac{1+i}{2}\right)(a+ix)^{4m+3}$$
$$-\left(\frac{1-i}{2}\right)(a-ix)^{4m+3}=-2\,\mathrm{Re}\left\{(x+ia)^{4m+3}\right\}-2\,\mathrm{Im}\left\{(x-ia)^{4m+3}\right\}$$
$$\frac{i}{2}[1+i(a-x-1)]^{4m+3}-\frac{i}{2}[1-i(a-x-1)]^{4m+3}+\frac{1}{2}(a-x-1+i)^{4m+3}$$
$$+\frac{1}{2}(a-x-1-i)^{4m+3}=2\,\mathrm{Re}\left\{(a-x-1-i)^{4m+3}\right\}$$

Giving

$$P(x,s)$$
$$=\sum_{m=0}^{\infty}\frac{(-1)^m s^{2m}}{(4m+3)!}\Big[-2(a-x)^{4m+3}-2\,\mathrm{Im}\left\{(a+x-1-i)^{4m+3}\right\}$$
$$+2\,\mathrm{Re}\left\{[a-1+i(x-1)]^{4m+3}\right\}+2\,\mathrm{Im}\left\{[a-1-i(x-1)]^{4m+3}\right\}-2\,\mathrm{Re}\left\{(x+ia)^{4m+3}\right\}$$
$$-2\,\mathrm{Im}\left\{(x-ia)^{4m+3}\right\}+2\,\mathrm{Re}\left\{(a-x-1-i)^{4m+3}\right\}\Big]$$

leading to the final form

$$\begin{aligned}P(x,s)=2\sum_{k=0}^{\infty}\frac{(-1)^k}{(4k+3)!}\Big[&-(a-x)^{4k+3}+\mathrm{Re}\left\{(a-x-1-i)^{4k+3}\right\}\\&-\mathrm{Im}\left\{(a+x-1-i)^{4k+3}\right\}+\mathrm{Re}\left\{[a-1+i(x-1)]^{4k+3}\right\}\\&+\mathrm{Im}\left\{[a-1-i(x-1)]^{4k+3}\right\}-\mathrm{Re}\left\{(x+ia)^{4k+3}\right\}\\&-\mathrm{Im}\left\{(x-ia)^{4k+3}\right\}\Big]s^{2k}\end{aligned}\tag{8.14}$$

8.6.2 Series Representation of $Q(x,s)$

Starting with equation (8.12) and using the definitions in Section 8.6,

$$\begin{aligned}Q(x,s)&=4(-1+\cos A\cosh A)\\&=4\left(-1+\frac{\cosh(A+iA)+\cosh(A-iA)}{2}\right)\\&=-4+2\cosh(A+iA)+2\cosh(A-iA)\\&=-4+2\sum_{k=0}^{\infty}\frac{(A+iA)^{2k}}{(2k)!}+2\sum_{k=0}^{\infty}\frac{(A-iA)^{2k}}{(2k)!}\\&=-4+2\sum_{k=0}^{\infty}\frac{(\sqrt{is}+i\sqrt{is})^{2k}}{(2k)!}+2\sum_{k=0}^{\infty}\frac{(\sqrt{is}-i\sqrt{is})^{2k}}{(2k)!}\end{aligned}$$

$$= -4 + 2\sum_{k=0}^{\infty} \frac{\sqrt{is}^{2k}}{(2k)!}\left[(1+i)^{2k} + (1-i)^{2k}\right]$$
$$= -4 + 2\sum_{k=0}^{\infty} \frac{(is)^{k}}{(2k)!}\underbrace{\left[(1+i)^{2k} + (1-i)^{2k}\right]}_{=0\,\forall\, k=1,3,5,\ldots}$$

To retain only non-zero terms, let $k = 2m$, $m = 0, 1, 2, \ldots$

$$Q(x,s) = -4 + 2\sum_{m=0}^{\infty} \frac{(is)^{2m}}{(4m)!}\left[(1+i)^{4m} + (1-i)^{4m}\right]$$
$$= -4 + 4 + \frac{16s^2}{4!} + \frac{64s^4}{8!} + \frac{256s^6}{12!} + \ldots$$
$$= \sum_{k=1}^{\infty} \frac{2^{(2k+2)}s^{2k}}{(4k)!}$$
$$= 4\sum_{k=1}^{\infty} \frac{2^{2k}s^{2k}}{(4k)!}$$

Giving the final expression

$$Q(x,s) = 4\sum_{k=1}^{\infty} \frac{4^k}{(4k)!}\, s^{2k} \tag{8.15}$$

8.6.3 Series Representation of $R(x,s)$

For the third expression, we start from equation (8.13) and use the definitions in Section 8.6:

$$\begin{aligned}
&R(x,s)\\
&= \frac{1}{A^3}\Big\{ \cosh B \sin A - \cosh C \sin D + \cosh E \sin F - \sin H + \cosh A \sin I - \cosh D \sin C\\
&+ \cosh F \sin E - \cos B \sinh A + \cos C \sinh D - \cos E \sinh F + \sinh H - \cos A \sinh I\\
&+ \cos D \sinh C - \cos F \sinh E \Big\}\\
&= \frac{1}{A^3}\Big\{ \frac{\sinh(B+iA) - \sinh(B-iA)}{2i} - \frac{\sinh(C+iD) - \sinh(C-iD)}{2i}\\
&+ \frac{\sinh(E+iF) - \sinh(E-iF)}{2i} - \sin H + \frac{\sinh(A+iI) - \sinh(A-iI)}{2i}\\
&- \frac{\sinh(D+iC) - \sinh(D-iC)}{2i} + \frac{\sinh(F+iE) - \sinh(F-iE)}{2i}\\
&- \frac{\sinh(A+iB) + \sinh(A-iB)}{2} + \frac{\sinh(D+iC) + \sinh(D-iC)}{2}\\
&- \frac{\sinh(F+iE) + \sinh(F-iE)}{2} + \sinh H\\
&- \frac{\sinh(I+iA) + \sinh(I-iA)}{2} + \frac{\sinh(C+iD) + \sinh(C-iD)}{2}\\
&- \frac{\sinh(E+iF) + \sinh(E-iF)}{2} \Big\}\\
&= \frac{1}{A^3}\Big\{ \frac{i}{2}\Big[\sinh(B-iA) - \sinh(B+iA)\Big] + \frac{i}{2}\Big[\sinh(C+iD) - \sinh(C-iD)\Big]\\
&+ \frac{i}{2}\Big[\sinh(E-iF) - \sinh(E+iF)\Big] - \sin H + \frac{i}{2}\Big[\sinh(A-iI) - \sinh(A+iI)\Big]
\end{aligned}$$

$$+\frac{i}{2}\Big[\sinh(D+iC)-\sinh(D-iC)\Big]+\frac{i}{2}\Big[\sinh(F-iE)-\sinh(F+iE)\Big]$$
$$-\frac{1}{2}\Big[\sinh(A+iB)+\sinh(A-iB)\Big]+\frac{1}{2}\Big[\sinh(D+iC)+\sinh(D-iC)\Big]$$
$$-\frac{1}{2}\Big[\sinh(F+iE)+\sinh(F-iE)\Big]+\sinh H-\frac{1}{2}\Big[\sinh(I+iA)+\sinh(I-iA)\Big]$$
$$+\frac{1}{2}\Big[\sinh(C+iD)+\sinh(C-iD)\Big]-\frac{1}{2}\Big[\sinh(E+iF)+\sinh(E-iF)\Big]\Big\}$$
$$=\frac{1}{A^3}\Big\{\frac{i}{2}\sinh(B-iA)-\frac{i}{2}\sinh(B+iA)+\left(\frac{1+i}{2}\right)\sinh(C+iD)+\left(\frac{1-i}{2}\right)\sinh(C-iD)$$
$$-\left(\frac{1-i}{2}\right)\sinh(E-iF)-\left(\frac{1+i}{2}\right)\sinh(E+iF)-\sin H+\frac{i}{2}\sinh(A-iI)-\frac{i}{2}\sinh(A+iI)$$
$$+\left(\frac{1+i}{2}\right)\sinh(D+iC)+\left(\frac{1-i}{2}\right)\sinh(D-iC)-\left(\frac{1-i}{2}\right)\sinh(F-iE)$$
$$-\left(\frac{1+i}{2}\right)\sinh(F+iE)-\frac{1}{2}\sinh(A+iB)-\frac{1}{2}\sinh(A-iB)+\sinh H-\frac{1}{2}\sinh(I+iA)$$
$$-\frac{1}{2}\sinh(I-iA)\Big\}$$

Bringing in the power series representations, placing the sinh and sin terms first:

$$R(x,s)$$
$$=\frac{1}{A^3}\Big\{\sum_{k=0}^{\infty}\frac{H^{2k+1}}{(2k+1)!}-\sum_{k=0}^{\infty}\frac{(-1)^kH^{2k+1}}{(2k+1)!}+\frac{i}{2}\sum_{k=0}^{\infty}\frac{(B-iA)^{2k+1}}{(2k+1)!}-\frac{i}{2}\sum_{k=0}^{\infty}\frac{(B+iA)^{2k+1}}{(2k+1)!}$$
$$+\left(\frac{1+i}{2}\right)\sum_{k=0}^{\infty}\frac{(C+iD)^{2k+1}}{(2k+1)!}+\left(\frac{1-i}{2}\right)\sum_{k=0}^{\infty}\frac{(C-iD)^{2k+1}}{(2k+1)!}-\left(\frac{1-i}{2}\right)\sum_{k=0}^{\infty}\frac{(E-iF)^{2k+1}}{(2k+1)!}$$
$$-\left(\frac{1+i}{2}\right)\sum_{k=0}^{\infty}\frac{(E+iF)^{2k+1}}{(2k+1)!}+\frac{i}{2}\sum_{k=0}^{\infty}\frac{(A-iI)^{2k+1}}{(2k+1)!}-\frac{i}{2}\sum_{k=0}^{\infty}\frac{(A+iI)^{2k+1}}{(2k+1)!}$$
$$+\left(\frac{1+i}{2}\right)\sum_{k=0}^{\infty}\frac{(D+iC)^{2k+1}}{(2k+1)!}+\left(\frac{1-i}{2}\right)\sum_{k=0}^{\infty}\frac{(D-iC)^{2k+1}}{(2k+1)!}-\left(\frac{1-i}{2}\right)\sum_{k=0}^{\infty}\frac{(F-iE)^{2k+1}}{(2k+1)!}$$
$$-\left(\frac{1+i}{2}\right)\sum_{k=0}^{\infty}\frac{(F+iE)^{2k+1}}{(2k+1)!}-\frac{1}{2}\sum_{k=0}^{\infty}\frac{(A+iB)^{2k+1}}{(2k+1)!}-\frac{1}{2}\sum_{k=0}^{\infty}\frac{(A-iB)^{2k+1}}{(2k+1)!}$$
$$-\frac{1}{2}\sum_{k=0}^{\infty}\frac{(I+iA)^{2k+1}}{(2k+1)!}-\frac{1}{2}\sum_{k=0}^{\infty}\frac{(I-iA)^{2k+1}}{(2k+1)!}\Big\}$$
$$=\frac{1}{\sqrt{is}^3}\Big\{\sum_{k=0}^{\infty}\frac{[\sqrt{is}(a-x)]^{2k+1}}{(2k+1)!}-\sum_{k=0}^{\infty}\frac{(-1)^k[\sqrt{is}(a-x)]^{2k+1}}{(2k+1)!}$$
$$+\frac{i}{2}\sum_{k=0}^{\infty}\frac{[\sqrt{is}(a+x-1)-i\sqrt{is}]^{2k+1}}{(2k+1)!}-\frac{i}{2}\sum_{k=0}^{\infty}\frac{[\sqrt{is}(a+x-1)+i\sqrt{is}]^{2k+1}}{(2k+1)!}$$
$$+\left(\frac{1+i}{2}\right)\sum_{k=0}^{\infty}\frac{[\sqrt{is}(x-1)+i\sqrt{is}(a-1)]^{2k+1}}{(2k+1)!}+\left(\frac{1-i}{2}\right)\sum_{k=0}^{\infty}\frac{[\sqrt{is}(x-1)-i\sqrt{is}(a-1)]^{2k+1}}{(2k+1)!}$$
$$-\left(\frac{1-i}{2}\right)\sum_{k=0}^{\infty}\frac{[\sqrt{is}\,x-i\sqrt{is}\,a]^{2k+1}}{(2k+1)!}-\left(\frac{1+i}{2}\right)\sum_{k=0}^{\infty}\frac{[\sqrt{is}\,x+i\sqrt{is}\,a]^{2k+1}}{(2k+1)!}$$
$$+\frac{i}{2}\sum_{k=0}^{\infty}\frac{[\sqrt{is}-i\sqrt{is}(a-x+1)]^{2k+1}}{(2k+1)!}-\frac{i}{2}\sum_{k=0}^{\infty}\frac{[\sqrt{is}+i\sqrt{is}(a-x+1)]^{2k+1}}{(2k+1)!}$$

$$+\left(\frac{1+i}{2}\right)\sum_{k=0}^{\infty}\frac{[\sqrt{is}(a-1)+i\sqrt{is}(x-1)]^{2k+1}}{(2k+1)!}+\left(\frac{1-i}{2}\right)\sum_{k=0}^{\infty}\frac{[\sqrt{is}(a-1)-i\sqrt{is}(x-1)]^{2k+1}}{(2k+1)!}$$

$$-\left(\frac{1-i}{2}\right)\sum_{k=0}^{\infty}\frac{[\sqrt{is}\,a-i\sqrt{is}\,x]^{2k+1}}{(2k+1)!}-\left(\frac{1+i}{2}\right)\sum_{k=0}^{\infty}\frac{[\sqrt{is}\,a+i\sqrt{is}\,x]^{2k+1}}{(2k+1)!}$$

$$-\frac{1}{2}\sum_{k=0}^{\infty}\frac{[\sqrt{is}+i\sqrt{is}(a+x-1)]^{2k+1}}{(2k+1)!}-\frac{1}{2}\sum_{k=0}^{\infty}\frac{[\sqrt{is}-i\sqrt{is}(a+x-1)]^{2k+1}}{(2k+1)!}$$

$$-\frac{1}{2}\sum_{k=0}^{\infty}\frac{[\sqrt{is}(a-x+1)+i\sqrt{is}]^{2k+1}}{(2k+1)!}-\frac{1}{2}\sum_{k=0}^{\infty}\frac{[\sqrt{is}(a-x+1)-i\sqrt{is}]^{2k+1}}{(2k+1)!}\Bigg\}$$

$$=\frac{1}{\sqrt{is}^{3}}\sum_{k=0}^{\infty}\frac{\sqrt{is}^{2k+1}}{(2k+1)!}\Bigg[(a-x)^{2k+1}-(-1)^{k}(a-x)^{2k+1}+\frac{i}{2}(a+x-1-i)^{2k+1}$$

$$-\frac{i}{2}(a+x-1+i)^{2k+1}+\left(\frac{1+i}{2}\right)[x-1+i(a-1)]^{2k+1}+\left(\frac{1-i}{2}\right)[x-1-i(a-1)]^{2k+1}$$

$$-\left(\frac{1-i}{2}\right)(x-ia)^{2k+1}-\left(\frac{1+i}{2}\right)(x+ia)^{2k+1}+\frac{i}{2}[1-i(a-x+1)]^{2k+1}$$

$$-\frac{i}{2}[1+i(a-x+1)]^{2k+1}+\left(\frac{1+i}{2}\right)[a-1+i(x-1)]^{2k+1}+\left(\frac{1-i}{2}\right)[a-1-i(x-1)]^{2k+1}$$

$$-\left(\frac{1-i}{2}\right)(a-ix)^{2k+1}-\left(\frac{1+i}{2}\right)(a+ix)^{2k+1}-\frac{1}{2}[1+i(a+x-1)]^{2k+1}$$

$$-\frac{1}{2}[1-i(a+x-1)]^{2k+1}-\frac{1}{2}(a-x+1+i)^{2k+1}-\frac{1}{2}(a-x+1-i)^{2k+1}\Bigg]$$

$$=\frac{1}{\sqrt{is}^{3}}\sum_{k=0}^{\infty}\frac{\sqrt{is}^{2k+1}}{(2k+1)!}\Big[f_{Q}(a,x,k)\Big]$$

It can be verified that

$$f_{Q}(a,x,k)=0 \qquad k=0,2,4,\ldots$$
$$f_{Q}(a,x,k)\neq 0\in\mathbb{R} \qquad k=1,3,5,\ldots$$

Introducing a change of variables to guarantee k odd, we obtain

$$k=2m+1$$
$$2k+1\rightarrow 4m+3$$
$$\frac{\sqrt{is}^{2k+1}}{\sqrt{is}^{3}}\rightarrow(-1)^{m}s^{2m}$$
$$(a-x)^{2k+1}\left[1-(-1)^{k}\right]\rightarrow 2(a-x)^{4m+3}$$

$R(x,s)$

$$=\sum_{m=0}^{\infty}\frac{(-1)^{m}s^{2m}}{(4m+3)!}\Bigg[2(a-x)^{4m+3}+\frac{i}{2}(a+x-1-i)^{4m+3}-\frac{i}{2}(a+x-1+i)^{4m+3}$$

$$+\left(\frac{1+i}{2}\right)[x-1+i(a-1)]^{4m+3}+\left(\frac{1-i}{2}\right)[x-1-i(a-1)]^{4m+3}-\left(\frac{1-i}{2}\right)(x-ia)^{4m+3}$$

$$-\left(\frac{1+i}{2}\right)(x+ia)^{4m+3}+\frac{i}{2}[1-i(a-x+1)]^{4m+3}-\frac{i}{2}[1+i(a-x+1)]^{4m+3}$$

$$+\left(\frac{1+i}{2}\right)[a-1+i(x-1)]^{4m+3}+\left(\frac{1-i}{2}\right)[a-1-i(x-1)]^{4m+3}-\left(\frac{1-i}{2}\right)(a-ix)^{4m+3}$$

$$-\left(\frac{1+i}{2}\right)(a+ix)^{4m+3}-\frac{1}{2}[1+i(a+x-1)]^{4m+3}-\frac{1}{2}[1-i(a+x-1)]^{4m+3}$$
$$-\frac{1}{2}(a-x+1+i)^{4m+3}-\frac{1}{2}(a-x+1-i)^{4m+3}\Big]$$

The following simplifications can be verified

$$\frac{i}{2}(a+x-1-i)^{4m+3}-\frac{i}{2}(a+x-1+i)^{4m+3}-\frac{1}{2}[1+i(a+x-1)]^{4m+3}$$
$$-\frac{1}{2}[1-i(a+x-1)]^{4m+3}=2\,\mathrm{Im}\left\{(a+x-1+i)^{4m+3}\right\}$$
$$\left(\frac{1+i}{2}\right)[x-1+i(a-1)]^{4m+3}+\left(\frac{1-i}{2}\right)[x-1-i(a-1)]^{4m+3}$$
$$+\left(\frac{1+i}{2}\right)[a-1+i(x-1)]^{4m+3}+\left(\frac{1-i}{2}\right)[a-1-i(x-1)]^{4m+3}$$
$$=2\,\mathrm{Re}\left\{[x-1+i(a-1)]^{4m+3}\right\}+2\,\mathrm{Im}\left\{[x-1-i(a-1)]^{4m+3}\right\}$$
$$-\left(\frac{1-i}{2}\right)(x-ia)^{4m+3}-\left(\frac{1+i}{2}\right)(x+ia)^{4m+3}-\left(\frac{1-i}{2}\right)(a-ix)^{4m+3}$$
$$-\left(\frac{1+i}{2}\right)(a+ix)^{4m+3}=-2\,\mathrm{Re}\left\{(x+ia)^{4m+3}\right\}-2\,\mathrm{Im}\left\{(x-ia)^{4m+3}\right\}$$
$$\frac{i}{2}[1-i(a-x+1)]^{4m+3}-\frac{i}{2}[1+i(a-x+1)]^{4m+3}-\frac{1}{2}(a-x+1+i)^{4m+3}$$
$$-\frac{1}{2}(a-x+1-i)^{4m+3}=-2\,\mathrm{Re}\left\{(a-x+1+i)^{4m+3}\right\}$$

Hence, we have

$$R(x,s)=\sum_{m=0}^{\infty}\frac{(-1)^m s^{2m}}{(4m+3)!}\Big[2(a-x)^{4m+3}+2\,\mathrm{Im}\left\{(a+x-1+i)^{4m+3}\right\}$$
$$+2\,\mathrm{Re}\left\{[x-1+i(a-1)]^{4m+3}\right\}+2\,\mathrm{Im}\left\{[x-1-i(a-1)]^{4m+3}\right\}-2\,\mathrm{Re}\left\{(x+ia)^{4m+3}\right\}$$
$$-2\,\mathrm{Im}\left\{(x-ia)^{4m+3}\right\}-2\,\mathrm{Re}\left\{(a-x+1+i)^{4m+3}\right\}\Big]$$

Leading to the final form

$$R(x,s)=2\sum_{k=0}^{\infty}\frac{(-1)^k}{(4k+3)!}\Big[(a-x)^{4k+3}+\mathrm{Im}\left\{(a+x-1+i)^{4k+3}\right\}$$
$$+\mathrm{Re}\left\{[x-1+i(a-1)]^{4k+3}\right\}+\mathrm{Im}\left\{[x-1-i(a-1)]^{4k+3}\right\}-\mathrm{Re}\left\{(x+ia)^{4k+3}\right\}$$
$$-\mathrm{Im}\left\{(x-ia)^{4k+3}\right\}-\mathrm{Re}\left\{(a-x+1+i)^{4k+3}\right\}\Big]s^{2k} \tag{8.16}$$

8.7 Flat Output Parametrization: Single-input

We now return to the s-domain solution (8.10),

$$W_1(x,s)=\frac{P(x,s)}{Q(x,s)}U(s) \qquad\qquad W_2(x,s)=\frac{R(x,s)}{Q(x,s)}U(s)$$

where $P(x,s)$, $Q(x,s)$ and $R(x,s)$ are given in infinite series form by (8.14), (8.15) and (8.16), respectively. This is a one-input system, so there is one flat output.

As in Section 3.5, we choose

$$U(s) = Q(x,s)\,Y(s)$$

as the system input parametrization by the transformed flat output. This gives

$$W_1(x,s) = \frac{P(x,s)}{Q(x,s)}\,Q(x,s)\,Y(s) \qquad W_2(x,s) = \frac{R(x,s)}{Q(x,s)}\,Q(x,s)\,Y(s)$$
$$W_1(x,s) = P(x,s)\,Y(s) \qquad W_2(x,s) = R(x,s)\,Y(s)$$

The $W_1(x,s)$ term becomes

$$\begin{aligned} W_1(x,s) = 2\sum_{k=0}^{\infty}\frac{(-1)^k}{(4k+3)!}\Big[&-(a-x)^{4k+3} + \mathrm{Re}\left\{(a-x-1-i)^{4k+3}\right\} \\ &- \mathrm{Im}\left\{(a+x-1-i)^{4k+3}\right\} + \mathrm{Re}\left\{[a-1+i(x-1)]^{4k+3}\right\} \\ &+ \mathrm{Im}\left\{[a-1-i(x-1)]^{4k+3}\right\} - \mathrm{Re}\left\{(x+ia)^{4k+3}\right\} - \mathrm{Im}\left\{(x-ia)^{4k+3}\right\}\Big] s^{2k}\,Y(s) \end{aligned}$$

Which can immediately be inverse transformed into the time domain:

$$\begin{aligned} w_1(x,t) = 2\sum_{k=0}^{\infty}\frac{(-1)^k}{(4k+3)!}\Big[&-(a-x)^{4k+3} + \mathrm{Re}\left\{(a-x-1-i)^{4k+3}\right\} \\ &- \mathrm{Im}\left\{(a+x-1-i)^{4k+3}\right\} + \mathrm{Re}\left\{[a-1+i(x-1)]^{4k+3}\right\} \\ &+ \mathrm{Im}\left\{[a-1-i(x-1)]^{4k+3}\right\} - \mathrm{Re}\left\{(x+ia)^{4k+3}\right\} - \mathrm{Im}\left\{(x-ia)^{4k+3}\right\}\Big] y^{(2k)}(t) \end{aligned} \tag{8.17}$$

Similarly, $W_2(x,s)$ and $U(s)$ transform back to the time domain as

$$\begin{aligned} w_2(x,t) = 2\sum_{k=0}^{\infty}\frac{(-1)^k}{(4k+3)!}\Big[&(a-x)^{4k+3} + \mathrm{Im}\left\{(a+x-1+i)^{4k+3}\right\} \\ &+ \mathrm{Re}\left\{[x-1+i(a-1)]^{4k+3}\right\} + \mathrm{Im}\left\{[x-1-i(a-1)]^{4k+3}\right\} - \mathrm{Re}\left\{(x+ia)^{4k+3}\right\} \\ &- \mathrm{Im}\left\{(x-ia)^{4k+3}\right\} - \mathrm{Re}\left\{(a-x+1+i)^{4k+3}\right\}\Big] y^{(2k)}(t) \end{aligned} \tag{8.18}$$

and

$$u(t) = 4\sum_{k=1}^{\infty}\frac{4^k}{(4k)!}\,y^{(2k)}(t) \tag{8.19}$$

For steering purposes, we need to interpret the effect of $y(t)$ on $w(x,t)$. We look at the ending equilibrium at $t = t_f$ when all the $y(t)$ derivatives are zero, such that only the $k = 0$ term remains:

$$w_1(x,t_f) = P_{k=0}y(t_f)$$
$$w_2(x,t_f) = R_{k=0}y(t_f)$$

By direct substitution,

$$P_{k=0} = \frac{8}{3} - 4a - 4x + 8ax$$
$$R_{(k=0} = \frac{8}{3} - 4a - 4x + 8ax$$
$$P_{k=0} = R_{k=0} = (8a-4)\,x + \left(\frac{8}{3} - 4a\right)$$

Therefore, the end configuration is always a straight line with both slope and offset being functions of a. Since we are using normalized coordinates, $0 \leq a \leq 1$. Therefore, we have three possibilities for the equilibrium slope:

- $0 \leq a < 0.5$: negative (downwards) slope
- $a = 0.5$: zero (flat) slope
- $0.5 < a \leq 1$: positive (upwards) slope

This result is consistent with the physics of a solid body subjected to an external force. This is illustrated in Figure 8.7, where the center of mass is located at $x = 0.5$ since the beam is homogenous.

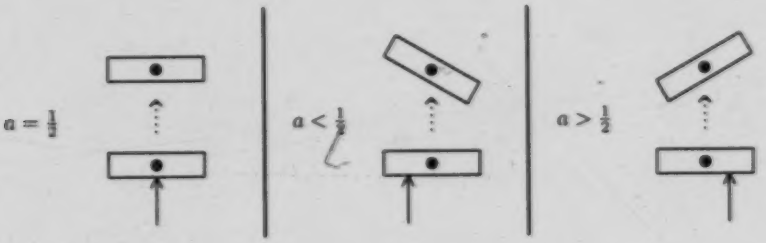

Figure 8.7: Effect of input force location on final configuration

For the special case of $a = \frac{1}{2}$, the final slope value is zero, and we can figure out the "DC gain" of the system:

$$\left[(8a-4)x + \left(\frac{8}{3} - 4a\right)\right]_{a=\frac{1}{2}} = \frac{2}{3}$$

In this situation, the flat output choice

$$y(t) = \left(\frac{3}{2}Y\right)\eta_7(t)$$

steers the beam to $w(x, t_f) = Y$, where $\eta_7(t)$ represents a Gevrey steering function on $[0, 1]$, given by (3.31).

For the more general case when $a \neq \frac{1}{2}$, it is still possible to pick a gain to control the ending displacement of the center of mass:

$$\left[(8a-4)x + \left(\frac{8}{3} - 4a\right)\right]_{x=\frac{1}{2}} = \frac{2}{3}$$

Therefore, choosing

$$y(t) = \left(\frac{3}{2}Y\right)\eta_7$$

as the flat output will guarantee $w(0.5, t_f) = Y$. However, the equilibrium slope will be a function of both a and Y $(= (8a-4)Y)$. The final slope of the beam is thus *uncontrollable* for a single input force. We will revisit this idea in Section 8.9, when we consider the two-input case.

8.8 Simulation of Single-input System

The system's open-loop trajectory and input can be directly calculated from the time-domain series expressions, as done in Section 5.1. Two different series are used to calculate $w(x,t)$, (8.17) for the $0 < x < a$ interval and (8.18) for $a < x < 1$. We compute $u(t)$ from (8.19).

A sample simulation is provided, using the parameters in Table 8.1. The beam displacement, beam deformation excluding rigid motion, and input are plotted in Figure 8.8.

Parameter	Value
Gevrey parameter γ	1.4
Input location a	0.25
End height Y	1
End time t_f	2
# of time points	100
# of space points	50
Series order (k_{max})	15

Table 8.1: Simulation parameters for a one-input beam

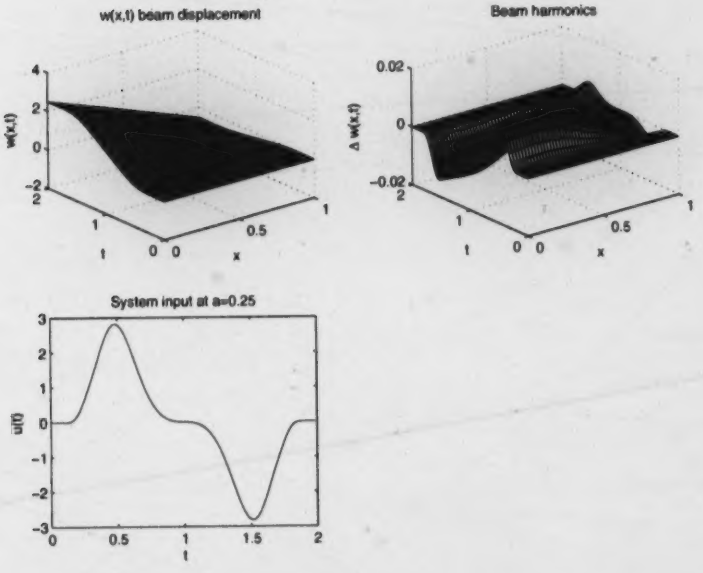

Figure 8.8: Simulation of 1-input beam

8.9 Two-input System

We first need to look at the issue of how to assign the flat output gains to steer the system to a desired end state. From flatness theory, we know that the number of system inputs equals the number of flat outputs, so we have two independent quantities to work with.

Also, unlike the one-input case, we intuitively expect the final beam configuration to be fully controllable.

From Section 8.7, we know that for one input, the steady-state relationship is

$$w_{a_1}(x, t_f) = \left[(8a_1 - 4)\,x + \left(\frac{8}{3} - 4a_1\right)\right] y_1(t_f)$$

where a_1 is the location where the input is applied, y_1 is the flat output connected to the input, and w_{a_1} is the resulting beam deformation.

For a second input, we have

$$w_{a_2}(x, t_f) = \left[(8a_2 - 4)\,x + \left(\frac{8}{3} - 4a_2\right)\right] y_2(t_f)$$

therefore

$$\begin{aligned} w(x, t_f) &= w_{a_1}(x, t_f) + w_{a_2}(x, t_f) \\ &= \left[(8a_1 - 4)\,x + \left(\frac{8}{3} - 4a_1\right)\right] y_1(t_f) + \left[(8a_2 - 4)\,x + \left(\frac{8}{3} - 4a_2\right)\right] y_2(t_f) \end{aligned} \tag{8.20}$$

due to superposition.

$w(x, t_f)$ is the two-input system's equilibrium configuration, with slope M and center of mass displacement Y. We need to express this in $y = mx + b$ form:

$$\begin{aligned} m &= \frac{y - y_1}{x - x_1} \\ M(x - 0.5) &= w(x, t_f) - Y \\ w(x, t_f) &= Mx + (Y - 0.5M) \end{aligned} \tag{8.21}$$

where $(x_1, y_1) = (0.5, Y)$ is a known point on the line.

Equating (8.20) and (8.21),

$$Mx + (Y - 0.5M) = \left[(8a_1 - 4)\,x + \left(\frac{8}{3} - 4a_1\right)\right] y_1(t_f) + \left[(8a_2 - 4)\,x + \left(\frac{8}{3} - 4a_2\right)\right] y_2(t_f)$$

therefore

$$\begin{aligned} M &= (8a_1 - 4)\,y_1(t_f) + (8a_2 - 4)\,y_2(t_f) \\ Y - 0.5M &= \left(\frac{8}{3} - 4a_1\right) y_1(t_f) + \left(\frac{8}{3} - 4a_2\right) y_2(t_f) \end{aligned} \tag{8.22}$$

(8.22) is a linear system of two equations in two unknowns $y_1(t_f), y_2(t_f)$ whose solution is

$$y_1(t_f) = \frac{M + 6Y - 12a_2Y}{8a_1 - 8a_2} \tag{8.23}$$

$$y_2(t_f) = \frac{M + 6Y - 12a_1Y}{8a_2 - 8a_1} \tag{8.24}$$

where Y is the desired center of mass displacement, M is the desired beam slope, and a_1, a_2 are the locations of u_1 and u_2 respectively.

Note that both (8.23) and (8.24) are singular when $a_1 = a_2$. Physically, this condition means the two inputs overlap, so we effectively revert back to the one-input case. We can still work with the beam, but we can control only end displacement *or* slope, but not both. In other words, $a_1 = a_2$ leads to a loss of controllability of the system.

8.10 Simulation of Two-input System

A sample simulation of a two-input beam is performed using the parameters in Table 8.2. The combined results are shown in Figure 8.9.

Parameter	Value
Gevrey parameter γ	1.4
Input location #1 a_1	0.25
Input location #2 a_2	0.8
End height Y	1
End slope M	1
End time t_f	3
# of time points	100
# of space points	50
Series order (k_{max})	15

Table 8.2: Simulation parameters for a two-input beam

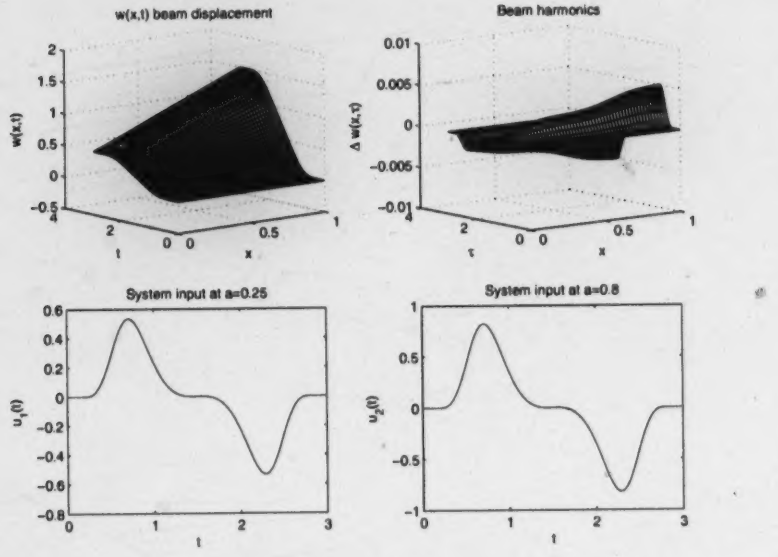

Figure 8.9: Simulation of 2-input beam

8.11 Discussion and Future Work

An interesting extension of the work in this chapter would be to design a closed-loop controller using the technique in Chapter 4. Hardware implementation would require the expressions to be un-normalized. Stabilization is an important problem in magnetic bearing systems, and the state-space model derived could be readily used to design a stabilizing controller.

Note that in practice the rotor is not restricted to move in one plane. Since there is no coupling between the motion in two orthogonal planes (assuming no shaft rotation), vertical and horizontal stabilizing controllers could be designed independently.

Chapter 9

Conclusions and Future Work

The flatness-based open and closed-loop tracking control of a flexible beam has been successfully designed and implemented in simulation and experiment. The approach relies on a series parametrization of the system state and input by a flat output function and its time derivatives. This parametrization is analogous to that found in flatness of finite-dimensional systems and allows the design of an open-loop control which achieves rest to rest motion. The closed-loop design is based on a state-space LTI system approximation which follows from truncating series parameterizations used in the open-loop control. Standard estimated state feedback tracking control can be readily applied to these approximate systems. An FEA model was derived in order simulate the closed-loop system and validate open-loop series results. Simulation and experimental results both indicate the proposed control design achieves robust tracking.

Future work on closed-loop control and experimental testing could investigate generalized beam models which include tip payloads, rotary inertia, and non-constant beam parameters (e.g. volumetric mass density). For example, the introduction of rotary inertia changes the nature of the parametrization of the system variables in terms of the flat output, and we expect distributed delays/predictions to appear as operators. The multi-input levitated beam discussed in Chapter 8 requires further study. In particular, non-uniform beams could be considered. To date, such configurations have not been treated using flatness. The levitated beam problems offers potentially interesting and industrially relevant experimental work as it models a shaft supported by magnetic bearings.

Bibliography

[1] Y. Aoustin, C. Chevallereau, A. Glumineau, and C. H. Moog. Experimental results for the end-effector control of a single flexible robotic arm. *IEEE Transactions on Control Systems Technology*, 2(4), December 1994.

[2] Y. Aoustin, M. Fliess, H. Mounier, P. Rouchon, and J. Rudolph. Theory and practice in the motion planning and control of a flexible robot arm using mikusiński operators. In *Proceedings of the 5th IFAC Symposium on Robot Control*, pages 287–293, Nantes, France, September 3–5 1997.

[3] R. N. Banavar and P. Dominic. An LQG/H_∞ controller for a flexible manipulator. *IEEE Transactions On Control Systems Technology*, 3(4):409–416, December 1995.

[4] F. P. Beer and E. R. Johnston, Jr. *Mechanics of Materials*. McGraw-Hill, London, second in si units edition, 1992.

[5] M. Bensosman and G. Le Vey. Control of flexible manipulators: A survey. *Robotica*, 22:533–545, 2004.

[6] C.-T. Chen. *Linear System Theory and Design*. Oxford University Press, New York, third edition, 1999.

[7] P. C. Chou and N. J. Pagano. *Elasticity – Tensor, Dyadic, and Engineering Approaches*. Dover, New York, 1992.

[8] R. F. Curtain and H. Zwart. *An Introduction to Infinite-dimensional Linear Systems Theory*. Springer-Verlag, New York, NY, 1995.

[9] X. Ding, T.-J. Tarn, and A. K. Bejczy. A novel approach to the modelling and control of flexible robot arms. In *Proceedings of the 27th Conference on Decision and Control*, pages 52–57, Austin, TX, 1988.

[10] D. Dochain. *Contribution to the Analysis and Control of Distributed Parameter Systems with Applications to (Bio)Chemical Processes and Robotics*. Ph.D., Universite Catholique de Louvain, Louvain, Belgium, July 1994.

[11] F. Dubois, N. Petit, and P. Rouchon. Motion planning and nonlinear simulations for a tank containing a fluid. In *Proceedings of the Fifth European Control Conference*, Karlsruhe, Germany, 1999.

[12] M. P. Fard. *Modelling and Control of Mechanical Flexible Systems*. Ph.D., Norwegian University of Science and Technology, Trondheim, Norway, 2001.

[13] M. Fliess, J. Levine, P. Martin, and P. Rouchon. Sur les systèmes non linéaires différentiellement plats. *Comptes Rendus de l'Académie des Sciences. Série I, Mathématique*, 315(5):619–624, 1992.

[14] M. Fliess, J. Levine, P. Martin, and P. Rouchon. Flatness and defect of nonlinear-systems – introductory theory and examples. *International Journal Of Control*, 61(6):1327–1361, 1995.

[15] M. Fliess, P. Martin, N. Petit, and P. Rouchon. Commande de l'équation des télégraphistes et restauration active d'un signal. *Traitement du Signal - Spécial*, 15:619–625, 1998.

[16] M. Fliess, H. Mounier, P. Rouchon, and J. Rudolph. Controllability and motion planning for linear delay systems with an application to a flexible rod. In *Proceedings of the 34th Conference on Decision and Control*, New Orleans, LA, December 1995.

[17] M. Fliess, H. Mounier, P. Rouchon, and J. Rudolph. Systèmes linéaires sur les opérateurs mikusiński et commande d'une poutre flexible. In *ESAIM: Proceedings*, volume 2, pages 183–193, 1997.

[18] M. Fliess, H. Mounier, P. Rouchon, and J. Rudolph. Controlling the transient of a chemical reactor: a distributed parameter approach. In *Computational Engineering in Systems Application IMACS Multiconference (CESA '98)*, Hammamet, Tunisia, 1998.

[19] M. Fliess, H. Mounier, P. Rouchon, and J. Rudolph. A distributed parameter approach to the control of a tubular reactor: a multi-variable case. In *Proceedings of the 37th Conference on Decision and Control*, pages 736–741, Tampa, FL, 1998.

[20] M. Gevrey. Sur la nature analytique des solutions des équations aux dérivées partielles. *Annales Scientifiques de l'École Normale Superieure*, 25:129–190, 1918.

[21] B.-Z. Guo, J.-M. Wang, and S.-P. Yung. Boundary stabilization of a flexible manipulator with rotational inertia. *Differential and Integral Equations*, 18(9):1013–1038, 2005.

[22] W. Haas and J. Rudolph. Steering the deflection of a piezoelectric bender. In *Proceedings of the 5th European Control Conference*, Karlsruhe, Germany, August 31–September 3 1999.

[23] L. R. Hunt and R. Su. Linear equivalents of nonlinear time-varying systems. In *International Symposium on the Mathematical Theory of Networks and Systems*, pages 119–123, Santa Monica, CA, 1981.

[24] M. Hussey. *Fundamentals of Mechanical Vibrations*. The Macmillan Press, London, 1983.

[25] IEEE Canada. The Shuttle Remote Manipulator System – The Canadarm. http://ieee.ca/millennium/canadarm/canadarm_about.html.

[26] D. J. Inman. *Engineering Vibration*. Prentice Hall, Upper Saddle River, New Jersey, second edition, 2001.

[27] B. Jakubczyk and W. Respondek. On linearization of control systems. *Bulletin de L'Academie Polonaise des Sciences, Série des Sciences mathématiques*, XXVII(1):517–522, 1980.

[28] R. H. C. Jr. and E. Schmitz. Initial experiments on the end-point control of a flexible one-link robot. *The International Journal of Robotics Research*, 3(3):62–75, Fall 1984.

[29] C. R. Koch, A. F. Lynch, and S. Chung. Flatness-based automotive solenoid valve control. In *Proceedings of the 6th IFAC Symposium on Nonlinear Control Systems (NOLCOS 2004)*, pages 1091–1096, Stuttgart, Germany, 2004.

[30] B. Laroche. *Extension de la Notion de Platitude à des Systèmes Décrits par des Équations aux Dérivées Partielles Linéaires.* Ph.D, École Nationale Supérieure des Mines de Paris, Paris, France, December 2000.

[31] B. Laroche and P. Martin. Motion planning for a 1-D diffusion equation using a Brunovsky-like decomposition. In *Proceedings of the Fourteenth International Symposium on Mathematical Theory of Networks and Systems*, Perpignan, France, 2000.

[32] B. Laroche, P. Martin, and P. Rouchon. Motion planning for a class of partial differential equations with boundary control. In *Proceedings of the 37th Conference on Decision and Control*, pages 736–741, Tampa, FL, 1998.

[33] B. Laroche, P. Martin, and P. Rouchon. Motion planning for the heat equation. *International Journal Of Robust And Nonlinear Control*, 10:629–643, 2000.

[34] L. Ljung. *System Identification: Theory for the User.* Prentice Hall, Upper Saddle River, New Jersey, second edition, 1999.

[35] A. Lynch and D. Wang. Flatness-based motion planning control of an euler-bernoulli beam in a gravitational field. In H. Şira-Ramirez and G. Silva-Navarro, editors, *Algebraic Methods in Flatness, Signal Processing and State Estimation*, pages 149–170. Innovacion Editorial Lagares, 2003.

[36] A. Lynch and D. Wang. Flatness-based control of a flexible beam in a gravitational field. In *Proceedings of the 2004 American Control Conference*, Boston, MA, 2004.

[37] A. F. Lynch. *EE 460 Lab 1: Rotary Inverted Pendulum.* Department of ECE, University of Alberta, 2005.

[38] A. F. Lynch and J. Rudolph. Flachheitsbasierte Randsteuerung parabolischer Systeme mit verteilten Parametern. *at — Automatisierungstechnik*, 48(10):478–486, Oct. 2000.

[39] A. F. Lynch and J. Rudolph. Flatness-based boundary control of a nonlinear parabolic equation modelling a tubular reactor. In A. Isidori, F. Lamnabhi-Lagarrique, and W. Respondek, editors, *Nonlinear Control in the Year 2000*, pages 45–54. Springer-Verlag, New York, NY, 2000.

[40] A. F. Lynch and J. Rudolph. Flatness-based boundary control of two coupled nonlinear pdes modelling a tubular reactor. In *Proceedings of the International Symposium on Nonlinear Theory and its Applications (NOLTA 2000)*, volume 2, pages 641–644, Dresden, Germany, 2000.

[41] A. F. Lynch and J. Rudolph. Flatness-based boundary control of a class of quasilinear parabolic systems. *International Journal of Control*, 75(15):1219–1230, 2002.

[42] R. Mahadevan and F. J. D. III. On-line optimization of recombinant product in a fed-batch bioreactor. *Biotechnol. Prog.*, 19:639–646, 2003.

[43] P. Martin, R. Murray, and P. Rouchon. Flat systems. In G. Bastin and M. Gevers, editors, *Plenary Lectures and Mini-Courses, 4th European Control Conference*, pages 211–264, Brussels, Belgium, 1997.

[44] J. L. Meriam. *Engineering Mechanics*, volume 2: Dynamics. John Wiley and Sons, New York, SI/English edition, 1978.

[45] T. Meurer and M. Zeitz. A novel design approach to flatness-based feedback boundary tracking control for nonlinear parabolic distributed parameter systems. In W. Kang, C. Borges, and M. Xiao, editors, *New Trends in Nonlinear Dynamics and Control*, pages 221–236. Springer-Verlag, New York, 2003.

[46] T. Meurer and M. Zeitz. Flachheitsbasierte steuerung und regelung eines wärmeleitungssystems. *at - Automatisierungstechnik*, 52:411–420, September 2004.

[47] J. Mikusiński. *Operational Calculus*, volume 1 of *International Series of Monographs in Pure and Applied Mathematics*. Pergamon Press, Oxford, England, second edition, 1983.

[48] Y. Mizoshita, S. Hasegawa, and K. Takaishi. Vibration minimized access control for disk drives. *IEEE Transactions on Magnetics*, 32(3), May 1996.

[49] H. Mounier, J. Rudolph, M. Petitot, and M. Fliess. A flexible rod as a linear delay system. In *Proceedings of the Third European Control Conference*, pages 3676–3681, Rome, Italy, 1995.

[50] S. P. Nagarkatti, D. M. Dawson, M. S. de Queiroz, F. Zhang, and B. Costic. Boundary control of a two-dimensional flexible rotor. *International Journal of Adaptive Control and Signal Processing*, 15:589–614, 2001.

[51] K. Ogata. *System Dynamics*. Prentice Hall, Upper Saddle River, New Jersey, third edition, 1998.

[52] K. Ogata. *Modern Control Engineering*. Prentice Hall, Upper Saddle River, New Jersey, fourth edition, 2002.

[53] F. Ollivier and A. Sedoglavic. A generalization of flatness to nonlinear systems of partial differential equations. Applications to the command of a flexible rod. In *Fifth IFAC Symposium on Nonlinear Control Systems (NOLCOS 2001)*, Saint-Petersburg, Russia, 2001.

[54] G. G. Parker, B. Petterson, C. Dohrmann, and R. D. Robinett. Command shaping for residual vibration free crane maneuvers. In *Proceedings of the American Control Conference*, Seattle, Washington, June 1995.

[55] N. Petit. *Systèmes à retards. Platitude en génie des procédés et contrôle de certaines équations des ondes*. Ph.D., École Nationale Supérieure des Mines de Paris, Paris, France, 2000.

[56] N. Petit and P. Rouchon. Motion planning for heavy chain systems. *SIAM Journal on Control and Optimization*, 40:275–495, 2001.

[57] N. Petit and P. Rouchon. Dynamics and solutions to some control problems for water-tank systems. *IEEE Transactions on Automatic Control*, 47(4):594–609, 2002.

[58] Quanser Consulting Advanced Teaching Systems. *Systems and Procedures*.

[59] R. Rothfuß, U. Becker, and J. Rudolph. Controlling a solenoid valve – a distributed parameter approach. In *Proc. 14th Int. Symp. Math. Theory of Networks and Systems — mtns'2000*, Perpignan, France, 2000.

[60] P. Rouchon. Motion planning, equivalence, infinite dimensional systems. In *Proceedings of the Fourteenth International Symposium on Mathematical Theory of Networks and Systems*, Perpignan, France, 2000.

[61] P. Rouchon and J. Rudolph. Réacteurs chimiques différentiellement plats : planification et suivi de trajectoires. In *Automatique et procédés chimiques — Réacteurs et colonnes de distillation*, chapter 5, pages 163–200. Hermès Science Publications, Paris, France, 2001.

[62] J. Rudolph. Randsteuerung von Wärmetauschern mit örtlich verteilten Parametern: ein flachheitsbasierter Zugang. *at — Automatisierungstechnik*, 48(8):399–406, Aug. 2000.

[63] J. Rudolph. *Flatness Based Control of Distributed Parameter Systems*. Shaker Verlag, Aachen, 2003.

[64] J. Rudolph, J. Winkler, and F. Woittennek. Exercise course – control of distributed parameter systems: "technological examples". Ecole Internationale d'Automatique de Lille, 2nd-6th September 2002.

[65] J. Rudolph and F. Woittennek. Flachheitsbasierte randsteuerung von elastischen balken mit piezoaktuatoren. *at Automatisierungstechnik*, 50:412–421, September 2002.

[66] J. Rudolph and F. Woittennek. Motion planning for euler-bernoulli beams. In H. Sira-Ramirez and G. Silva-Navarro, editors, *Algebraic Methods in Flatness, Signal Processing and State Estimation*. Innovacion Editorial Lagares, 2003.

[67] R. Scibor-Marchocki. Hyperbolic trigonometric functions. http://www.geocities.com/ResearchTriangle/2363/hyperbol.html.

[68] J.-J. E. Slotine and W. Li. *Applied Nonlinear Control*. Prentice-Hall, Englewood Cliffs, New Jersey, 1991.

[69] C. Trautman and D. Wang. Experimental H_∞ control of a single flexible link with a shoulder joint. In *IEEE International Conference on Robotics and Automation*, pages 1235–1241, 1995.

[70] J. v. Löewis. *Flachheitsbasierte Trajektorienfolgeregelung Elektromechanischer Systeme*. Ph.D, TU-Dresden, Dresden, Germany, 2002.

[71] M. J. van Nieuwstadt and R. M. Murray. Real-time trajectory generation for differentially flat systems. *Int. J. Robust Nonlinear Control*, 8:995–1020, 1998.

[72] D. Wang and M. Vidyasagar. Transfer functions for a single flexible link. *The International Journal of Robotics Research*, 10(5):540–549, Oct. 1991.

[73] F.-Y. Wang and G. Guan. Influences of rotatory inertia, shear and loading on vibrations of flexible manipulators. *Journal of Sound and Vibration*, 171(4):433–452, 1994.

[74] F. Woittennek and J. Rudolph. Motion planning and boundary control for a rotating timoshenko beam. *Proceedings in Applied Mathematics and Mechanics*, 2:106–107, 2003.

[75] K. Yuan. Control of slew maneuver of a flexible beam mounted non-radially on a rigid hub: a geometrically exact modelling approach. *Journal of Sound and Vibration*, 204(5):795–806, 1997.

Appendix A

Electrical Drive Subsystem

The hub and ruler combination is driven by a DC motor through a gear train. We model the system [51, pp. 148-149] to obtain the relationship between the input power supply voltage $u(t)$, and the output torque $\tau(t)$ acting on the hub.

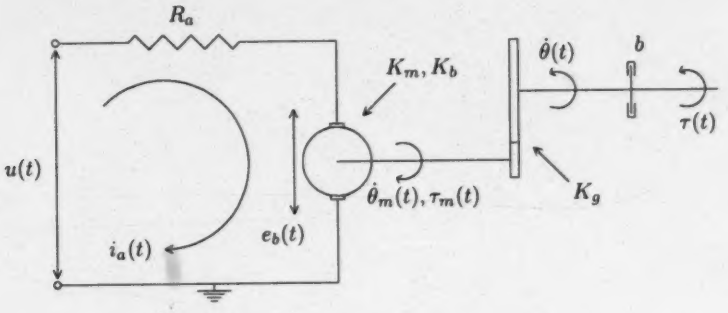

Figure A.1: Electric drive system diagram

A diagram of the system is shown in Figure A.1. The symbols used are:

R_a	Armature resistance
$i_a(t)$	Armature current
$u(t)$	Input voltage
$e_b(t)$	Motor back EMF
K_m	Motor torque constant
K_b	Back EMF constant
K_g	Gear ratio
$\dot{\theta}_m(t)$	Motor shaft angular velocity
$\tau_m(t)$	Motor torque
b	Total system viscous friction
$\dot{\theta}(t)$	Hub angular velocity
$\tau(t)$	Torque on hub

The motor-hub gear train multiplies torque but divides angular speed

$$\tau(t) = K_g \tau_m(t) \tag{A.1}$$

$$\dot{\theta}(t) = \frac{1}{K_g} \dot{\theta}_m(t) \tag{A.2}$$

The torque produced by the motor is proportional to the armature current

$$\tau_m(t) = K_m\, i_a(t) \tag{A.3}$$

The voltage drop across the motor is proportional to the motor shaft speed

$$e_b(t) = K_b\, \dot{\theta}_m(t) \tag{A.4}$$

The viscous friction opposes the output torque and is proportional to the hub angular speed

$$\tau_f(t) = -b\dot{\theta}(t) \tag{A.5}$$

Writing down the equation for the electrical part of the system using Kirchoff's voltage law, then using (A.4) and (A.2),

$$\begin{aligned} R_a\, i_a(t) + e_b(t) &= u(t) \\ R_a\, i_a(t) + K_b\, \dot{\theta}_m(t) &= u(t) \\ R_a\, i_a(t) + K_b K_g\, \dot{\theta}(t) &= u(t) \end{aligned} \tag{A.6}$$

For the mechanical part, we use a moment balance with (A.3) and (A.5), then substitute in result (A.6):

$$\begin{aligned} \tau(t) &= K_g \tau_m(t) - b\dot{\theta}(t) \\ &= K_g K_m i_a(t) - b\dot{\theta}(t) \\ &= K_g K_m \left(\frac{u(t) - K_b K_g\, \dot{\theta}(t)}{R_a} \right) - b\dot{\theta}(t) \end{aligned}$$

$$\tau(t) + \left(\frac{K_g^2 K_m K_b}{R_a} + b \right) \dot{\theta}(t) = \left(\frac{K_g K_m}{R_a} \right) u(t) \tag{A.7}$$

Appendix B

Closed-loop Step Identification Test

Two of the experimental plant parameters, the hub inertia J_{hub} and the viscous friction b, required a closed-loop step response test to be identified [37]. For these tests, the flexible ruler was detached from the hub.

Writing down the equation of motion of the system without beam and then using input expression (A.7), we get

$$J_{\text{hub}}\,\ddot{\theta}(t) = \tau(t)$$

$$J_{\text{hub}}\,\ddot{\theta}(t) = \left(\frac{K_g K_m}{R_a}\right) u(t) - \left(\frac{K_g^2 K_m K_b}{R_a} + b\right)\dot{\theta}(t)$$

$$\ddot{\theta}(t) + \underbrace{\left(\frac{K_g^2 K_m K_b}{R_a\, J_{\text{hub}}} + \frac{b}{J_{\text{hub}}}\right)}_{K_1}\dot{\theta}(t) = \underbrace{\left(\frac{K_g K_m}{R_a\, J_{\text{hub}}}\right)}_{K_2} u(t)$$

where K_1,K_2 are introduced for compactness. The open-loop transfer function of this system is obtained by applying the Laplace transform to the equation above, giving

$$s^2\Theta(s) + K_1\, s\,\Theta(s) = K_2 U(s)$$

$$\frac{\Theta(s)}{U(s)} = \frac{K_2}{s^2 + K_1 s}$$

The closed-loop control law $u(t) = K(\theta_d - \theta(t))$ is now added to the system, where K is a proportional gain and θ_d is the desired output angle. The closed-loop system is shown in Figure B.1. From classical control theory, the transfer function of this system can be shown to be

$$\begin{aligned}\frac{\Theta(s)}{\Theta_d(s)} &= \frac{\frac{KK_2}{s^2+K_1 s}}{1 + \frac{KK_2}{s^2+K_1 s}} \\ &= \frac{KK_2}{s^2 + K_1 s + KK_2}\end{aligned} \tag{B.1}$$

Following [52, Section 5.3], (B.1) is rewritten as

$$\frac{\Theta(s)}{\Theta_d(s)} = \frac{\omega_n^2}{s^2 + 2\zeta\omega_n s + \omega_n^2} \tag{B.2}$$

where $\omega_n = \sqrt{KK_2}$ is the natural frequency of the system, and $\zeta = \frac{K_1}{2\omega_n}$ is the damping ratio. A second-order system of the form (B.2), assuming it is underdamped ($0 < \zeta < 1$),

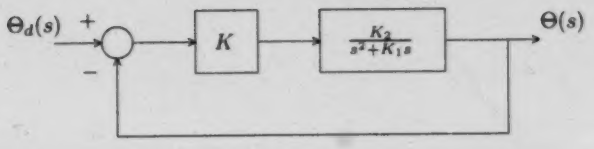

Figure B.1: Closed-loop setup for parameter identification

and subject to a step input, can be shown [52, p.232] to have the peak time

$$t_p = \frac{\pi}{\omega_n \sqrt{1-\zeta^2}} \tag{B.3}$$

and the percent overshoot

$$PO = 100 \exp\left(\frac{-\zeta\pi}{\sqrt{1-\zeta^2}}\right) \tag{B.4}$$

The procedure to identify J_{hub} and b is summarized below

1. Implement the closed-loop setup shown in Figure B.1 in hardware
2. Pick a step amplitude, then tune K to provide an underdamped system response without saturating the input voltage $u(t)$
3. Using the step response data, identify the values of t_p and PO
4. From equations (B.3) and (B.4), solve for ω_n and ζ
5. Use the definitions of K_1 and K_2 to solve for J_{hub} and b

The data obtained to identify our system parameters is plotted in Figure B.2. A step value of 90° was used, with a gain of $K = 0.2$. Note the input voltage remains below the $22V$ saturation limit, and the system response is underdamped.

Using the first graph in Figure B.2, we estimated $t_p = 0.175$s, $PO = 4.2035\%$. The parameter values were calculated to be $J_{\text{hub}} = 3.6391 \times 10^{-3}$ kg m^2, $b = 0.020939$ N m s.

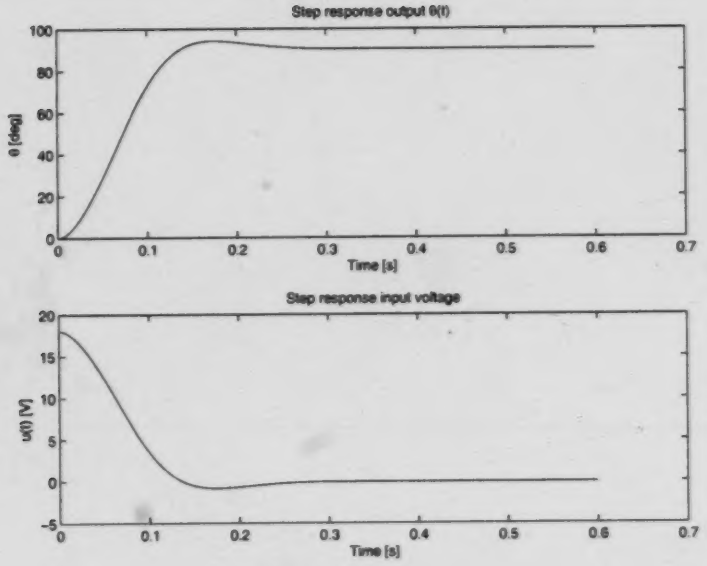

Figure B.2: Input/Output data for system step response